5-1-2016

# Inhaled multiwalled carbon nanotubes induce systemic inflammation and endothelial dysfunction via MMP-9 induction

Mario Aragon

Mario Aragon
*Candidate*

Biomedical Sciences Graduate Program
*Department*

This dissertation is approved, and it is acceptable in quality and form for publication:

*Approved by the Dissertation Committee:*

Matthew Campen , Chairperson

Scott Burchiel

Mary Walker

Nany Kanagy

Aaron Erdely

# Inhaled Multiwalled Carbon Nanotubes induce Systemic Inflammation and Endothelial Dysfunction via MMP-9 Induction

**by**

**MARIO ARAGON**

**B.S. Biomedical Engineering, Tulane University**

**DISSERTATION**

Submitted in Partial Fullfillment of the
Requirement for the Degree of

**Doctor of Philosophy**
**Biomedical Sciences**

The University of New Mexico
Albuquerque, New Mexico

May 2016

## Acknowledgements

First and foremost I would like to thank my mentor, Matt Campen, for everything he has done over the years. He has always been available when I needed to talk to him or had a problem that I needed help solving. He has given me a solid foundation to continue my toxicology training, while simultaneously squirreling away a few stories of some of my less than impressive moments in the lab. I would also like to thank my committee members Scott Burchiel, Nancy Kanagy, Mary Walker and a special thanks to Aaron Erdely for making the trips back and forth from West Virginia to New Mexico.

I would also like to thank current and former members of the lab. From my first day to my last there have been people that have helped me a long. Special thanks go Sage Colombo, Sarah Robertson, Selita Lucas, Bethany Sanchez, Guy Herbert, Megan Channell, and Katie Zychowski. Everyone mentioned has helped with assays, exposures, and just generally been there to provide feedback.

I would like to thank my family, specifically my parents, for everything they have done over the years. They have encouraged me in every major endeavor I have gone through in my life, both the highs and lows. They supported when I moved away and to various parts of the country, and they were right there when I got married in grad school.

Lastly, and most importantly I would like to thank my wife. She has been a rock by my side through thick and thin and I consider myself extremely lucky to

have met her in my first year of grad school. Her support and loyalty have been unwavering. Everything is more fun when she is around. I am very excited to take our next step in life together.

# Inhaled Multiwalled Carbon Nanotubes induce Systemic Inflammation and Endothelial Dysfunction via MMP-9 Induction

By

**Mario Aragon**

B.S. Biomedical Engineering, Tulane University

Ph.D. Biomedical Sciences, University of New Mexico, 2016

## Abstract

Assessing the mechanisms underlying adverse cardiovascular effects induced by inhaled toxins presents a substantial research challenge. We propose that blood carries an as yet unknown “inflammatory potential” consisting of modified proteins or other biomolecules and reaction byproducts that affects a pathological bioactivity which can be assessed using naïve endothelial cells and blood vessels. The approach involves applying serum from exposed animals to cultured primary endothelial cells or ex vivo isolated arteries. Mice were exposed to multi-walled carbon nanotubes (MWCNT; 0, 10 or 40 μg) or other pollutants

via pharyngeal aspiration and serum was collected at 4 and 24 h post-exposure. Serum from exposed mice increased endothelial cell surface vascular cell adhesion molecule-1 (VCAM-1) and intracellular adhesion molecule-1 (ICAM-1) expression and proinflammatory transcripts, and decreased ATP-stimulated nitric oxide (NO) production. The functional impact of this loss of NO bioavailability was confirmed via myography, in which serum from pollutant-exposed mice significantly impaired vasodilation to acetylcholine. In addition, serum from pollutant-exposed mice reduced cell migration in a traditional scratch assay experiment. In vivo MWCNT exposure was able to both increase the permeability of the Blood Brain Barrier (BBB), as well as induce transcription of pro-inflammatory cytokines in the hippocampus and frontal cortex regions of the brain. This affect was abolished with the treatment of fasudil, or the absence of CD36. There was also evidence of astrocyte activation in the short and microglia activation at 24 hours. CD 36 has also been identified as playing a key role in mediating loss of vasodilatory properties ex vivo. In conclusion, pulmonary exposure to MWCNT dynamically alters circulating factors, which promotes endothelial cell activation, decreased NO bioavailability, and altered functionality all directionally predicting adverse cardiovascular outcomes.

# Table of Contents

# List of Figures

# List of Tables

# INTRODUCTION

## 1.1 Cardiovascular Disease

According to the world health organization, cardiovascular disease (CVD) is the number 1 cause of death globally. Presently, more people die from cardiovascular disease annually than from any other cause. In 2012, an estimated 17.5 million people died from CVD, this number represented 31% of all global deaths. CVD includes a wide range of disorders of the heart and blood, involving a wide range of vascular beds, such as the cerebrovascular (stroke) and coronary (myocardial infarction, heart failure). These specific beds are of greatest interest, due to the high frequency of disease incidence and potential for environmental factors to negatively impact this large population. The World Health Organization estimates that inhaled pollutants represent one of the largest global health concerns, specifically in terms of exacerbating cardiovascular disease, owing to the commonality of pollutant exposures in the home, workplace, and ambient environment in many urban regions of the world[1,2].

One of the hallmarks of common, chronic CVD, such as atherosclerosis, is the activation of the endothelium. The endothelium is a layer of cells that line the vasculature of the body. Under normal conditions the endothelium works to maintain a state of homeostasis in the body, with blood flowing freely and accessing the different organs of the body, as needed. However, when vascular injury occurs, the endothelium becomes “activated”, resulting in three main outcomes that initiates the process of atherosclerosis[3].

### 1.1.1 Activation of the Endothelium

The first outcome of an activated endothelium is the expression of adhesion molecules[4] on the surface of the cell, followed by secretion of pro-inflammatory cytokines[5] to both further activate the endothelium as well as activate circulating monocytes in the blood. Circulating monocytes adhere to the endothelium, migrate into the sub-endothelial space, and undergo further differentiation into monocyte-derived macrophages[6]. This process was originally thought to be mediated by an abundance of cholesterol and low-density lipoproteins (LDL) in the body as a result of a bad diet and/or poor lifestyle. Recent evidence however has found that atherosclerosis has a stronger inflammatory and immune[7] component than originally thought. A recently identified molecule, called oxidized-low density lipoprotein (ox-LDL)[8], has been identified as one of the primary drivers of this inflammation. Ox-LDL is formed when LDL particles in blood plasma invade the endothelium and become oxidized[9]. This oxidation is the result of a complex set of biochemical reactions involving enzymes and free radicals in the endothelium.

The initial migration of monocytes into the sub-endothelial space is further propagated by intracellular signaling through adhesion molecules, including intercellular adhesion molecule -1 (ICAM-1), vascular cell adhesion molecule – 1 (VCAM-1)[10] and various selectins, most notably p-selectin. Monocyte migration into the interstitial tissue results in the differentiation of monocytes into macrophages. Macrophage-colony stimulating factor (M-CSF) is required to catalyze this conversion of monocytes into macrophages[11].

The second outcome of an activated endothelium is the increased permeability of the endothelium[12-14]. Tight junctions can become destabilized, allowing for gaps in the endothelial cells to form; this is most often the result of stimulation by cytokines/chemokines and close communication with activated monocytes[15]. This increased permeability allows for adherent monocytes to transmigrate into the sub-endothelial space and eventually differentiate into macrophages[16,17]. A second consequence of this increased permeability is the potential for LDL or ox-LDL to bind proteoglycans in the extracellular matrix and become trapped in the vascular wall, eventually becoming engulfed by the sub-endothelial macrophages.

A third consequence of an activated endothelium is the decreased production of vasodilatory and antithrombotic molecules, primarily through reduced expression and/or function of endothelial nitric oxide synthase (eNOS)[18,19]. eNOS produces the diffusible gas, nitric oxide (NO), which functions as an endogenous vasodilator, platelet inhibitor, antioxidant and regulator of vascular endothelium[20,21]. NO production is a tightly regulated process that is required in response to diverse physiological and pathophysiological stimuli. eNOS is regulated by multiple interdependent control mechanisms and signaling pathways that act throughout the various states of the enzyme's life history. Intra-cellular calcium is a critical determinant of eNOS activity; this is due to the fact that maximal catalytic function of eNOS requires calmodulin[22] binding to a 50-amino acid domain in order to facilitate transfer of oxygen-derived electrons between the enzyme's reductase and oxygenase domains, which facilitates the

conversion of L-arginine to L-citrulline plus NO. Normally, eNOS is bound to membrane invaginations called caveolae; binding of calcium to calmodulin disrupts this inhibitory binding and allows eNOS to become activated.

Numerous pathways converge on mobilization of intercellular calcium transients to provide the most rapid mechanisms of eNOS activation via calmodulin[23]. A diverse group of agonists, including bradykinin and acetylcholine, activates a G-protein dependent signaling pathways that ultimately releases intracellular calcium stores[24]. In this pathway, phospholipase C cleaves membrane component phosphatidylinositol 4,5 trisphosphate into diaclyglycerol and inositol 1,4,5-triphosphate (IP3) which binds to IP3 receptors that are found in high concentrations in caveolae and regulate intra-cellular calcium through pleiotropic effects.

In addition to calcium activation of eNOS, phosphorylation and de-phosphorylation act as major post-translation regulatory influences on eNOS activity. Key serine and threonine residues in eNOS regulatory loci include phosphorylations at Ser 1177, Ser 635, and Ser 617 are stimulatory, while phosphorylations at Thr 495[25], and Ser 116 act to inhibit activation. The activation of eNOS catalytic function by Ser 1177 phosphorylation is due to inhibition of calmodulin dissociation from eNOS, as well as enhancement of the internal rate of eNOS electron transfer. Ser 1177 phosphorylation is catalyzed by numerous kinases including Akt as well as cyclic AMP-dependent protein kinase, AMP-activated protein kinase, PKG, and calcium/calmodulin-dependent protein kinase II[26]. At present the relative contributions of these different kinases are

unknown, but is it known that different extra-cellular stimuli activate distinct kinase pathways leading to eNOS phosphorylation[27]. **(Figure 1.1)**

These three processes of endothelial activation (increased adhesion/chemotactic signaling; increased permeability; decrease NO production) occur throughout the development of chronic atheromatous lesions in major blood vessels. In early lesion development, the activated endothelium is the first step in recruiting macrophages to begin the lesion formation. In latter stages of atheroma development, the inability to generate NO impairs relaxation and allows greater activation of circulating platelets. Importantly, these endothelial outcomes appear to be triggered by numerous environmental factors and represent an important biological readout to assess the potency of exogenous toxicants.

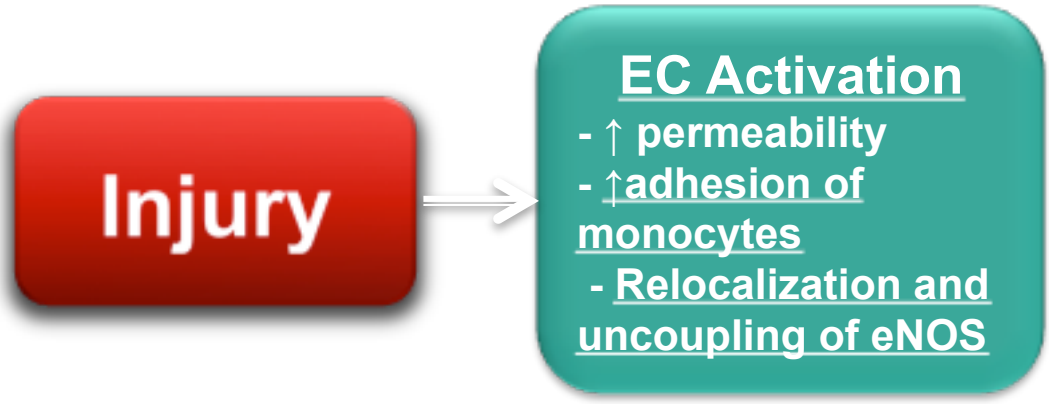


**Figure 1.1: Initial Consequences of an activated endothelium.**

Activation of the endothelium results in increased permeability, increased adhesion of circulating monocytes, and uncoupling of eNOS.

### 1.1.2 Risk Factors for CVD

Risk factors for CVD include both modifiable and non-modifiable risk factors. Non-modifiable risk factors include age, male gender due to the lack of

the cardio protective properties of estrogen, and a family history of CVD at a young age. Modifiable risk factors include lifestyle and environmental exposures that can be impacted by changes in behavior, diet, or medication, such as dyslipidemia, or elevated LDL and decreased HDL, smoking or other toxicant exposures, hypertension, and obesity. The risk factor we are most interested in is modifiable environmental exposures, specifically the inhalation of airborne particulates.

## 1.2 Particulates

Particulates are defined as microscopic solid or liquid matter suspended in earth's atmosphere[28]. Particulates have been designated a group 1 carcinogen by the WHO and are heavily associated with asthma and lung cancer, but also premature death and increased risk of hospitalizations, especially as related to CVD outcomes. Respirable particles have an aerodynamic diameter of 10 micrometers or less, with fine particles having a diameter of <2.5 micrometers and ultrafine particles having a diameter of <0.1microns or 100 nanometers.

### 1.2.1 Toxicity of Particulates

The size of a particle is the most important determinant of its toxicity, which partially determines its reactive surface area, as well as where in the respiratory tract it will deposit, once inhaled[29]. Larger particles (2.5-10 microns) are generally filtered in the nose and throat, but smaller particles can settle deeper in the lungs and bronchi and cause more significant health problems[30]. Fine or ultrafine particles, due to their small size, can penetrate into the gas

exchange (alveolar) regions of the lung. While size is a large determinant of the toxicity and the depth of penetration of particles, shape and chemical composition play a role, as well. In general, inhalable particles penetrate the airways no further than the bronchi and are quickly removed out by the mucociliary tract of the major conduit airways, where they are swallowed or expectorated. Smaller particles can penetrate into terminal bronchioles and the alveoli, the deep region of the lung where gas exchange occurs, where they must be removed by alveolar macrophages. These smaller particles that penetrate deep into the airways necessarily will have a prolonged retention time and the potential for greater toxicity.

## 1.3 Lung Defenses

The lungs have the largest surface area of the body, approximately the size of a tennis court, and as a result are exposed to a wide range of pathogens, toxins, and allergens. To combat this, the lungs employ a wide range of defenses. These defenses include the mucociliary escalator, xenobiotic metabolism, the innate immune system, and the epithelial lining fluid (ELF).

### 1.3.1 Mucociliary Escalator

The portion of the respiratory tract that conducts air into the gas exchange region of the lungs is largely lined with a ciliated airway respiratory epithelium. A thin fluid film of mucus, derived from secretory goblet cells, surrounds cilia. On top of that is a second viscous film of mucus, in which deposited foreign particles and microorganisms become trapped. Within the thin fluid film of mucus the cilia

act out movements coordinated in direction towards the pharynx. Thereby, the viscous film of mucus, including its freight, is transported away in direction towards the mouth, where it is either swallowed or expelled via coughing. Important for effective mucociliary clearance are the number of cilia, their structure, activity, and coordinated movement. Optimal functionality of the cilia requires a specific temperature and humidity[31]. Conditions of insufficient temperature and humidity can result in the ciliary cells suspending their transport function. Under such circumstances, bacterial germinal colonization is facilitated. Pulmonary infections and damaging of the pulmonic tissues may result. The mucociliary escalator generally functions to remove larger particles that deposit in the upper airways; smaller particles or gases require the lungs to employ other defense mechanisms[32].

### 1.3.2 Xenobiotic Metabolism

The lungs also contain a wide range of xenobiotic metabolizing cytochrome p450s[33], located largely in airway club cells (previously termed Clara cells). These xenobiotic enzymes include cyclo-oxygenases and flavine dependent monooxygenases, as well as phase II conjugating enzymes such as glutathione S-transferases, UDP-glucuronyltransferases, and DT-diaphorases. All of these enzymes play a role in the early cellular defense against acute and delayed pulmonary toxicity. The susceptibility of the lung to xenobiotics depends on the metabolic balance between toxication and detoxication pathways[34]. Notably, as all blood flows through the lung in a given circuit, the lung is highly responsible for the condition and content of the blood. Major metabolic pathways

for regulation of blood volume, such as angiotensin converting enzyme, are predominantly located in the lung tissue.

### 1.3.3 Anti-oxidants and the Lung Surfactant

In the alveoli of the lower respiratory tract, the functional interface between the atmosphere and the body is found, allowing the exchange of oxygen and carbon dioxide between air and blood. As a result of this interface, the cells composing the alveolar walls are placed under a burden of toxic oxygen radicals that is often found to be greater than that of any other tissue. The parenchymal cells of the lower respiratory tract are able to suppress the intracellular burden of oxidants with a wide array of anti-oxidants that include superoxide dismutase (SOD)[35], catalases[36], and the glutathione system[37]. These anti-oxidants function to either convert oxidants to water and oxygen, or to make them water-soluble so they become easier to excrete. The anti-oxidant defense systems of the parenchyma are well characterized, but the unique situation of the alveolar structures with their potential exposure to a wide range of oxidants in the extracellular milieu, creates the possibility that there may be more oxidant defense mechanisms that would serve as more of a first line of defense out of the parenchymal cells.

Additionally, in the deep lung as well as lining the conducting airways, there is a phospholipid surfactant layer that contains high concentrations of anti-oxidants such as urate, ascorbate, and glutathione. This surfactant is typically very thin, to avoid compromising the gas exchange in alveoli or mucociliary tract

action of the upper airways, but very effective in scavenging reactive gaseous air pollutants[38].

### 1.3.4 Alveolar Macrophages

In the deepest regions of the lungs the last line of defense is the presence of alveolar macrophages[39]. Alveolar macrophages (AMs) serve as the primary phagocytes of the innate immune system, clearing the air spaces of infectious, toxic, or allergic substrates that have evaded the defenses of the respiratory tract, such as nasal passages and the mucociliary escalator[40], or formed in situ. AMs employ secretion of oxygen metabolites, lysozyme, antimicrobial peptides, and proteases to help eliminate pathogens. In addition to their phagocytic capabilities, recent evidence suggests that AMs have an equally important role in resolving inflammation within the airspace. As an inflammatory response subsides, neutrophils in the lung undergo apoptosis. During apoptosis, neutrophil surface membranes remain intact, containing their potentially tissue damaging cytoplasmic contents. If apoptotic neutrophils are not efficiently cleared, devitalized neutrophils further degrade and leak their proteases into the alveolus, producing further tissue injury and perpetuating inflammation. Phagocytosis of neutrophils reduces macrophage secretion of pro-inflammatory cytokines and also stimulates production of anti-inflammatory cytokines, such as transforming growth factor-β and interleukin-10[41,42].

AMs have proven to be extremely efficient at clearing inhaled particles. Particles they were unable to phagocytize, such as asbestos, have resulted in

long-term health effects. Termed “frustrated” macrophages, long fibers that are morphologically impossible to phagocytize can lead to accumulation of immune cells and focal regions of inflammation and remodeling[43,44]. Particles with a high ascpect ratio of concern to public health include carbon nanotubes. These engineered particles share morphological characteristics with asbestos and have raised concerns regarding potential for inefficient alveolar removal.

## 1.4 Carbon Nanotubes

Presently >100 tons of nanotubes are produced each year, or roughly 1/3 of all nanoparticles created that are carbon-based. Their unique physiochemical characteristics allows for a wide range of biological effects. Most importantly, their small aerodynamic size creates the potential for them to penetrate deeply into the alveolar regions of the lungs. One result of such a high volume of production is the increased probability for accidental exposures to occur in an occupational setting, with inhalation of particles having the potential for the greatest amount of toxicity.

## 1.5 Multiwalled Carbon Nanotubes (MWCNTs)

MWCNTs are a subset of nanotubes that are highly desired to their ability to withstand a high degree of functionalization[45]. This means that they are ideal platforms for a number of different applications including electronics, consumer goods, imaging, and as drug delivery platforms[46]. MWCNTs consist of graphene that has either been rolled around itself, dubbed the “parchment model” due to its resemblance to rolled parchment. Or they can consist of sheets of graphite

arranged in concentric cylinders, e.g. a single-walled nanotube within a larger single-walled nanotube. The number of layers can vary from 2−50 depending on the desired properties of the nanotubes. **(Figure 1.2)**

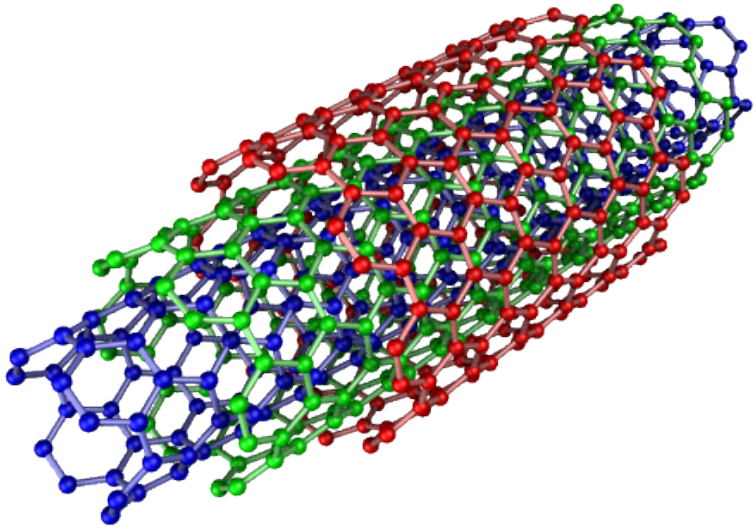

**Figure 1.2: Model of a Multiwalled Carbon Nanotube.**
An example of the Russian Doll model of MWCNTs.

### 1.5.1 Properties of MWCNTs

MWCNTs are the strongest and stiffest materials yet discovered in terms of tensile strength and elastic modulus respectively[47]. These two properties are chief among the reasons they are so highly desired. Their strength results from the $sp^2$ bonds that form between the individual carbon atoms[48]. A comparison of their mechanical properties to other well-known materials indicates that their strength exceeds that of both Kevlar and stainless steel, respectively.

The symmetry and unique electronic structure of graphene, the parent substrate of MWCNTs, strongly affects the electrical properties of MWCNTs. For a given (where n=length,and m=external diamter) nanotube, if n=m the nanotube

is metallic; if n-m is a multiple of 3 then the nanotube is semiconducting with a very small band gap, otherwise the nanotube is a moderate semiconductor[48].

The mechanical properties of MWCNTs allow them to undergo a high degree of manipulation, but during this process the potential for crystallographic defects can occur and, as such, alteration of the material properties. Defects can occur in the form of atomic vacancies, high levels of which can dramatically lower the tensile strength of the nanotube, i.e. enhancing the fragility of the tubes. Defects can also result in loss of electrical properties and thermal conductivity, with the size of the defect being the biggest determinant of the loss of electrical and thermal conductivity[49].

### 1.5.2 Surface Characteristics

Many of the unique properties of MWCNTs can be attributed to the interactions that occur at the surface. In the absence of any kind of surface coating, MWCNTs are highly lipophilic and tend to aggregate in liquid suspensions, instead of staying evenly dispersed[50]. Coating with surfactant is an example of a surface modification that can prevent the aggregation of nanotubes, and is an important consideration in the conduct of the present research[45]. The degree of nanotube dispersion in a composite material is based on the nanotube surface interaction with the surrounding material or solution. Toxicity, gas adsorption, and catalytic activity are all strongly affected by the surface characteristics. The small size of nanoparticles results in a tremendous amount of surface area and increases the potential for toxicity. Surface area

measurement of carbon nanotubes is most commonly based upon $N_2$ gas adsorption. Surface area measurements must be performed at the boiling point of absorbate, this makes the use of nitrogen even more appealing due to the fact that liquid nitrogen is very readily available[51].

### 1.5.3 Density

Density of carbon nanotubes is important for several reasons; it helps determine the mass of the particle, the aerodynamic behavior that determines pulmonary deposition, as well as the degree of functionalization that can be achieved. Currently, three different kinds of density are generally assessed. These include the bulk density, skeletal density, and the packing density. These three types of densities are all taken into account when determining the manipulation of the nanotube in pursuit of a final outcome[52].

### 1.5.4 Current Applications

The many desirable properties of MWCNTs have created the potential for a number of applications across a wide range of industries. Unfortunately, the process of scaling nanotubes from the individual tube to a finished product has presented numerous challenges. Current use and application of nanotubes has been limited to the use of bulk nanotubes, which translates to a mass of unorganized fragments of nanotubes[53]. Presently, bulk nanotube material is unable to achieve a tensile strength that is on par to that of the individual tubes. Despite this, bulk composites may still be able to yield strengths sufficient for many applications[54]. In spite of this inability to maintain the tensile strength of

individual particles, bulk carbon nanotubes have already been used as composite fibers in polymers to strengthen the applications of the composite. Nanotubes can currently be found in bicycles, airplanes, wind turbines, skis, and baseball bats.

### 1.5.5 Synthesis of MWCNTs

There currently exist multiple methods to fabricate nanomaterials depending on the desired properties. The most common method currently used to fabricate nanotubes is called plasma arcing. This method employs plasma, which is an ionized gas. A potential difference is placed between two electrodes and the gas in between ionizes. A typical arcing device is made of two electrodes and an arc that passes from one electrode to the other. The first electrode vaporizes as electrons are taken from it by the potential difference. These positively charged ions pass to the other electrode, pick up electrons and are deposited to form nanotubes.

The second most common technique employed to synthesize nanomaterials is called chemical vapor deposition. In this method, the material to be deposited is first heated to its gas form and then allowed to deposit as a solid on a fmetal catalyst. The deposition can be direct or through a chemical reaction so that the material deposited is different from the volatilized. This process is normally performed under vacuum and is used to make nanopowders of oxides and carbides of metals. At present, chemical vapor deposition is the most promising method for low-cost, large-scale production of MWCNTs[55].

## 1.6 Occupational Exposure to MWCNTs

As mentioned previously, >100 tons of nanotubes are synthesized each year. When CNT synthesis moved from the lab to factories and the products became more widespread, there was a great concern about the toxicity of these fibrous materials and the potential for exposure in an occupation setting[56]. The occupational workforce handling CNT and carbon nanofiber (CNF) currently employs 500 workers at 61 different companies in the US with an expected growth rate of 22% annually[57]. Economically, the global market shows that CNTs represent 28% of the total engineered nanomaterial market share, with MWCNTs accounting for 94% of the total CNT production value.

Carbon nanotubes were discovered 25 years ago, but have only entered the realm of large scale manufacturing in the last 10 years. A result of this very recent growth in production has limited epidemiological research detailing the long-term effects of workplace exposures to CNTs. Exposure to CNTs is currently assessed via sampling of a worker's Personal Breathing Zone (PBZ). PBZ samples are attached to the lapel of the worker while the area samplers are positioned within three feet of the specific process. Direct reading measurements are then co-located to assess a number of different factors including particle number, active surface area, and respirable mass[58,59].

Early exposure assessment on CNT materials focused on collecting samples to estimate CNT mass gravimetrically, which does not differentiate CNT from other airborne dusts. Studies based on total gravimetric mass reported inconsistent data. These studies reported concentrations ranging from not

detectable (ND) to 331.7μg/m$^3$. A study by Maynard et al estimated the inhalable mass of CNFs based on the concentration of metal catalyst and reported PBZ exposures ranging from 0.7-53μg/m$^3$[3,60]. Studies that quantified CNT as respirable PBZ elemental carbon (EC) found CNF exposures ranging from 45 to 80μg/m$^3$[3,61].

### 1.6.1 Methodology to Assess MWCNT Exposure and Toxicity

To better understand the potential health risks of MWCNT, not only is information on exposure needed, but also the concentration-response relationship for adverse health outcomes. Ideally, controlled MWCNT exposure research would be conducted in human subjects to get an accurate representation of the health consequences of exposure, but medical and ethical principles limit the extent of such research. Aside from that, animal inhalation exposure would be the most appropriate means to assess the toxicity of nanotubes in the lungs. This approach also presents many challenges. Inhalation exposures are often time consuming, expensive, and require special equipment to conduct correctly. Other factors associated with conducting an inhalation study include difficulty in generating a controlled CNT concentration, monitoring particle size and maintaining the exposure level throughout the duration of the experiment.

The technical difficulty and cost associated with inhalation exposure forced scientists to assess the effects of CNT exposure in the lung in an alternative manner. A process termed intratracheal instillation (ITI) was developed[62,63]. ITI administers nanotubes in a bolus into the trachea of a small

animal, and relies upon the idea that the nanotubes will be drawn deeper into the lung during breathing. One factor that must be taken into account when utilizing this route of exposure is to choose the appropriate delivery vehicle. An ill-chosen delivery vehicle can result in aggregation of the nanotubes and prevents both the delivery into the deep portions of the lungs, as well as failing to achieve a uniform distribution. This type of exposure does employ an unnatural route of administration and causes a great deal of stress to the animal as a result of the traching process. An appropriately designed ITI study including carefully chosen doses and the appropriate reference compounds does allow for an accurate assessment of the toxicity of the test material in respirable doses[64,65]. It is worth noting that exposures given by ITI have resulted in similar toxicity in the lungs when compared to inhalation[66].

It has been further refined to a method known as pharyngeal aspiration (PA), which is especially valuable in mice where IT is challenging. Briefly, an animal is put under light anesthesia and hung from their teeth so their mouth is open. The tongue is then pulled to the side and a dose of nanotubes, suspended in a physiologic dispersion media, is slowly pipetted to the back of the throat, allowing the animal to aspirate the particle-containing solution as they come out of the anesthesia. When compared to IT, it allows for a better distribution of the particles in the lungs and causes less stress to the animal. As with IT, appropriate delivery vehicles and doses must be chosen to ensure a level of toxicity comparable to inhalation[67].

## 1.7 Respiratory Health Effects of MWCNTs

As the production of nanotubes increased the potential for exposure in the workplace became more apparent, researchers stepped in to determine if there was the potential for any type of toxicity in the lungs following an exposure. Researchers have conducted studies in mice and rats utilizing both IT and PA exposures, they have found a number of effects including: inflammation, fibrosis, granulomas, and cytotoxicity[68-70]. Two of the more relevant studies will be covered here.

The first study was conducted in rats by Muller et al testing two forms of MWCNTs: unprocessed and those that had been ground. The ground MWCNTs became carbon black, which has a smaller surface area and density when compared to the unprocessed MWCNTs. Sprague-Dawley rats were given a single IT dose of either 0.5, 5, or 5mgs of MWCNTs in their lungs and 60 days later the researchers analyzed the lungs for markers of inflammation. They found evidence of inflammation, granuloma formation, and fibrosis. This study suggested the toxic potential for MWCNTs but the doses employed for ITI exposure were extremely high and unlikely to occur in an occupational setting[71].

To date Porter et al has conducted the most thorough study investigating the pulmonary toxicity of MWCNT exposure utilizing a PA exposure. Their study investigated the dose-response and time course of MWCNTs in mice to assess their ability to induce pulmonary inflammation, cytotoxicity, and fibrosis. The authors of this study employed doses ranging from 10μg to 80μg. They also assessed their various end points at 1 day following exposure, and explored out

to 56 days to assess whether any persistent effects remained. The authors found significant increases in neutrophils in the BALF, lactate dehydrogenase (LDH) and albumin across all doses, with most peaking at either 1 or 7 days following exposure. By 56 days these markers were still elevated but were reduced and presumably returning to baseline. Fibrosis was also evident in all groups at all time points. An interesting finding from this study separate from the toxicity in the lungs was light micrograph evidence of AMs that had taken up multiple MWCNTs. This indicated that MWCNTs could be phagocytized and cleared by AMs[72,73]. The implication of this AM clearance is that, unlike asbestos, concerns regarding pulmonary persistence of MWCNTs are largely mitigated.

## 1.8 Systemic Effects of MWCNTs

While the adverse respiratory effects of MWCNTs are well established, the systemic effects associated with MWCNTs are still being established. Presently, MWCNT exposure is known to induce systemic inflammation, immune suppression, and has been shown to exacerbate the progression of cardiovascular disease. These studies have included both PA and inhalation exposure methodologies. Mechanistic studies that describe pathways by which systemic organs are negatively affected by inhalation are currently lacking, although one was proposed for the manner in which MWCNTs exert their immunosuppressive effects.

The laboratory of Peter Møller and Steffen Loft conducted research investigating the association between pulmonary exposure to MWCNT and a

plaque progression. ApoE$^{-/-}$ mice were fed a high fat diet to accelerate the development of plaque progression while simultaneously being exposed to MWCNTs. The authors analyzed liver and lung tissues and found gene expression responses related to oxidative stress (heme-oxygenase 1), inflammation (CcL2 and NOS2), and vascular activation (VCAM-1 and VEGF-A). They also found evidence for plaque progression in the aorta as a result of nanotube exposure, an effect not seen in WT mice[74].

Erdely et al conducted a study utilizing a single dose of MWCNTs to evaluate the immediate systemic response following exposure, characterized by increased gene expression in circulating white blood cells as well as soluble proteins released into the circulation. They found that following exposure increases in biomarkers of a neutrophilic response, including CXCL2, IL-8r, and Mac-1. Genes associated with stress including Hif-3α, MMP-9, and arginase II were up regulated. Inflammatory serum proteins were also up regulated including IL-6, IL-5, CCL-11 and CCL22[75].

Erdely et al followed this study up with one looking at some of the longer term systemic effects following MWCNT exposure. This study found that at 24 hours following MWCNT exposure there was a significant increase in levels of acute phase proteins including C-reactive protein (CRP), haptoglobin, and serum amyloid P (SAP) in the serum. They further confirmed these findings by showing significant elevations of serum amyloid A1 (SAA-1), SAP, and haptoglobin gene expression in the liver[75,76].

Lastly MWCNT exposure has been associated with systemic immune suppression. Mitchell and colleagues[63] conducted a whole body inhalation exposure to MWCNTs to assess their interaction on the immune system. Immune function measurements of splenic cells following MWCNT exposure showed suppressed T-cell dependent antibody responses, decreased proliferation of T cell following mitogen simulation, and altered natural killer (NK) cell killing. These results were accompanied by increased NQO1 and IL-10 gene expression in the spleen, but not in the lung. The authors followed up this study by elucidating the mechanism responsible for the systemic immunosuppression they observed as a result of MWCNT inhalation. The results of this study found that Transforming Growth Factor-β (TGF-β) was released from the lung upon inhalation exposure to MWCNTs. This cytokine activated the cyclooxygenase pathway in the spleen leading to prostaglandin and IL-10 production and release ultimately resulting in T cell dysfunction and altered systemic immunity[77,78].

Taken together, these data provide strong evidence that inhaled MWCNTs exert systemic effects across multiple organs. The time table following exposure could help explain pro-inflammatory effects as well the evidence for altered immune function. The mechanism(s) underlying the pro-inflammatory effects that extend beyond the lung, however, remain largely unknown.

## 1.9 Mechanisms through which Inhaled Particles Cause Systemic Effects

There are currently three different ideas that have been promulgated to explain the how inhaled toxicants cause systemic effects. All three ideas as well as any supporting evidence are described below.

### 1.9.1 Direct Translocation of Particles

The first idea that was proposed was the theory that particles had the ability to directly translocate from the alveolar regions of the lungs into the systemic circulation[79]. As a result of this translocation, particles would be able to directly interact with the endothelium resulting in an activated endothelium and the initiation of a pro-inflammatory state. Research on the deleterious effects of other forms of inhaled particulate matter in the early 90's led to the idea first being proposed that particles had the ability to directly translocate from the lungs to the systemic circulation. With the advent of nanotechnology in the past 15 years, this idea of direct translocation was reignited.

At present the literature on the translocation of very small particles from the lungs into the blood is limited and conflicting. While inhaled particles can translocate beyond the lung, the uptake is inefficient and the few observations of particulates physically located at extrapulmonary sites (such as the heart or brain) have not been able to establish that those translocated particles are exerting a toxic effect. A study utilizing human volunteers reported deposition and clearance by 2 hr of an ultrafine technetium-99m-labeled aerosol. No significant radioactivity was found in the liver or the blood following exposure[80]. Kawakami et al have reported the presence of radioactivity in blood immediately

after inhalation of $^{99m}$Tc-Technegas in human volunteers[81]. Experimental animal studies have reported extra pulmonary translocation of ultrafine particles via IT or inhalation exposure[82-85]. Other studies have detailed the ability of IT exposure to promote thrombosis and adversely affect cardiac function[86]. While these studies indicate that particles, specifically those in the ultrafine range, do have the ability to translocate, the amount that actually makes it into the blood and extrapulmonary organs differs significantly between studies. While there is no clear consensus the majority of studies have found that while translocation of particles can occur, it generally results in a very small amount of particles making it into the systemic circulation. Further detracting from this theory is the fact that direct exposures of systemic cells (such as endothelial cells or cardiomyocytes) to particulate matter typically require in excess of 1,000,000-fold greater concentrations than are observed even in occupational settings (e.g. 10-100 μg/ml in cell culture, compared to 10-100 μg/m$^3$ in the air) to induce measureable adverse effects. This small amount of particles suggests that other mechanisms are responsible for the systemic effects observed following pulmonary particle exposure.

### 1.9.2 Activation of the Autonomic Nervous System

The second mechanism proposed to explain the systemic effects of particles involves activation of the autonomic nervous system[87-89]. This mechanism posits the idea that particle inhalation activates airway sensory nerves, which due to neural plasticity, can modify autonomic nervous system control of cardiovascular function. This neural plasticity can manifest in both the

short-term and long-term. Changes in autonomic tone are often the most immediate response of particle exposure and involve several different reflex arcs[86,90]. Much of the evidence linking changes in cardiac autonomic tone with exposure to particles comes from studies observing Heart Rate Variability (HRV). HRV is defined as the degree of difference in the inter-beat intervals of successive heartbeats and is considered an indicator of the balance between sympathetic and parasympathetic branches of the ANS[91]. Increased HRV has traditionally been considered positive because the heart has the ability to respond rapidly to changing environments. Descreased HRV, reflecting increased sympathetic tone, is generally associated with an increased risk of cardiac arrhythmia[92] and an increased risk of mortality in people with heart disease[93,94]. Research has found low HRV to be associated with exposure to PM and ozone[95-99], while other studies have demonstrated associations between PM exposure and increased HRV[100,101]. While the mechanisms triggering changes in HRV, and thus autonomic tone, have not been fully delineated and are likely numerous and diverse in nature, the best studied is associated with pulmonary neural reflexes. While activation of the ANS as a result of exposure to particles has stronger supporting evidence than the translocation theory, it fails to fully explain the relationship between particle exposures and cardiovascular disease. This theory is likely most pertinent in early responses to exposures (i.e., within hours), while the latter stages of exposure response (hours to days) are influenced by factors derived from lung interactions that “spill over” into the circulation[102].

## 1.10 Spillover of Inflammatory Mediators from the Lung

The third mechanism that has been proposed, dubbed the "spillover" hypothesis, and the one that has the largest body of supportive evidence, states that particle exposure elicits its effects by triggering pulmonary oxidative injury and systemic inflammation with an increase in pro-inflammatory biomarkers. This local response can lead to systemic oxidative stress and inflammation characterized by an increase in activated white blood cells, platelets and cytokine expression. The major consequence of this theory is that the resultant systemic inflammation injures the vascular endothelium, promoting vasoconstriction, thrombosis, and inflammation[103]. Kaufman et al found that inhalation of diesel exhaust in healthy human subjects caused an increased platelet count 22 hours following exposure[104]. This observation was also seen in mice exposed to concentrated ambient particles that showed an increase in their platelet count with evidence of platelet activation[105].

Van Eeden et al showed that human alveolar macrophages produce TNF-α in a dose dependent manner when exposed to atmospheric particles[106]. Kido et al found the lung to be a major source of systemic circulating IL-6 levels in mice exposed to ambient PM[107]. These observations are in line with a large cohort study by Boucud et al that found significant positive associations of short-term exposure to PM10 with circulating IL-1β, IL-6, and TNF-α levels[108].

Mercer and colleagues at NIOSH conducted one of the most thorough and compelling studies in support of the spillover hypothesis. The purpose of this study was to determine the fate of MWCNTs in the body following an inhalation

exposure. Mice were exposed to whole-body inhalation of MWCNTs at 5 mg/$m^3$, for 5 hours/day for 12 days. At 1 and 336 days after the 12-day exposure, mice were anesthetized and lungs, lymph nodes, and extra pulmonary tissues were analyzed to determine the number of MWCNTs per gram of tissue as a percentage of the lung burden the mice were exposed to. The authors found that following exposure, the largest number of particles was found in lymph nodes, followed by the liver. The heart and brain each had <0.01% of the total number of particles; given that both of these organs receive a disproportionately high volume of blood flow to support the high metabolic needs, this lack of uptake was telling. From this data the authors concluded that while MWCNTs did have limited ability to translocate from the lungs to the systemic circulation, the numbers of particles getting through the lungs was insufficient to account for the adverse effects associated with particle exposure, providing more evidence to the idea that another mechanism must be responsible for the observed effects.

Recently our lab has published a number of studies providing further support for the spillover hypothesis; specifically the idea that following exposure an inflammatory signal arises that is carried in the serum component of the blood. A study by Channell et al found that human serum was able to induce gene expression of VCAM-1 when incubated on primary human endothelial cells following exposure to either diesel or nitrogen dioxide[109]. Robertson and colleagues found that serum from mice exposed to ozone, a reactive gas that is unable to translocate beyond the lungs, was able to significantly decrease the ability of eNOS mediated relaxation *ex vivo*[110]. This effect was abolished in the

absence of CD 36, a class B scavenger receptor that has been shown to play a role in a wide range of diseases including atherosclerosis[111]. Importantly, these studies did not observe increases in circulating inflammatory factors, such as C-reactive protein or TNFα, which might explain the increased bioactivity of the serum/plasma. It was hypothesized that perhaps modified proteins or peptide fragments arising from extracellular protease activity might be a driver of systemic effects.

This serum bioactivity can be assessed in multiple ways across a range of end points. Incubation of exposed serum on naïve cells or vessels can be used for both gene expression or vessel reactivity. Serum bioactivity bolsters the argument that inflammatory spillover is a possible mechanism for the manner in which inhaled pollutants cause systemic effects. The origin of those circulating bioactive factors remains unknown, although evidence from earlier work suggests that air pollution-triggered proteolytic activity in the lungs may lead to degraded or fragmented peptides that have altered biological activity. Matrix metalloproteinase 9 (MMP9) was noted as a potential mediator of such fragments[112]. Additionally, it is unknown how factors in the serum may act on the endothelium, but important information from exposure to other inhaled pollutants, such as ozone or ambient particulate matter suggests that scavenger receptors such as CD36[113], TLR4[114], or LOX-1[115] may be central mediators of endothelial cell activation.

## 1.11 Matrix Metalloproteinase

One of the studies conducted by Erdely et al included a chart of the various pro-inflammatory mediators that were measured following a MWCNT exposure and whether that mediator went up, down, or was unchanged. **(Table 1.1)**

| Name | Lung RNA | Blood RNA | Serum Proteins |
|---|---|---|---|
| IL-1β (ng/mL) | ↑ | ↑ | ↔ |
| CD 40 (pg/mL) | ↔ | ↓ | ↑ |
| CCL11(pg/mL) | ↑ | ↔ | ↑ |
| IL-5(ng/mL) | ↑ | ↔ | ↑ |
| IL-6(pg/mL) | ↑ | ↔ | ↑ |
| CXCL1(ng/mL) | ↑ | ↔ | ↑ |
| CCL22(pg/mL) | ↑ | ↔ | ↑ |
| MMP-9(ng/mL) | ↑ | ↑ | ↑ |
| Osteopontin (ng/mL) | ↔ | ↑ | ↓ |
| CXCL2(pg/mL) | ↑ | ↑ | ↔ |

**Table 1.1: Chart of inflammatory mediators and their response to MWCNT exposure.**

While various mediators were altered following MWCNT exposure, MMP-9 was the only enzyme consistently found to up-regulated across all measured samples.

Close inspection of this table revealed one mediator, MMP9, was up regulated in both lung and blood gene expression, as well as in the serum. Matrix

metalloproteinases are zinc-dependent endopetidases that are capable of degrading a wide range of extracellular matrix proteins. They are known to be involved in cleavage of cell surface receptors, the release of apoptotic ligands, and are thought to play a role in cytokine inactivation[116]. MMP-9 in particular utilizes a collagen-based substrate that it can further cleave into distinct fragments. MMP-9 is secreted by a wide number of cell types, including neutrophils, macrophages, and fibroblasts. MMP-9 degrades ECM with subsequent activation of major proangiogenic factors such as vascular endothelial growth factor[117,118]. Macrophages have shown to be a potent source of MMP-9 secretion[119,120], this is important because MWCNT exposure has been shown to elicit a large number of alveolar macrophages following exposure. The fragments generated by MMP-9 have been shown to result in a positive feed back loop that induces the expression of both MMP-9 mRNA and protein.

## 1.12 Scavenger Receptor, CD36

Once in the circulation, factors from the lung are hypothesized to exert detrimental action on the vascular endothelium via cell surface receptors. CD36 has been previously identified as a putative receptor that mediates endothelial cell dysfunction cause by inhalation ozone-induced circulating factors[110]. Furthermore, Rao and colleagues[113] found that CD36 was central to the progression of atherosclerosis cause by inhaled ambient particulate matter in apolipoprotein E-deficient mice, an effect plausibly mediated by enhanced generation and phagocytic uptake of oxidized cholesterol by macrophages. Activation of CD36 has been linked to endothelial dysfunction, anti-angiogenesis

and inflammation in other condition[121,122], making this a compelling target to investigate as a mediator of MWCNT-induced cerebrovascular outcomes.

## 1.13 Hypothesis and Specific Aims

This information allows me to form a hypothesis and subsequent specific aims to test this hypothesis. I hypothesize that **inhalation of multiwalled carbon nanotubes will result in systemic inflammation and vascular dysfunction via MMP-9 activation in the lungs.**

### 1.13.1 Specific Aim 1

First, I will explore the dynamics of serum-based *in vitro* and *ex vivo* assays to determine how serum bioactivity is altered by inhalation of environmentall-relevant particles and gases. Specifically, we will examine re-suspended road dust particles, mixtures of vehicular emissions (gases and particles) and hardwood smoke emissions. Serum will be tested for its ability to induce inflammatory responses in cultured endothelial cells and to reduce vasorelaxation in myographic preparations.

### 1.13.2 Specific Aim 2

My second specific aim will look at the ability of MWCNT exposure to activate the endothelium and decrease NO bioavailability via loss of eNOS activation. This aim will utilize both *in vitro* and *ex vivo* approaches. *In vitro* approaches will center on MWCNT exposed serum's ability to adversely affect NO bioavailability as measured by electron paramagnetic resonance. This will be followed by an acellular assay to determine if the exposed serum has any ability

to scavenge NO. *Ex vivo* approaches will look at serum from MWCNT exposed mice to affect eNOS mediated relaxation in isolated mouse aorta. CD 36 null vessels will be used in the same manner to determine the role of the scavenger receptor and its interaction will eNOS. Lastly, MMP-9 deficient mice will be treated with MWCNT to test the role of MMP9 in generating the bioactive circulating factors.

1.13.3 Specific Aim 3

My third aim will detail the ability of MWCNT exposure to elicit systemic inflammation, with a special focus on activation of endothelial cells that compromise the blood brain barrier, a specialized structure that controls the transport of molecules into and out of the brain. This aim will utilize both *in vivo* and *in vitro* approaches. *In vivo* analysis will focus on BBB permeability, pro-inflammatory cytokine expression in the brain, and immunohistochemistry to identify astrocyte and microglial activation following MWCNT exposure. *In vitro* analysis will focus on serum from MWCNT exposed mice ability to induce expression of pro-inflammatory mediators at the gene and protein level, as well as its ability to negatively affect cell mobility in a “wound healing” assay. Primary cerebrovascular endothelial cells will be used of the *in vitro* asays. Lastly mechanisms of neuroinflammation will be investigated by utilizing fasudil, a Rho kinase inhibitor, to modulate BBB permeability. $CD36^{-/-}$ mice will be used to determine the role of the scavenger receptor in inducing BBB permeability and neuroinflammation. We will further examine the role of MMP9 in driving these effects using transgenic mouse models. **(Figure 1.3)**

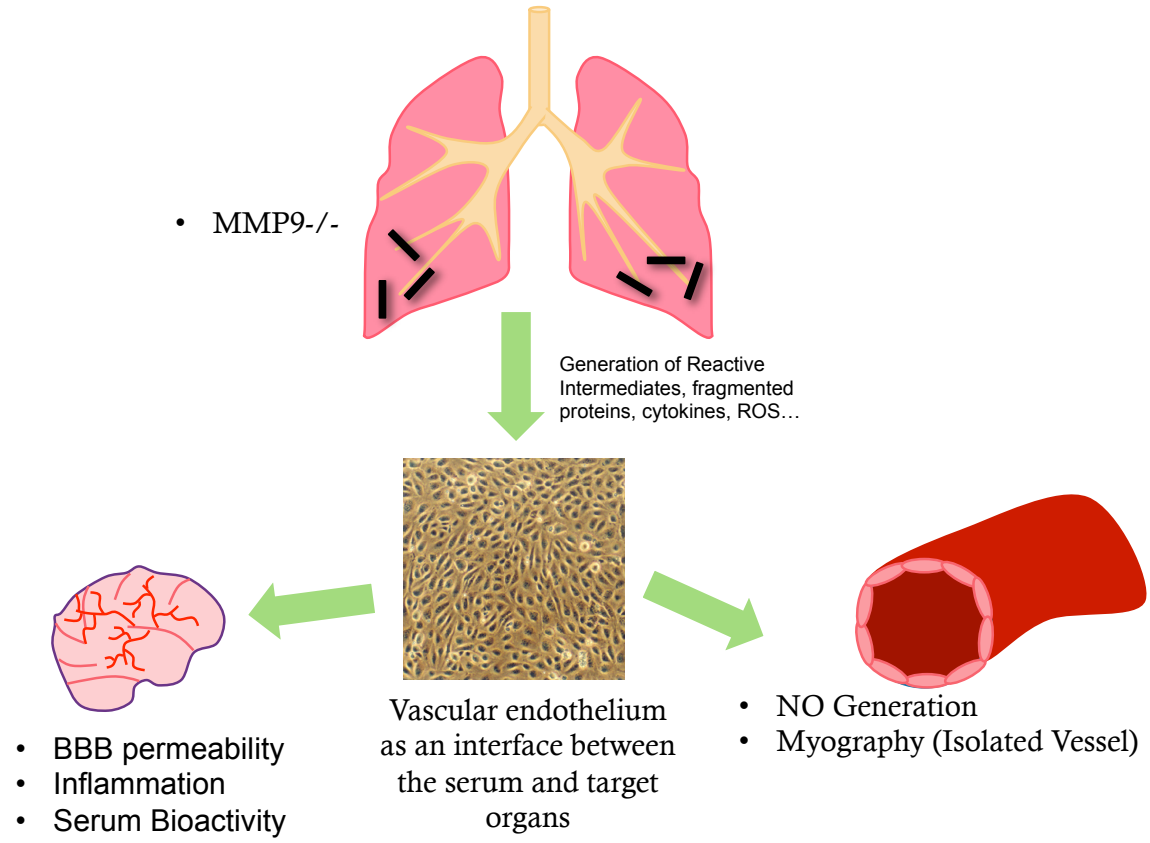


**Figure 1.3: Schematic Representation of Specific Aims.**

# 2. Inflammatory and Vasoactive Effects of Serum Following Inhalation of Varied Complex Mixtures

*Published in Cardiotoxicity, March 2015*

Mario Aragon[1]*, Izabela Chrobak[2,3]*, Jeremy Brower[3], Luis Roldan[1], Laura E. Fredenburgh[2,3], Jacob D. McDonald[3], Matthew Campen[1]

*Denotes equal contributions

[1]College of Pharmacy, University of New Mexico, Albuquerque, NM

[2]Brigham and Women's Hospital, Boston, MA

[3]Lovelace Respiratory Research Institute, Albuquerque, NM

**Corresponding Author:** Matthew J. Campen

MSC09 5360

1 University of New Mexico

Albuquerque, NM 87131

505 925-7778

mcampen@salud.unm.edu

**Running title:** Complex Emissions-Induced Serum Bioactivity

**Word Count:** 4819

**Acknowledgements and Funding:** This study was funded by grants from the National Institutes of Health (R01 ES014639, R01 HL114839, HL115106, T32 HL007736) and the Environmental Protection Agency (RD-83479601-0). The views expressed in this document are solely those of the authors and the U.S. EPA does not endorse any products or commercial services mentioned in this publication.

## 2.1 ABSTRACT

Chronic cardiovascular disease is associated with air pollution exposure in epidemiology and toxicology studies. Inhaled toxicants can induce changes in serum bioactivity that impact endothelial inflammatory gene expression in vitro and impair vasorelaxation ex vivo, which are common precursors to atherosclerosis. Comparisons between single pollutants and common combustion mixtures, in terms of driving such serum inflammatory and vasoactive effects, have not been characterized. Healthy C57BL/6 mice were exposed to a single 6h period of contrasting pollutant atmospheres: road dust, mixed vehicle emissions (MVE; a combination of gasoline and diesel engine emissions) particulate matter (MVE-PM), mixed vehicle emissions gases (MVE-G), road dust plus ozone, road dust plus MVE, and hardwood smoke. Serum obtained from mice 24h after these exposures was used as a stimulus to assess inflammatory potential in two assays: incubated with primary murine cerebrovascular endothelial cells for 4h to measure inflammatory gene expression, or applied to naïve aortic rings in an ex vivo myographic preparation. Road dust and wood smoke exposures were most potent at inducing inflammatory gene expression, while MVE atmospheres and wood smoke were most potent at impairing vasorelaxation to acetylcholine. Responses are consistent with recent reports on MVE toxicity, but reveal novel serum bioactivity related to wood smoke and road dust. These studies suggest that the compositional changes in serum and resultant bioactivity following inhalation exposure to pollutants may be highly dependent on the composition of mixtures.

**KEYWORDS:** diesel, particulate matter, gasoline, exhaust, cardiovascular, wood smoke, endothelium

## 2.2 INTRODUCTION

Air pollution exposure is associated with adverse cardiovascular outcomes[123,124] despite limited direct systemic absorption or translocation of pollutant components into the body [38,125,126]. In recent studies, serum or plasma obtained after pollutant exposures has been shown to possess a pathologic bioactivity capable of inducing inflammation, arresting growth, and impairing vasodilation in cell culture or isolated organ experiments [109,110,127]. Because these studies employed such varied pollutants as diesel exhaust, nitrogen dioxide, ozone, and nickel nanoparticles, it is difficult to gauge the relative potency of these pollutants in driving a serum-borne bioactivity without head-to-head experiments.

Ambient air pollution is comprised of a complex and dynamic mixture of gaseous and particulate substances that may all have varying cardiovascular impact [128]. Emissions arising from traffic have been shown to have a focused impact on cardiovascular outcomes in epidemiological studies [129,130] and diesel exhaust inhalation impairs vasoreactivity in healthy individuals [131]. However, overall ambient air pollution remains an important contributor to chronic cardiovascular disease and numerous source apportionment studies have drawn different conclusions regarding the relative potency of ambient airshed

constituents. A recent examination of cardiovascular hospital admissions in the Northeast U.S. implicated road dust contributions, moreso than motor vehicles, oil combustion, sea salt, or regional sources, as being a principal driver [132]. However, earlier studies suggested a stronger association with mobile source emissions and cardiovascular hospital admissions [129]. The current lack of understanding of the pathogenesis on cardiovascular health impacts of inhaled materials substantially impedes our ability to derive congruous conclusions from large-scale population studies.

The overarching hypothesis of the present work is that inhaled materials lead to compositional changes in the blood that are then conveyed by the circulation to vulnerable sites, such as atherosclerotic regions of the coronary or cerebrovascular arterial beds, and there the bioactive serum may promote inflammatory responses or impair vasodilation. Given the myriad potential compositional changes of the circulation, the present study utilizes two related functional outcomes, inflammatory response and vasorelaxation, under an endothelial cell biosensor assay paradigm. Using healthy mice exposed to a battery of varied complex pollutant atmospheres, we examined the relative impact of serum changes on inflammatory and vasoactive impairments.

## 2.3 METHODS

### 2.3.1 Animals:

Male C57BL/6 (Jackson Laboratories) and Apolipoprotein E-null ($ApoE^{-/-}$; Taconic Laboratories) mice were obtained at 6-8 weeks of age and quarantined

for 14 days prior to exposures. Mice were housed in standard shoebox caging under AAALAC-approved conditions for temperature and humidity, with food and water available ad libitum, except during exposures. Following exposures, mice were euthanized by humane means (pentobarbital) and tissues collected. For myograph experiments, male C57BL/6 mice were also used as donors for aortic rings. Donor mice were euthanized via exsanguination while under anesthesia (isoflurane; concentration 1.5-2%). All procedures were approved by both the University of New Mexico and the Lovelace Respiratory Research Institute animal care and use committees.

2.3.2 Exposures:

All exposures with C57BL/6 mice were conducted for a single 6h period, and serum was obtained 18h following the cessation of exposures (N=6 per group). All exposure systems have been rigorously characterized in terms of chemical composition and each is described in brief, below. Exposures were conducted in 1 or 2 $m^3$ whole-body rodent inhalation chambers (Lab Products, Inc., Maywood, NJ) that were ventilated with exposure atmospheres at ~500 lpm, for a residence time of approximately 4 min. The chambers contain sampling ports above each cage unit to facilitate characterizing spatial homogeneity of exposures and to provide multiple sample locations for exposure characterization (Figure 1). During the exposures, concentrations of particulate matter were measured by gravimetric analysis of filter samples three times during each exposure. For each exposure condition, a matched cohort of mice exposed to filtered air (FA) was included as a sham control group.

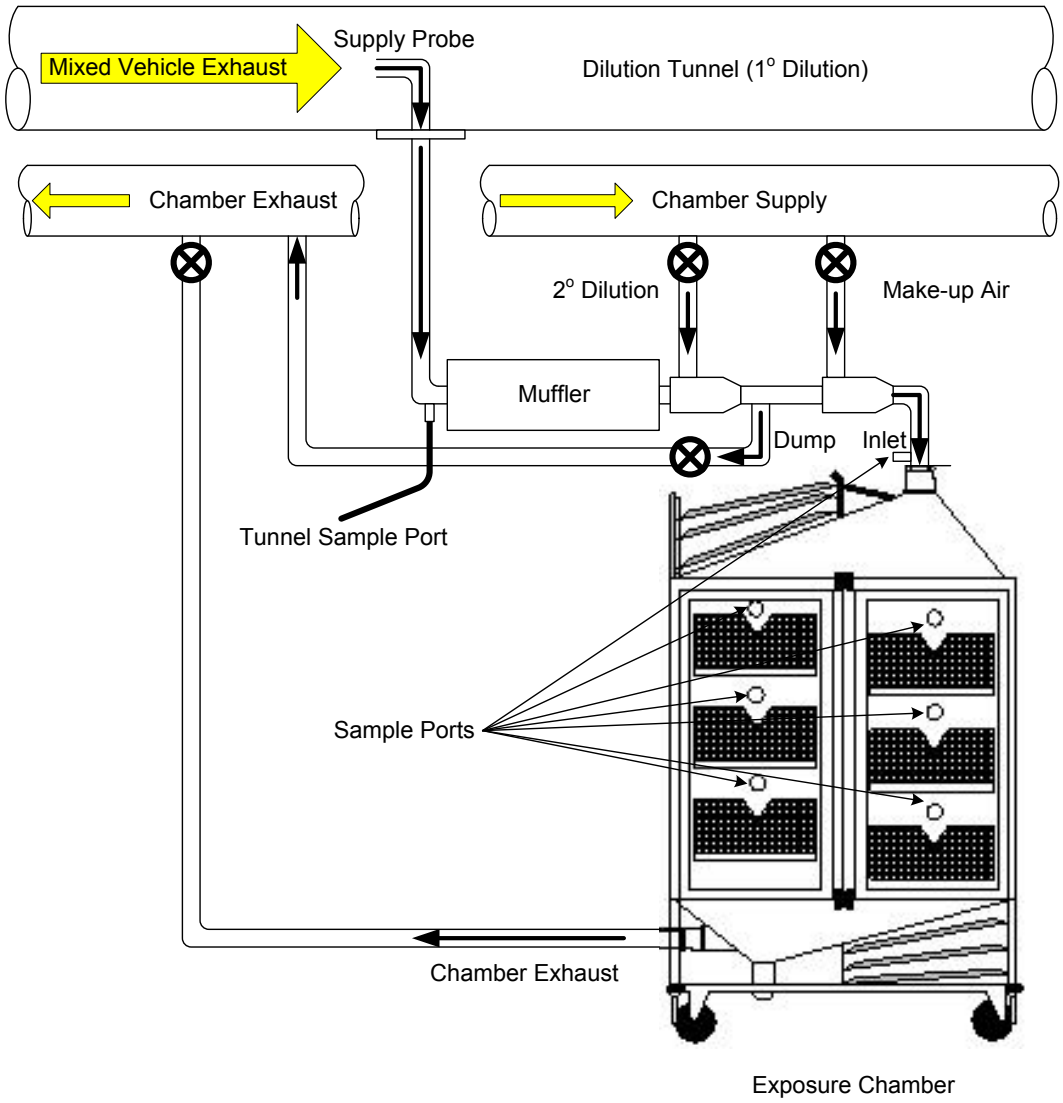


**Figure 2.1: General schematic for inhalational exposures.**

*Road dust* was obtained from roadway surfaces on residential streets and urban arterials in Phoenix and Tucson, AZ [128]. Material was vacuumed from street surfaces with a commercially- available, standardized, low-volume surface sampler (CS3, Inc., Sandpoint, ID). The sampler excluded particulate material >10 microns during collection. Particulate samples were subsequently sieved on an orbital shaker and the finest fraction (<38 μm bulk material diameter) was retained. Aerosol generation was conducted with a Wright-dust feeder that was

coupled to a PM2.5 cyclone on the effluent stream to remove particles >2.5 microns. This size selective cut was used to ensure the material was in the respirable range for a rodent.

*Ozone* was generated using a Sander Ozonisator (Model IV, Sander Company, West Germany), diluted to 0.3 ppm, and monitored with a Teledyne Ozone Analyzer (Model 465L, Teledyne, San Diego, California).

*Mixed vehicle emissions* (MVE) were generated by combining exhausts from a diesel generator (single-cylinder, 5500-watt, Yanmar diesel-engine generator [133] using Number 2 Diesel Certification Fuel) pulling a constant 90% load during operation with a gasoline engine (1996 General Motors 4.3 L V6 gasoline engine) connected to an eddy current dynamometer [134]. The ratio of diesel PM to gasoline engine PM was approximately 5:1, but gasoline contributed greater ratios of gaseous components. Oxides of nitrogen (NOx) and carbon monoxide (CO) concentrations were monitored and recorded at approximately 30–60 minute intervals throughout the exposures.

*Woodsmoke* was generated by a PineRidge wood-burning stove burning a supply of solid oak logs.

*National Particulate Component Toxicity Initiative Study:* Additionally, serum was available from previous studies using 50-day exposures in $ApoE^{-/-}$ mice. In the present manuscript, serum from road dust, road dust with MVE gases, and MVE gases was used in *in vitro* assays, described below. These

exposures are described in detail elsewhere [128] and are the basis for exposures above.

2.3.3 Serum Inflammatory Potential:

Cell culture of murine cerebrovascular endothelial cells and isolation of RNA was performed similarly to previously described methods. Briefly, murine cerebrovascular endothelial cells (mCECs) were obtained from a commercial vendor (Cell Biologics). Serum from each subject was added to individual wells of a 24-well plate at a ratio of 1:40 (2.5%) with complete culture media and incubated for 4h at 37°C. Following incubation, cell supernatants were collected and mCECs were washed with PBS, lysed and immediately cell lysates were pooled and collected for RNA purification. Total RNA was isolated using RNeasy Mini Prep Kits (Qiagen) and RNA was reverse-transcribed using High-Capacity cDNA Reverse Transcription Kits (Applied Biosystems) prior to quantitative real-time PCR (qPCR) assessment of endothelial adhesion markers. Amplification of target message was performed in Taqman® universal master mix following manufacturer's recommended conditions with Taqman® Gene expression assays for inflammatory markers included the arachidonic acid metabolizing enzyme cyclooxygenase-2 (COX2 aka PTGS2), adhesion molecules (ICAM1, VCAM1), and cytokines (IL-6, CXCL1, CCL2, and CCL5) with endogenous TATA-box binding protein (TBP) as the housekeeping gene. Relative gene expression was analyzed by the $2^{-\Delta\Delta CT}$ method [135] using a relative amount of mRNA for each sample normalized to TATA-box binding protein.

2.3.4 Ex Vivo Serum Effects on Vasorelaxation:

Serum from exposed mice was applied to aortic rings from naïve mice to assess the impact on acetylcholine-mediated relaxation, similar to that previously described [110]. Briefly, thoracic aortas were isolated from naïve C57BL/6 mice and cleaned of connective tissue. Ring segments of aorta (2-3 mm length) were then mounted in a myograph system (610 M; DMT, Inc, Atlanta, USA) and submerged in physiological salt solution (composition in mM: 119.0 NaCl, 25.0 $NaHCO_3$, 5.5 glucose, 4.7 KCl, 1.2 $MgSO_4$, 1.2 $KH_2PO_4$, 0.027 ethylenediaminetetraacetic acid, 2.5 $CaCl_2$) bubbled at 37ºC with 21%$O_2$-5%$CO_2$-balance $N_2$, and left to equilibrate at 2 g of tension for approximately 30 min. Tension was gradually applied over 10 min to an optimal passive tension of 10 mN. Vessel viability was confirmed by a contractile response on addition of high potassium PSS (KPSS in mM: 64.9 NaCl, 25.0 $NaHCO_3$, 5.5 glucose, 58.9 KCl, 1.2 $MgSO_4$, 1.2 $KH_2PO_4$, 0.027 ethylenediaminetetraacetic acid, 2.5 $CaCl_2$), repeated twice.

After a 30-min equilibration period, vessels were incubated with 1% serum obtained from WT mice following exposure to FA or other pollutant atmosphere (N=5-7 per group). To generate a control relaxation curve for the various atmospheres, serum from 1-2 mice per control group were used and the data from these ACh-response curves were pooled (n=7). This allowed for control data to be collected in parallel with all other atmospheres. Addition of serum to the myography bath induced contraction of aortic rings and cumulative concentration-response curves to ACh ($10^{-9}$-$10^{-4}$) were performed after response to serum had stabilized (approx. 20 min). Data were acquired by a MacLab/4e

analogue-digital convertor displayed through Chart™ software (AD Instruments, USA). Relaxation data are expressed as a percentage of serum-induced contraction, with baseline tension subtracted.

2.3.5 Statistics:

Serum effects on gene expression were compared by an unpaired Student's t-test with each exposure linked to the simultaneously-conducted filtered air control group. Subchronic studies in ApoE$^{-/-}$ mice were compared with an ANOVA with Dunnett's Multiple Comparison Test. Myographic studies were compared with a two-way analysis of variance considering exposure and acetylcholine concentration as the two factors, and post-hoc comparisons at specific acetylcholine concentrations were conducted using a Fisher's Least Significant Difference test (GraphPad Prism, v 6.0). To generate a control relaxation curve for the various atmospheres, serum from 1-2 mice per control group were used and the data from these ACh-response curves were pooled (n=7). Other comparisons were conducted with a standard one-way analysis of variance.

## 2.4 RESULTS

2.4.1 Exposure Generation:

Particulate matter and gas concentrations for each exposure atmosphere, both target and measured values, are shown in Table 1. Filtration of the MVE atmosphere effectively removed approximately 96% of particulate mass compared to the pre-filtration atmosphere. In contrast, denuding the MVE

atmosphere to reduce the gaseous fraction effectively removed 84% of NOx and 85% of CO compared to the pre-denuded atmosphere.

| | PM (µg/m$^3$) | | NOx (ppm) | | CO (100 ppm) | |
|---|---|---|---|---|---|---|
| **EXPOSURE** | **Target** | **Actual** | **Pre** | **Post** | **Pre** | **Post** |
| **Road Dust** | 300 | 349 | - | - | - | - |
| **Road Dust + MVE** | 200+100 | 342 | 10.2 (2.5) | - | 25.6 (8.2) | - |
| **MVE Gases** | 0 | 13 | 28.6 (5.1) | 25.6 (6.3) | 66.2 (24.4) | 58.5 (26.6) |
| **MVE PM** | 300 | 328 | 24.6 (8.0) | 4.0 (1.2) | 54.6 (9.3) | 8.0 (3.1) |
| **Road Dust + 0.33 ppm Ozone** | 300 | 344 | - | - | - | - |
| **Woodsmoke** | 300 | 380 | - | - | - | - |
| **MVE (for ApoE-/- mice)** | 300 | 349 | 17.8 (4.8) | - | 32.4 (8.2) | - |

**Table 2.1. Concentrations of major atmosphere components, PM, NOx, and CO in the 7 test atmospheres.**

For Nox and CO, values for "pre" and "post" indicate values upstream and downstream of the denuder or filter, when in use. Values are given and mean and (SD).

2.4.2 In Vitro Serum Inflammatory Potential:

We analyzed a panel of inflammatory markers expressed in cultured endothelial cells at the mRNA level, as an indicator of the cumulative inflammatory potential of serum from exposed mice. Serum obtained from C57BL/6 mice exposed for a single 6 h period to Road Dust was able to potently induce several inflammatory genes, namely cytokines IL-6, CXCL1, CCL2, and CCL5 (**Figure 2.2**). Interestingly, serum from mice exposed to Road Dust + MVE did not display this inflammatory induction on endothelial cells. Consistent responses were observed with serum from Road Dust + $O_3$, however, with endothelial transcription of CCL2, ICAM-1, and VCAM-1 being significantly

elevated. Serum from mice exposed to MVE PM or MVE gases failed to elicit any induction of the inflammatory genes that were assessed in cultured mCECs.

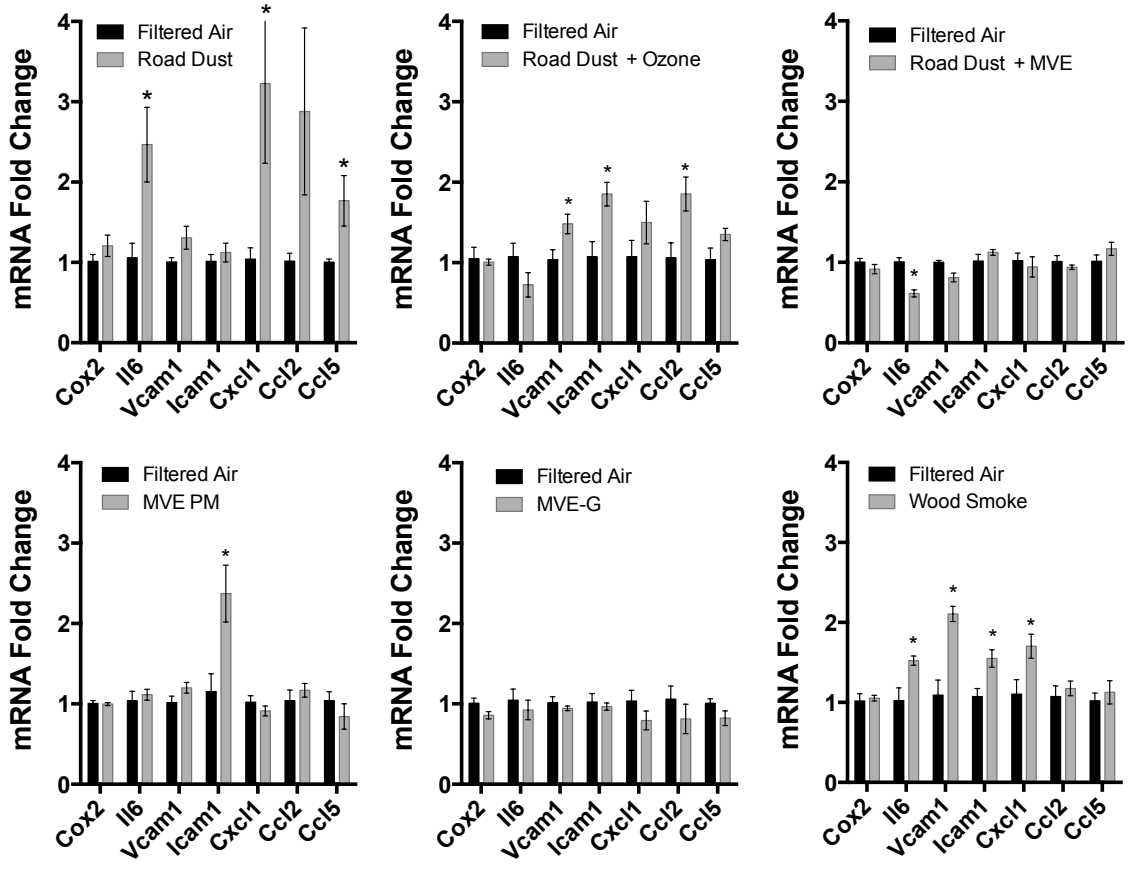


**Figure 2.2: Serum-induced endothelial cell gene expression in an in vitro assessment of inflammatory potential.**

Serum was obtained 24h after C57BL/6 mice were exposed for 6h to one of 6 atmospheres. Each exposure group (N=6) had a unique filtered air control group (N=6). Results for each gene are compared by a Student's t-test, with asterisks indicating $p<0.05$.

Given the divergent responses between Road Dust and Road Dust + MVE, we retrieved banked serum from previous studies on these pollutant atmospheres[128]. This previous research involved the exposure of $ApoE^{-/-}$ mice to Road Dust (the same source material and concentration used in the single day exposure), Road Dust + MVE gases, and MVE gases, albeit for a subchronic study design (6 h/d x 50d) [128]. In co-incubations with mCECs, we also noted that

serum obtained from Road Dust had a substantial impact on expression of CXCL1, CCL2, and CCL5 (**Figure 2.3**). Combined with the gaseous fraction of MVE, however, Road Dust failed to confer such inflammatory potential on the serum, consistent with the 1-d studies (**Figure 2.3**). The MVE gas fraction alone was similarly ineffective at increasing serum inflammatory potential. These data suggest that certain gases in the complex mixture may act to inhibit inflammatory responses of endothelial cells or the formation of inflammatory intermediates in the serum.

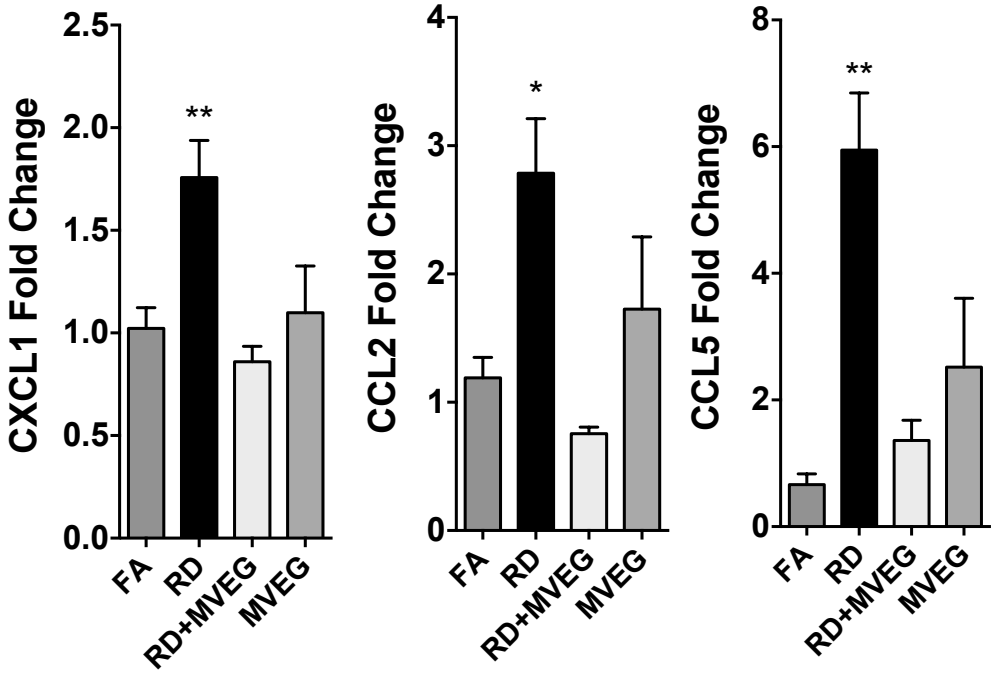


**Figure 2.3: Serum-induced endothelial cell gene expression in an *in vitro* assessment of inflammatory potential.**

Serum was obtained 24h after ApoE$^{-/-}$ mice were exposed for 6h/d x 50d to one of 3 atmospheres. Exposure groups (N=6 per group) were conducted in parallel with a single filtered air control group (N=6). Results for each gene are compared by an ANOVA with Dunnett's Multiple Comparison Test. Asterisks indicate significant difference from control (*$p<0.05$; **$p<0.01$).

2.4.3 Serum from Exposed Mice Impacts on Vasorelaxation:

In contrast to inflammatory markers in cultured cells, serum from Road Dust and Road Dust + $O_3$ exposure mice had no apparent effect on vasorelaxation in co-incubated aortic rings from naïve mice, compared to serum from control (filtered air exposed) mice (**Figure 2.4**). However, all atmospheres that contained complex emissions gases induced changes in serum that impaired relaxation *ex vivo*. Additionally, PM from MVE, with copollutant gases removed by denudation, was also able to reduce vasorelaxation responses to acetylcholine. In terms of magnitude of response, the atmospheres MVE PM, MVE Gases, wood smoke, and Road Dust +MVE could not be statistically differentiated, with all inducing a 20-40% reduction to the maximal effect in FA controls (**Supplemental Fig 1**). Additionally, all serum applications in the *ex vivo* bath led to some degree of contraction from the baseline tension. Serum from mice exposed to MVE PM or Road Dust + MVE induced the greatest contraction, relative to FA controls (**Figure 2.5**), even at a substantial dilution, suggesting the induction of pro-constrictive factors in the serum.

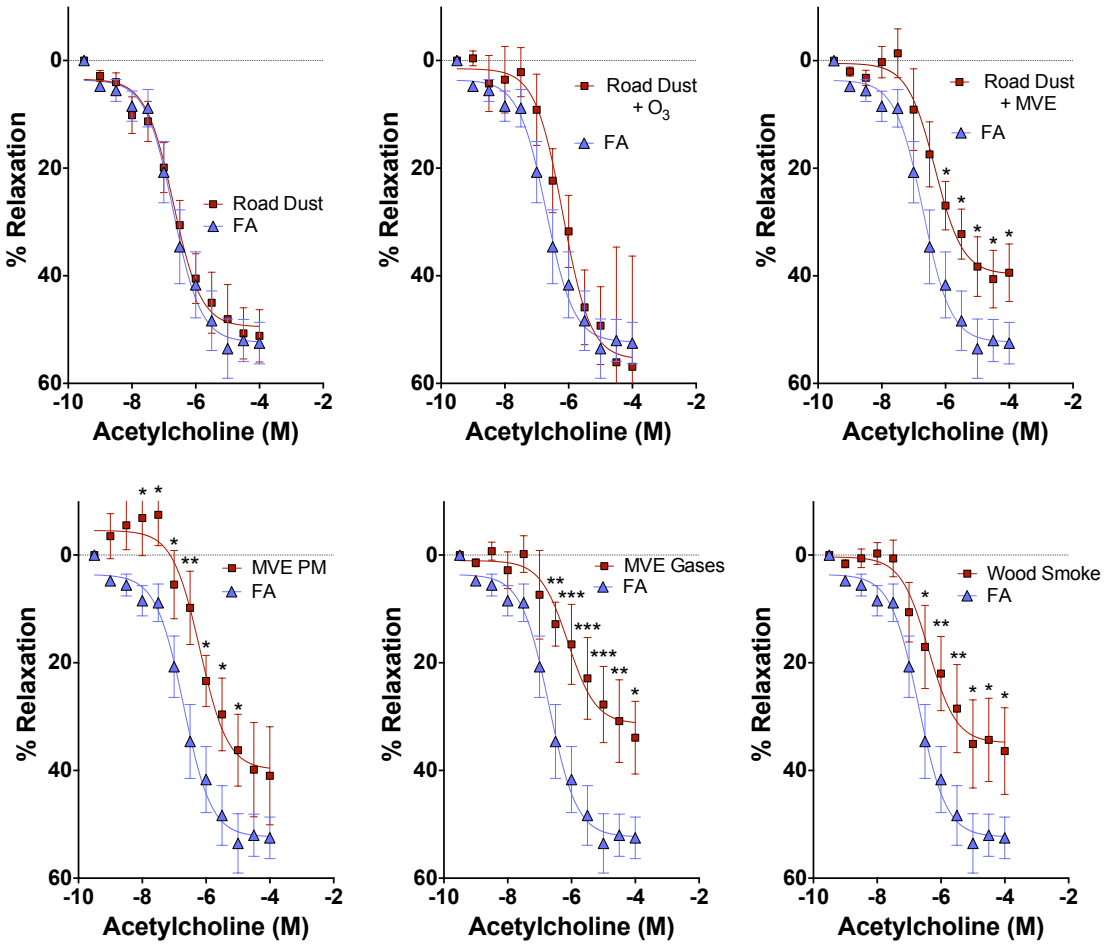


**Figure 2.4: Serum-induced impairments of vasorelaxation response to acetylcholine.**

Results are compared by a two-factor ANOVA, considering exposure and acetylcholine concentration as factors, with a Fisher's Least Significant Difference test to compare specific concentrations (GraphPad Prism, v 6.0). Asterisks indicate significant difference from control (*p<0.05; **p<0.01, ***p<0.001).

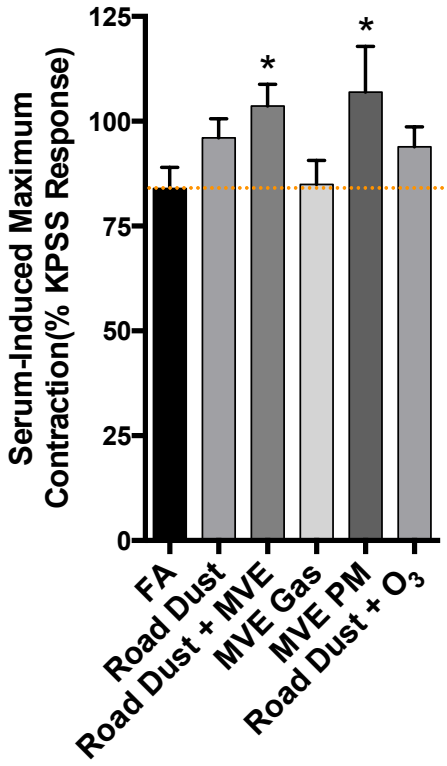


**Figure 2.5: Serum-induced contraction in aortic rings.**

Upon incubation with serum in the tissue bath, aortic rings developed spontaneous tone relative to baseline that was comparable to that induced by KPSS. Asterisk indicates significant difference from filtered air (FA) controls by ANOVA with an Uncorrected Fisher's Least Significant Difference test ($P<0.05$).

## 2.5 DISCUSSION

This study represents the first head-to-head comparison of inflammatory potential and vasoactivity of serum resulting from various complex pollutant exposures. Several conclusions can be inferred from the outcomes. First, a single day of exposure to these complex pollutant atmospheres in healthy C57BL/6 mice readily drove a varied bioactivity that was carried by the serum. Second, impairment of acetylcholine-induced vasorelaxation was not induced by the same serum modifications that caused inflammation, as there was very little

overlap in these outcomes across different atmospheres. This suggests that specific serum compositional modifications may result from exposures to varied pollutants, resulting in divergent biological impacts. The exception to this was wood smoke exposure, which caused serum bioactivity that induced both inflammatory and vasoactivity changes. Specific differences in the responses to the atmospheres belie simplistic interpretation, but the overall bioactivity of the serum is consistent with recent studies in mice and humans [109,110,127].

Divergent inflammatory effects from the three atmospheres containing Road Dust are the most difficult to explain. The potent induction of inflammatory chemokine transcripts by serum from Road Dust exposures was confirmed with serum obtained from a sensitive model ($ApoE^{-/-}$ mice) exposed subchronically (50d). While it is not clear form our study design whether the serum inflammatory potential was increased by the repeated exposure or the hypercholesterolemic model, the end result is coherent with the single day exposures. Additionally, the lack of effect of combined RD and MVE or MVE gases in both models helps to strengthen this unexpected finding. Speculatively, one or more components of the combustion mixture could diminish the pulmonary interactions with the Road Dust particles, such as anti-inflammatory gases like carbon monoxide [136]. In the analysis of aortic pathological outcomes of the 50d Road Dust and MVE gas exposures, we did not see protective effects, but the deleterious interactions seen between MVE gases and other particles (MVE PM, sulfate PM and nitrate PM) were invariably more pronounced than for Road Dust [128].

Serum-induced impairments in vasorelaxation were evident in 4 of the 6 atmospheres tested. Road Dust alone failed to induce any changes, along with Road Dust + $O_3$. Serum obtained from mice exposed to $O_3$ at higher levels (1 ppm) induced substantial diminution of vasorelaxation to acetylcholine in a similar model, a response that did not appear to be dependent on lung inflammation but was dependent on vascular CD36 [110]. MVE PM, however, did lead to the induction of bioactivity in serum that impaired vascular responses to acetylcholine. Both MVE PM and MVE gases caused similar effects on serum in a 50d study, but the relative potency was reversed, with MVE PM eliciting the strongest loss of relaxation [137]. The substitution of a portion of MVE PM with Road Dust PM in the whole MVE led to similar changes in serum bioactivity as MVE PM alone. As recently postulated [128], combining combustion-source gases from fresh emissions with aged or secondary particles may enhance particle toxicity. Furthermore, we have confirmed the clinical relevance of diesel-induced serum bioactivity in human studies, showing not only induction of genes used in the present study (IL-8, ICAM-1, VCAM-1), but also a more complete microarray analysis of the endothelial cell response to plasma post-exposure (Channell *et al*., 2012; Schisler *et al*., 2015). The microarray analysis noted induction of more global inflammatory pathways in the endothelial cells treated with plasma post-diesel exposure, as well as induction of transcription factors previously unassociated with air pollution effects, including FOXO4, FOXF2, and TCF3 (Schisler et al., 2015).

Wood smoke findings are relatively novel and few studies have addressed cardiovascular health effects of biomass combustion. Epidemiological studies related to wildfires are suggestive of a possible cardiovascular effect, but roughly equal numbers of positive and negative findings reflect a high variability of exposures associated with such sporadic natural events [132]. Forchhammer and colleagues observed no adverse effects in exposed human subjects at up to 354 μg PM/$m^3$ wood smoke for 3 hours [138]. Microvascular function assays were conducted 6 h after and blood samples were taken at 0, 6, and 20 hours after exposure for measures of oxidative stress and inflammation, with no obvious changes detected. Unosson and colleagues reported increased arterial stiffness in response to a comparable wood smoke exposure in health human subjects[139], although in a follow-up study in firefighters, wood smoke exposure did not compromise vasodilatory capacity [140]. Utilizing filtrations systems to reduce indoor wood smoke PM levels in participating households in British Columbia, however, significantly improved vascular hyperemic response along with a 30% decrease in circulating C-reactive protein levels [141]. However, controlled wood smoke exposures in mice have not resulted in substantial cardiovascular toxicity [142,143]. Thus, the current findings showing that serum contains some potentially adverse bioactivity suggest that further research may be needed to identify specific factors responsible, and possibly factors that confer vulnerability.

The value of utilizing serum from exposed mice to test the inflammatory potential on endothelial cells lies in the rigor and pertinence of the inhalation methodology. As opposed to treating endothelial cells in vitro with unjustifiably

high concentrations of particulates – with no consideration of co-pollutants – the present approach incorporates true inhalation exposures and then exposes endothelial cells to factors that would definitely be in direct contact with the endothelium *in vivo*. Furthermore, the treatments are at a highly dilute manner, owing to the requisite conditions for cell culture and isolated organ techniques. We do not propose what factor(s) may be responsible for these outcomes, as thousands of biomolecules are present in the serum and the present study is designed to assess the cumulative impact. Furthermore, the subsequent step of extrapolating the present outcomes to whole animal pathophysiology is less clear. We have recently shown that similar serum bioactivity exists in clinical syndromes, such as coronary artery disease, and clinical trials with the polyphenol resveratrol showed that reductions in serum inflammatory potential could be elicited in otherwise healthy human subjects (Cung et al., 2015). Quantitative links between the inflammatory potential in humans and laboratory species, in addition to linkages between short-term endothelial responses and chronic inflammatory diseases simply do not exist at present, owing to the novelty of the approach.

Overall, the findings of the present study reveal a consistent pattern of serum modifications following inhalation exposure to complex pollutants that lead to altered bioactivity. Both outcomes assessed – inflammatory pathways and impaired relaxation – are presumed to be part of a continuum of the early stages leading to atherosclerosis [144]. It was somewhat surprising that there was not more overlap between the pollutant atmospheres and serum-induced outcomes.

The main gap in the present study is a lack of serum compositional characterizations to examine potential candidate molecules to drive the varied effects. However, a thorough investigation, via proteomic or metabolomic approaches, is likely to yield more candidates than can be adequately confirmed in a single study. Future research will need to link complex compositional data sets with functional assay outcomes such as were developed in the present study to better delineate causal components.

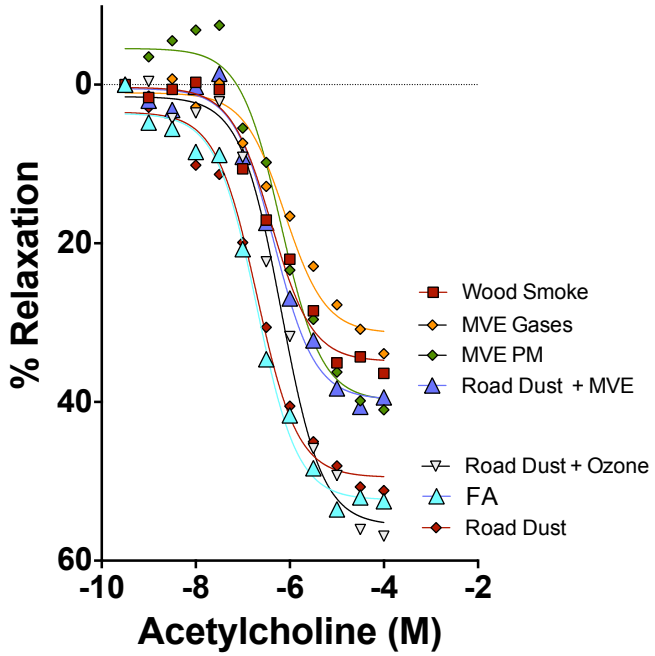


**Figure 2.6 (Supplemental Figure 1): Acetylcholine response curves from Figure 2.4 overlaid to compare the relative magnitudes of impairment.**

Atmospheres that caused any significant diminution of response (wood smoke, MVE PM, MVE Gases, Road Dust + MVE) did not clearly separate, causing approximately the same level of loss of the relaxation response to acetylcholine.

**Compliance with Ethical Standards:** The authors confirm that they have no conflicts of interest, financial or otherwise, with the contents of this manuscript.

Studies were conducted with full approval by the Institutional Animal Care and Use Committees of both the University of New Mexico and Lovelace Respiratory Research Institute.

# 3. MMP-9-Dependent Serum-Borne Bioactivity Caused by Multi-walled Carbon Nanotube Exposure Induces Vascular Dysfunction Via the CD36 Scavenger Receptor

Submitted to Toxicological Sciences October 2015

Mario Aragon[1] (MJAragon@salud.unm.edu), Aaron Erdely[2] (efi4@cdc.gov), Lindsey Bishop[2] (xgl5@cdc.gov), Rebecca Salmen[2] (zvj4@cdc.gov), Jonathon Weaver[1] (JMWeaver@salud.unm.edu), Jim Liu[1] (KLiu@salud.unm.edu), Pamela Hall[1] (PHall@salud.unm.edu), Tracy Eye[2] (tmh7@cdc.gov), Vamsi Kodali[2] (ywu0@cdc.gov), Patti Zeidler-Erdely[2] (paz9@cdc.gov), Jillian E. Stafflinger[3] (jstafflinger@mymail.vcu.edu), Andrew K. Ottens[3] (akottens@vcu.edu), Matthew J. Campen[1] (mcampen@salud.unm.edu)

[1]Department of Pharmaceutical Sciences, University of New Mexico College of Pharmacy, Albuquerque, NM 87131; [2]National Institute for Occupational Safety and Health, Morgantown, WV 26508; [3]Department of Anatomy and Neurobiology, Virginia Commonwealth University School of Medicine, Richmond, VA 23298

**Corresponding Author:** Matthew J. Campen
MSC09 5360
1 University of New Mexico
Albuquerque, NM 87131
505 925-7778
mcampen@salud.unm.edu



## 3.1 ABSTRACT

Inhalation of multi-walled carbon nanotubes (MWCNT) causes systemic effects including vascular inflammation, endothelial dysfunction, and acute phase protein expression. MWCNTs translocate only minimally beyond the lungs, thus cardiovascular effects thereof may be caused by generation of secondary biomolecular factors from MWCNT-pulmonary interactions that spill over into the systemic circulation. Therefore, we hypothesized that induced matrix metalloproteinase-9 (MMP-9) is a generator of factors that, in turn, drive vascular effects through ligand-receptor interactions with the multiligand pattern recognition receptor, CD36. To test this, wildtype (WT; C57BL/6) and MMP-9-/- mice were exposed to varying doses (10 or 40 μg) of MWCNTs (MWCNT-7) via oropharyngeal aspiration and serum was collected at 4 and 24 h post-exposure. Cells treated with serum from MWCNT-7-exposed WT mice exhibited significantly reduced NO generation, as measured by EPR, an effect that was independent of NO scavenging. Serum from MWCNT-7-exposed WT mice inhibited acetylcholine-mediated relaxation of aortic rings at both time points. Absence of CD36 on the aortic rings abolished the serum-induced impairment of

vasorelaxation. MWCNT-7 exposure induced MMP-9 protein levels in both bronchoalveolar lavage and whole lung lysates. Serum from MMP-9-/- mice exposed to MWCNT did not diminish the magnitude of vasorelaxation in naïve WT aortic rings, although a modest right shift of the acetylcholine dose-response curve was observed in both MWCNT-7 dose groups relative to controls. In conclusion, pulmonary exposure to MWCNT-7 leads to elevated MMP-9 levels and MMP-9-dependent generation of circulating bioactivity that promotes endothelial dysfunction and decreased NO bioavailability via interaction with vascular CD36.

## 3.2 INTRODUCTION

Pulmonary exposure to nanomaterials such as carbon nanotubes is associated with the progression of cardiovascular disease [76]. However, gaps exist in our understanding of the pathways by which inhaled substances affect the systemic vasculature, and this hinders our ability to predict risk and identify potentially vulnerable subpopulations. Inhaled nanomaterials, such as multi-walled carbon nanotubes (MWCNTs), have limited ability to translocate into the systemic circulation [125] and evidence for a direct interaction between nanomaterials and vascular cells at relevant exposure concentrations is lacking. Several studies have demonstrated more profound systemic vascular effects arising from particle inhalation [145-147] as compared to gavage or even direct intravenous injection [148,149], suggesting that secondary, circulating factors induced by pulmonary responses to exposure contribute to adverse cardiovascular effects.

Central to the development of cardiovascular disease is the activation of the endothelium, characterized by the increased expression of adhesion molecules, extravasation of leukocytes, and the loss of endothelial nitric oxide synthase (eNOS) function [150]. eNOS produces the diffusible molecule nitric oxide (NO), which is anti-inflammatory, anti-coagulatory, and vasodilatory [20,21,151]. In an atherosclerotic state, eNOS becomes “uncoupled” leading to the loss of NO bioavailability [19]. Loss of NO enhances the pro-inflammatory environment that is central to the progression of atherosclerosis. Mounting evidence suggests that pattern recognition (e.g. TLR4) or scavenger receptors (e.g. CD36) play a

prominent role in mediating endothelial activation [121,152]. Lipid peroxidation products present in the lung lining fluid following exposure to particulate matter (PM) mediate systemic cellular inflammatory responses through Toll-like receptor 4, and such modified lipids have been shown to be present following exposure to concentrated ambient particulate matter [114]. CD36, a class B scavenger receptor, recognizes many ligands and is widely expressed on the surface of multiple cell types, including macrophages and endothelial cells [153,154]. CD36 is involved in atherosclerosis and inflammation [111] and is required for the endothelial dysfunction induced by inhalation to the reactive gas ozone [110].

One potential source of circulating ligands that interact with pattern recognition receptors following inhalation exposure is activation of matrix metalloproteinases (MMPs) in the lung [155]. MMPs have been shown to be involved in a wide range of process including development, wound healing, and host defense [156]. MMP-9, an MMP that binds collagen based substrates, has been shown to be unregulated and activated following exposure to PM and PM-containing combustion mixtures [112,115,155]. Erdely and colleagues reported increased gene expression of MMP-9 in the lung, as well as an increase in circulating MMP-9 as a result of pulmonary MWCNT-7 exposure [75]. The pathophysiological relevance of MMP9 activation following pulmonary exposure to nanomaterials remains unknown.

Currently, no studies exist investigating the potential links between vascular dysfunction, MMPs, CD36, and nanomaterial exposure. We hypothesized that MWCNT-7 exposure activates MMPs in the lung, leading to

the generation of circulating ligands that may directly impact vascular function through the CD36 receptor. To test this hypothesis, we applied an innovative ex vivo methodology for assessing potential cumulative effects of circulating mediators on vascular function. In this study, we demonstrated that MWCNT-7 exposure induces the generation of circulating bioactive factors that diminish stimulated NO production, impair vasorelaxation, and are not linearly associated with MWCNT-7 dose.

## 3.3 MATERIALS AND METHODS

### 3.3.1 Animals

Specific pathogen-free, male C57BL/6J and MMP-9-/- (B6.FVB(Cg)-Mmp9tm1Tvu/J) mice from Jackson Laboratory (Bar Harbor, ME) and CD36-/- mice on a C57BL/6 background, bred in-house, were used in this study. C57BL/6J and MMP9-/- mice for exposures were housed in the AAALAC-approved NIOSH Animal Facility, while naïve mice (C57BL/6J and CD36-/-) donating aortas were housed in AAALAC-approved facilities at the University of New Mexico. All mice were provided food and tap water ad libitum in ventilated cages in a controlled humidity and temperature environment with a 12 hr light/dark cycle. Animal care and use procedures were conducted in accordance with the “PHS Policy on Humane Care and Use of Laboratory Animals” and the “Guide for the Care and Use of Laboratory Animals” (NIH publication 86-23, 1996). These procedures were approved by the respective Institutional Animal

Care and Use Committees of the National Institute for Occupational Safety and Health and the University of New Mexico.

Mice, 8 weeks of age, were treated via oropharyngeal aspiration with MWCNT (MWNCT-7 / Mitsui-7) at 0 μg, 10 μg, or 40 μg (n=12 for each group was needed to generate enough serum for all tests). The MWCNT were prepared in a physiologic dosing media (DM) for the vehicle that consisted of mouse serum albumin (0.6 mg/ml) and 1,2-dipalmitoyl-sn-glycero-3-phosphocholine (10 μg/ml) in PBS. The MWCNT used in this study, MWCNT-7, have been extensively characterized previously [72]. Mice were euthanized at 4 and 24 h following pulmonary exposure. Serum was collected and the left lung lobe was ligated and removed to preserve for MMP-9 protein determinations. Bronchoalveolar lavage was performed on the right lung lobes and the first lavage supernatant was assessed for lactate dehydrogenase activity, albumin concentration, and MMP9 levels.

### 3.4 Fractionation and Mass Spectrometry

Serum was first processed through a 0.1 μm Ultrafree-MC filtration unit (EMDMillipore, Billerica, MA) per manufacturer instructions. The clarified serum (100 μL) was then processed through a pre-cleaned Amicon Ultra-0.5 centrifugal filter with Ultracel-30 membrane (EMDMillipore) per manufacturer instructions at 10°C. Filtered sera (n = 5 per 0, 10, 40 μg MWCNT-7 groups) were prepared for liquid chromatography - tandem mass spectrometry (LC/MSMS). Samples (32 μL) were acidified with 8 μL of 1% formic acid, with 4 μL loaded onto a Symmetry C18 reversed-phase trap column using a NanoAcquity UPLC (Waters, Milford,

MA). Separation was performed with a 150 mm x 75 µm HSS T3 reversed-phase capillary column at 55°C online with a nano-electrospray equipped Synapt G2 HDMS tandem mass spectrometer (Waters). Separation and data-independent mass spectrometric analysis with ion mobility was performed as described previously [157,158] with the modifications that gradient elution was performed from 2% to 42% acetonitrile in water (formic-acid modified) and spectra were collected between 200 and 1800 m/z, with a collision energy ramp from 32 to 52 eV. All spectra were post-processed employing PLGS ion processing software (Waters). Generated ion tables were clustered and aligned by retention time (+/- 1.0 min), drift time (+/- 4 bins) and ion mass (MH+, +/- 12 ppm) using Isoquant software (v1.6 beta) [159,160]. Results were filtered to include only reproducible ion events (observed in four or more biological replicates per group). Ion mass tables per group were then evaluated and compared using histogram analysis with a minimum size of 500 Da.

### 3.4.1 Cell Culture

Mouse cerebrovascular endothelial cells (mCECs) were obtained from a commercial vendor (Cell Biologics) and maintained according to manufacturer's recommendations at 37° and 5% CO2 – 95 O2 with complete endothelial cell medium supplemented with 10% Fetal Bovine Serum (FBS). All experiments were performed between passages 3-8. Assays were batched by exposure to enhance consistency and comparability across samples.

3.4.2 Spin trapping of MCEC-generated NO using electron paramagnetic resonance.

To test the generation of NO, serum from control or MWCNT-7-treated mice (4h post) was added to the mCECs at a ratio of 1:9 (10%) with basal endothelial cell medium. Electron paramagnetic resonance (EPR) spectroscopy was conducted according to previously described methods with some modifications [161]. Following serum treatment, mCECs were incubated with the iron-chelate NO-spin trap Fe2+-di(N-methyl-D-glutaminedithiocarbamate) (Fe2+(MGD)2; 1mM, final concentration) for 5 min. The iron-chelator Fe2+(MGD)2 was freshly prepared by mixing a stock solution of ferrous sulfate (FeSO4; 20 mM, dissolved in deionized water under N2) and an equal volume of sodium N-methyl-D-glucamine dithiocarbamate (NaMGD; 100 mM, dissolved in deionized water under N2) to give a molar ratio of 1:5, respectively, prior to each experiment. Following the incubation period, the incubation medium (400 µL) containing spin trapped NO was immediately transferred into custom-made gas permeable Teflon tubing (Zeus Industries, Raritan, NJ), folded four times, and inserted into a quartz EPR tube open at each end. The quartz EPR tube was inserted within the cavity of a Bruker EleXsys E540 X-band EPR spectrometer (Billerica, MA) operating at 9.8 GHz and 100 kHz field modulation and spectra was recorded after spectrometer tuning at room temperature. The EPR spectrum of spin trapped-NO were acquired from untreated mCECs with a scan time of 40s, and 10 scans were obtained and averaged to produce significant signal-to-noise ratio. EPR measurements from mCECs stimulated with 2 mM ATP to induce NO release were performed under the same conditions. Instrument

settings were as follows: magnetic field, 3440 G; scan range, 100 G; microwave power, 21 mW; modulation frequency, 100 kHz; modulation amplitude, 1.0 G; time constant, 20 ms. The EPR spectra were collected, stored, and manipulated using the Bruker Software Xepr (Billerica, MA). NO levels were quantified and peak-to-peak measurements were taken and expressed in relative units.

mCECs were grown to confluence on six-well plates and incubated with 10% MWCNT exposed serum for 4 h. Following serum treatment, mCECs were incubated with Fe2+(MGD)2. Following application of the trap, a supernatant sample was isolated and NO was measured to assess a baseline reading. NO generation at baseline was negligible. Endothelial cells were subsequently stimulated with 2 mM adenosine triphosphate (ATP) for 5 min, followed by measurement of NO in a second supernatant sample.

### 3.4.3 *Ex vivo* vascular function using myography

Rings from the thoracic aorta were isolated and cleaned of connective tissue. Segments of aorta (2 mm length) were mounted in a 4-chamber myograph (610M; Danish Myo Technology A/S, Aarhus, Denmark). Vessels were submerged in physiological saline solution (composition in millimolar: 119.0 NaCl, 25.0 NaHCO3, 5.5 glucose, 4.7 KCl, 1.2 MgSO4, 1.2 KH2PO4, 0.025 EDTA, 2.5 CaCl2) bubbled at 37°C with 21% O2-5% CO2 balance N2 and left to equilibrate for 30 min. Tension was applied in 2 mN stepwise increments over 30 min to an optimal passive tension of 9 mN. Preliminary experiments showed that this tension produced optimal contraction and relaxation responses. Data from

force transducers were processed by a MacLab/4e A-DI converter displayed through LabChart software (AD Instruments).

Vessel viability was confirmed by a contractile response to the addition of potassium containing physiological salt solution (KPSS in millimolar: 64.9 NaCl, 25.0 $NaHCO_3$, 5.5 glucose, 58.9 KCl, 1.2 $MgSO_4$, 1.2 $KH_2PO_4$, 0.025 EDTA, 2.5 $CaCl_2$) repeated twice. Aortic rings isolated from naïve C57BL/6J or CD36-null mice were mounted in a myograph and challenged twice with KPSS as described above. After a 30-min equilibration period, vessels were incubated with 1% serum that was collected from mice exposed to dispersion media or MWCNT. Because the addition of serum induced contraction of aortic rings, the cumulative concentration-response curves to ACh (10-9-10-4) were acquired only after the response to serum had stabilized.

### 3.4.4 Matrix Metalloproteinase Protein Levels in Lung

Lung lavage fluid and whole lung homogenates were assayed for MMP-2 and MMP-9 protein concentrations according to manufacturer's instructions (Boster, Pleasanton, CA).

### 3.4.5 Statistics

Myographic studies were compared with a two-way analysis of variance considering exposure and acetylcholine concentration as the two factors, and post-hoc comparisons at specific acetylcholine concentrations were conducted using Fisher's least significant difference testing (GraphPad Prism, v 6.0). Other comparisons were conducted with a standard one-way analysis of variance.

## 3.5 RESULTS

### 3.5.1 Multi-walled Carbon Nanotube Exposure results in Lung Cytotoxicity and Permeability Changes

MWCNT-7 used in the present study have been previously characterized [72]. The average diameter was 49 nm with a mean length of 3.86 μm (geometric standard deviation = 1.94; **Figure 3.1A,B**). Purity was >99% carbon. Exposure to MWCNT-7 resulted in a dose-dependent increase in bronchoalveolar lavage (BAL) lactate dehydrogenase (LDH) activity at the 4 h time point, which also remained elevated at the 24 h time point. The 40 μg dose approximately doubled LDH levels compared to controls at both time points, with the 10 μg dose resulting in a 50% increase at both time points (**Figure 3.1C**). There was no significant difference in albumin levels between groups at the 4 h time point; however, both the 10 and 40 μg doses showed elevated albumin at the 24 h time point when compared to controls. (**Figure 3.1D**).

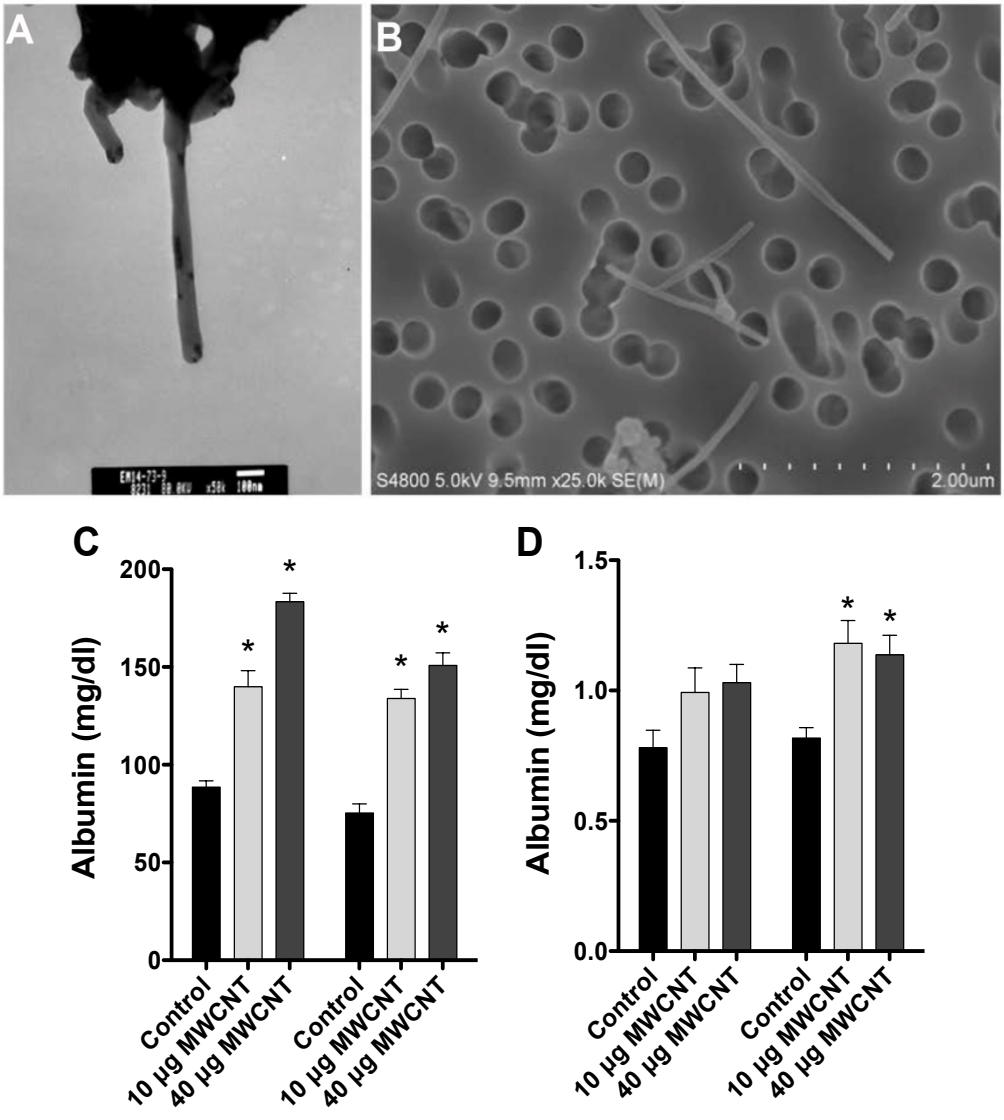


**Figure 3.1**

**A,B.** MWCNT-7 characterization by electron microscopy demonstrates the relative size and adequacy of dispersion. **C,D.** Markers of injury in the lung lavage, LDH and albumin levels, were increased following exposure (*$p<0.05$ vs DM by ANOVA, N=4-8 per group).

### 3.5.2 Serum from MWCNT-Exposed Mice Decreases Endothelial NO Generation In Vitro

The supernatant of serum-treated endothelial cells, when treated with ATP and the NO spin-trap MGD, afforded a strong signal detectable by electron paramagnetic resonance spectroscopy (**Figure 3.2A**). Baseline measurements of unstimulated endothelial cells resulted in negligible amounts of NO production between groups treated with exposed or control serum. In ATP-stimulated cells, however, serum from MWCNT-7-exposed mice decreased NO bioavailability by 30% when compared to cells incubated with serum from DM control mice (**Figure 3.2B**).

These results led us to speculate that the serum from MWCNT-7-exposed mice was able to directly affect eNOS or that the serum had the capacity to "scavenge" produced NO. To address this question we applied an acellular assay, bypassing the contribution of eNOS. MGD in iron-free media was incubated with serum from MWCNT-exposed mice and the NO-donor spermine NONOate (1M) as in previous studies with serum from ozone-exposed rodents [161]. However, serum from MWCNT-7-exposed mice had no effect on NO bioavailability when compared to serum from control mice (**Figure 3.2C**). These results suggested that serum from MWCNT-7-exposed mice diminishes eNOS generation of NO, rather than NO bioavailability.

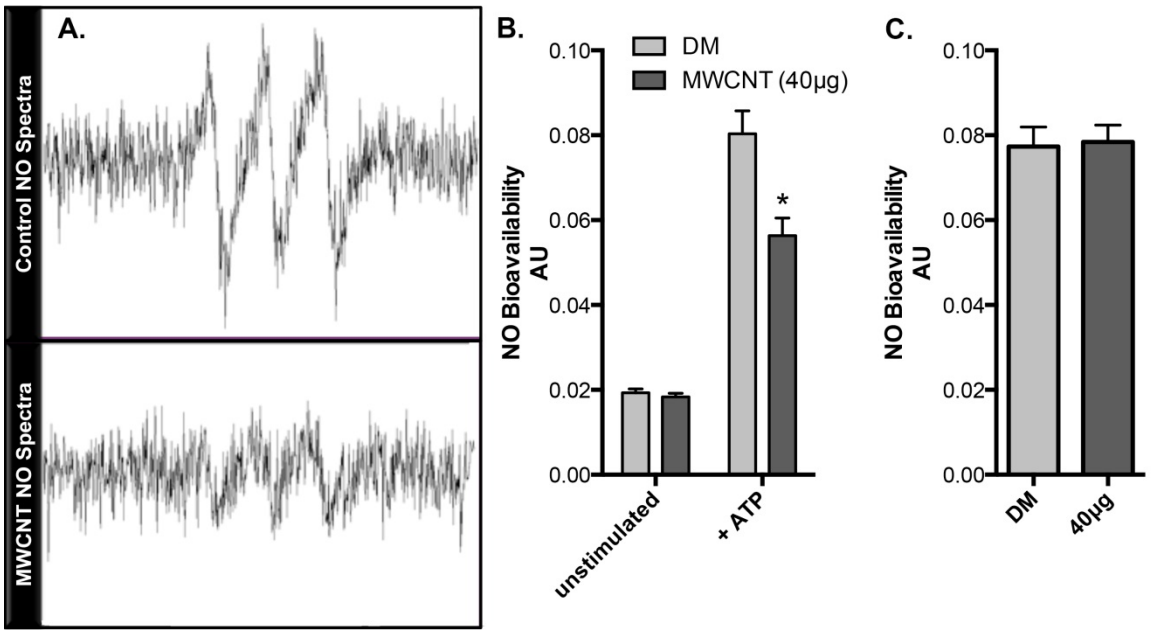


**Figure 3.2 Effects of serum from MWCNT-7-exposed mice on NO generation and bioavailabilty.**

**A.** Representative EPR spectra from endothelial cells incubated with control serum and serum from MWCNT-7-exposed mice. **B.** Unstimulated endothelial cells exhibited minimal baseline levels of detectable NO, which was not different when incubated with serum from DM (control) or MWCNT-7-treated mice. However, when stimulated by ATP, endothelial cells incubated with control serum demonstrated a significantly greater capacity to generate NO than cells treated with serum from MWCNT-7-exposed mice (*$p<0.05$, N=3 per group). **C.** In an acellular assay, levels of NO in iron-free media containing a known concentration of the NO donor, spermine NONOate, were not different in the presence of serum from control or MWCNT-7-treated mice.

### 3.5.3 Serum from MWCNT-7-Exposed Mice Diminishes Vasorelaxation Ex Vivo

We next examined the role that MWCNT exposure might have in a functional physiological system. We employed force-transduction myography with an isolated aortic ring preparation to test the serum bioactivity. Serum from both doses of MWCNT-7-exposed mice was able to significantly reduce acetylcholine (ACh)-induced relaxation (**Figure 3.3**). Interestingly, the serum from 10 µg-treated mice collected 4 h post-exposure (**Figure 3.3A**) was more potent in terms of inhibiting relaxation than was serum from 40 µg-treated mice, with the lower dose reaching a maximum relaxation of only 13.6%, compared to 27.1% for the higher dose and 49.4% for vehicle controls. This effect persisted at least 24 h

post-exposure (**Figure 3.3B**), although more variability was noted. At 24 h post exposure, serum from both low and high dose groups similarly inhibited relaxation (26.9% and 28.5%, respectively), as compared to DM control serum.

In addition to ACh responses, we assessed whether the initial contraction induced by serum treatment was similar between groups. Maximum vessel constriction induced by serum was measured and normalized to a potassium physiological saline solution (KPSS) response. There were no differences between control and MWCNT doses at 4 h with complete serum (**Figure 3A right panel**). However, serum obtained 24 h following MWCNT exposure did induce a modest but significantly higher average constriction in the 40 μg group (101% vs 80% for the low dose and 87% for the control; **Figure 3.3B right panel**).

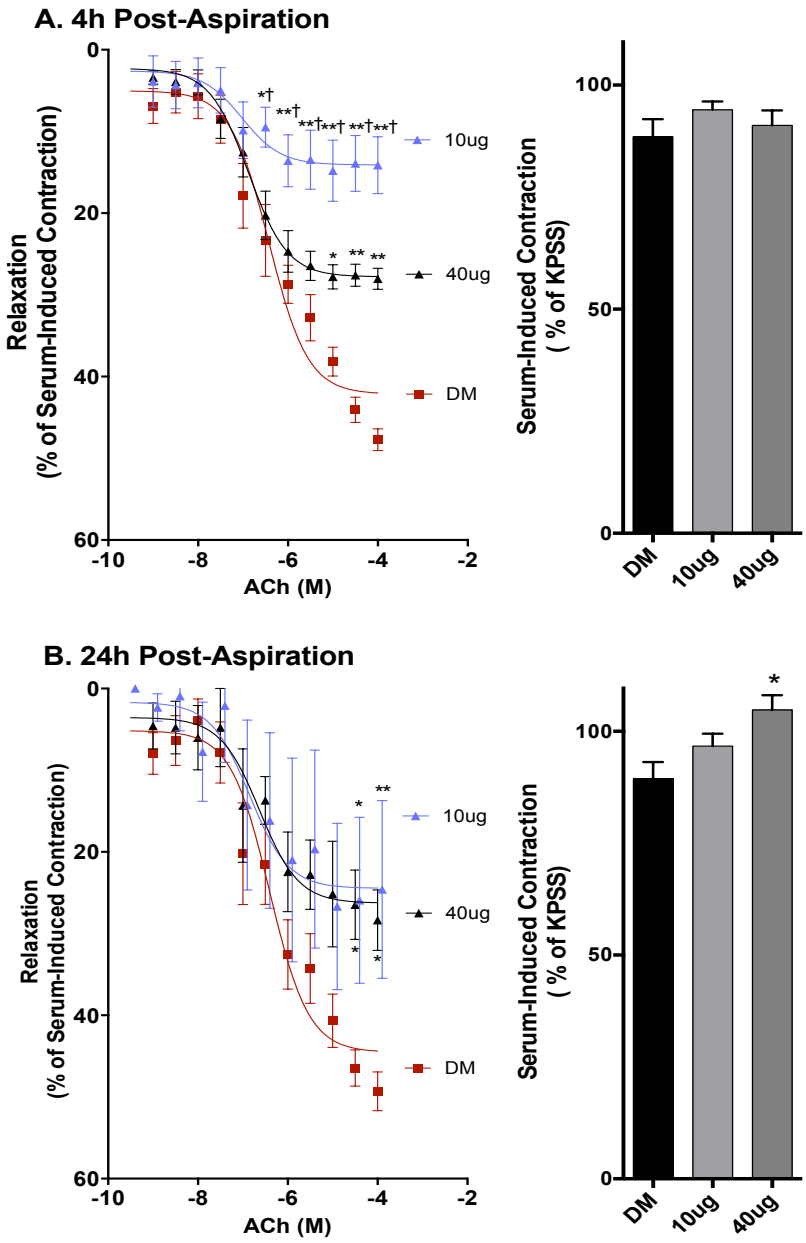


**Figure 3.3**

**A.** Mouse serum obtained 4 h following MWCNT-7 treatment inhibited ACh-mediated vasorelaxation in aortic rings from untreated (naïve) mice (left) and maximum vessel constriction induced by serum (normalized to a KPSS response; right). Interestingly, the serum from low dose-treated mice was more potent than serum from high dose-treated mice. Asterisks indicates significant difference from control by two-way ANOVA with Tukey's multiple comparison test (*p<0.05, **P<0.001), dagger represents significant difference between the 10 and 40 μg doses (†p<0.01; N=10 per group). **B.** Mouse serum obtained 24 h following MWCNT-7 treatment inhibited ACh-mediated vasorelaxation in aortic rings from untreated (naïve) mice (left), however the increased potency of the low dose exposure at 4 h was no longer observed. Maximum vessel constriction induced by serum (normalized to a KPSS response) is also shown (right of each relaxation curve). *Indicates significant difference from DM control by two-way ANOVA (*p<0.05, **P<0.01; N=6–8 per group).

### 3.5.4 Impact of Serum Fractionation on Vasorelaxation Responses

As an initial attempt to understand how serum bioactivity is driven by altered biochemistry and to exclude a direct nanomaterial effect on vasorelaxation, the serum was filtered to resolve smaller components (< 10 kDa) for aortic ring treatments. Notably, the filtered serum allowed for greater overall relaxation to ACh compared to whole serum, with an average relaxation of 77.39% for aortic rings incubated with filtered serum from DM-treated mice. In the 4 h post-exposure samples, the <10 kDa biomolecules induced a prominent anti-relaxation effect of serum from both doses of MWCNT-7-exposed mice, although the specific enhanced potency of the 10 μg dose was no longer observed (Figure 3.4A). The anti-relaxant effect of filtered serum components from MWCNT-7-treated mice was largely abolished in the 24 h post-exposure serum (**Figure 4B**), suggesting that the <10 kDa biomolecules may have complexed with larger biomolecules or that larger biomolecules contribute to a persistent effect. There were no differences in initial contraction between control and MWCNT doses with 4 h filtered serum (removal of large, >10 kD proteins), or with 24 h filtered serum (**Figure 3.4A,B right panels**, respectively).

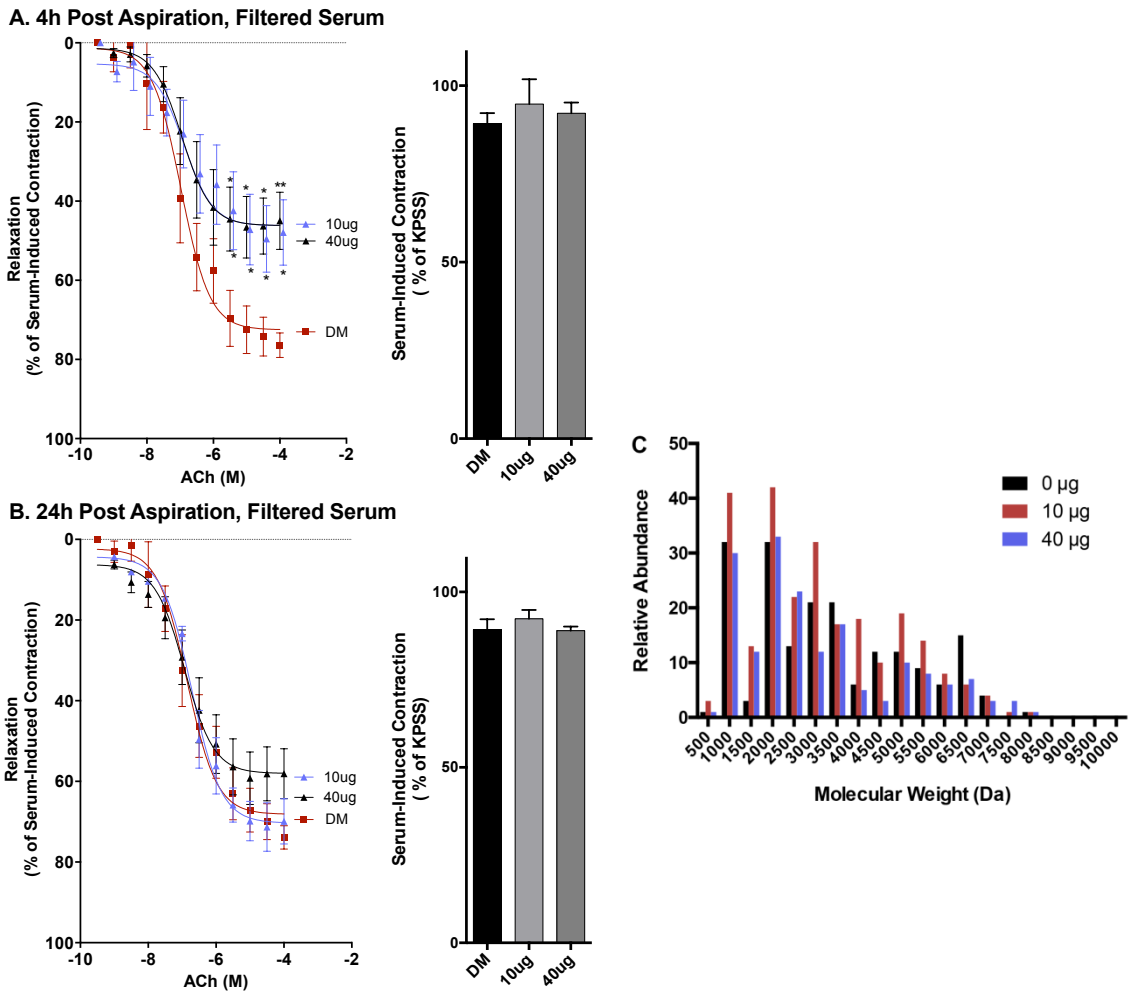


**Figure 3.4**

**A.** Mouse serum obtained 4 h following MWCNT-7 treatment was filtered to remove all larger proteins, leaving only biomolecules < 10 kD. This filtered serum still inhibited ACh-mediated vasorelaxation in aortic rings from untreated (naïve) mice. Asterisks indicate significant difference from control by two-way ANOVA with Tukey's multiple comparison test (*p<0.05, **p<0.01; N=5 per group). **B.** Filtered mouse serum obtained 24h following MWCNT-7 treatment did not affect ACh-mediated vasorelaxation in aortic rings from untreated mice (N=5 per group). **C.** Mass spectroscopic confirmation of numerous biomolecules ranging from 0.5 – 10 kDa remaining after filtration. Individual peaks are collected into bins of the histogram and separated by dose group for the 4 h post-treatment serum.

We employed LC/MSMS analysis to confirm that the serum fraction consisted of biomolecules below 10 kDa (**Figure 3.4C**). Further, in comparing the < 10 kDa serum fraction between treatment groups, we resolved differences in the mass distribution among doses, consistent with the observations of

nonlinear dose effects. Importantly, findings with filtered sera demonstrate that bioactivity can be induced without any possibility of direct nanomaterial or leukocyte interaction with the endothelium.

### 3.5.5 Vascular CD36 Mediates Endothelial Dysfunction Induced by Serum from MWCNT-7-Exposed Mice

Aortas harvested from CD36-null mice were employed to determine if the scavenger-receptor mediated effects of serum from MWCNT-7-exposed mice were similar to previous findings with ozone and ambient PM [110,113]. CD36-null aortic relaxation in response to ACh was not impacted by serum from MWCNT-7-exposed mice compared to serum from control mice (**Figure 3.5**). All three groups reached an average maximum relaxation of ~50% (comparable to WT vessels), with no discernible differences between the groups at either time point. These results denote that the bioactive compounds in the serum following MWCNT-7 exposure interact with CD36 to impair vasorelaxation.

Interestingly, however, serum from MWCNT-7-exposed mice applied to CD36-/- vessels was observed to induce a greater average contraction of 100% for the lower and 104% for the higher dose group at the 4 h mark compared to aortic rings treated with control serum (87%; **Figure 3.5A right panel**). By 24 h, the high dose group achieved a contraction of 101%, while the low dose was not different from controls (Figure 3.5B right panel). These findings contrast with the vasorelaxation data in that CD36 is not required to induce contraction due to MWCNT-induced, serum-borne components.

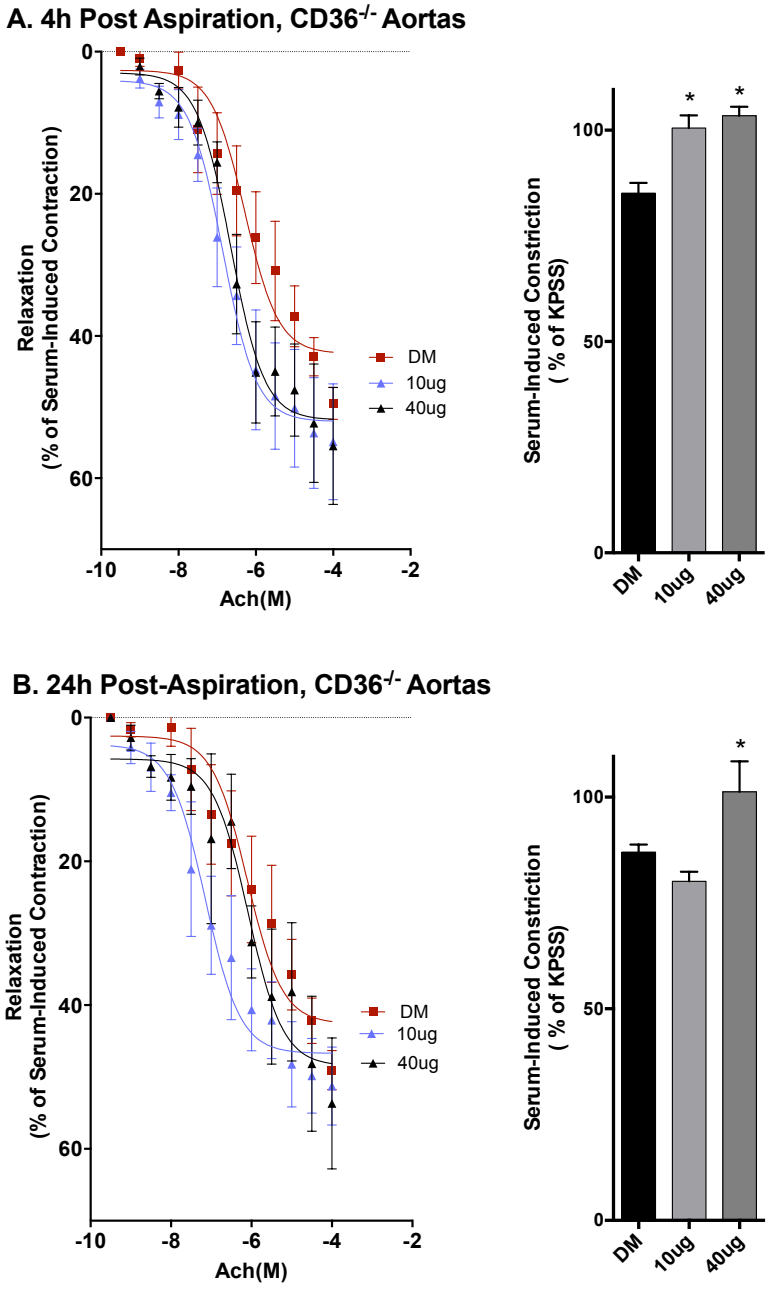


**Figure 3.5**

**A.** Mouse serum obtained 4 h following MWCNT-7 treatment had no effect on ACh-mediated vasorelaxation in aortic rings from untreated CD36-null mice (N=5 per group). Significant differences in the contractile response to the serum addition was noted for serum from MWCNT-7-treated mice. Asterisks indicate significant difference from control by ANOVA with Dunnett's multiple comparison test (*p<0.05; n=5 per group). **B.** Filtered mouse serum obtained 24 h following MWCNT-7 treatment had no effect on ACh-mediated vasorelaxation in aortic rings from untreated CD36-null mice (N=4–5 per group). Significant differences in the contractile response to the serum addition was noted for serum from the 40 µg MWCNT-7-treated mice. Asterisks indicate significant difference from control by ANOVA with Dunnett's multiple comparison test (*p<0.05; n=5 per group).

### 3.5.6 Serum from MMP-9 Deficient Mice Exhibits Reduced Vascular Bioactivity after MWCNT-7 Exposure

Lastly, we investigated the potential role of MMP-9 as a source of circulating ligands that are generated as a result of MWCNT-7 exposure. MMP-9 levels in WT mice treated with 10 and 40 μg MWCNT-7 were measured in the lung and BAL at the protein level. MMP-9 was up regulated in the BAL at both 10 and 40 μg doses at 4h, and in the 40 μg dose at 24h (**Figure 3.6A and B**). MMP-9 was also significantly upregulated in the lung lysate in the 40 μg dose at 24h (**Figure 3.6D**). In contrast, MMP-2 protein levels were unchanged in the lung lavage (Supplemental Figure 1).

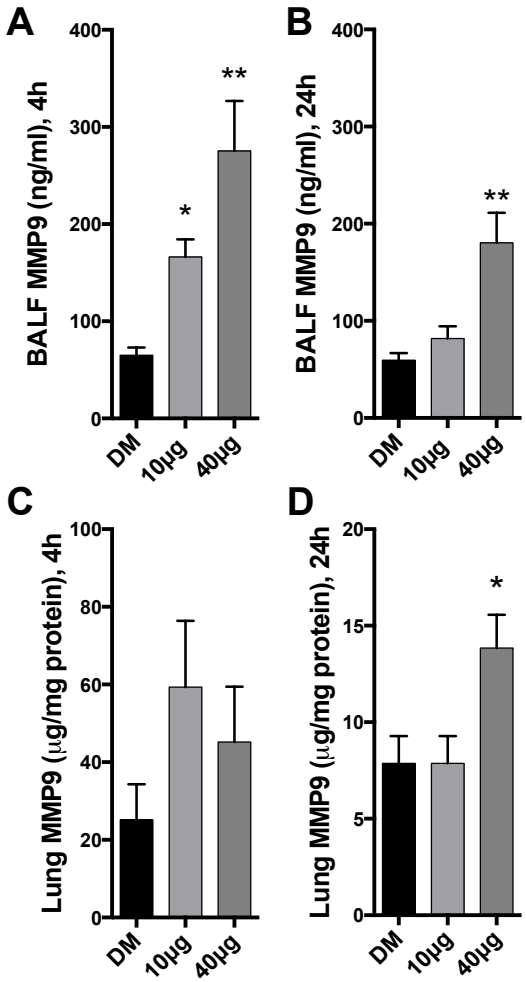


**Figure 3.6: MMP-9 protein levels in bronchoalveolar lavage**

(**A**,**B**) and whole lung lysates (**C**,**D**) from MWCNT-7-exposed mice. Asterisks indicate significant difference from control by ANOVA with Dunnett's multiple comparison test (*p<0.05; **p<0.01).

Building on the finding of MWCNT-7-induced pulmonary MMP-9 expression, MMP-9-/- mice were exposed to MWCNT-7 and the bioactivity of the serum was tested for its ability to affect eNOS mediated vasorelaxation ex vivo. Deficiency of MMP-9 (**Figure 3.7**) appeared fully protective relative to WT outcomes (**Figure 3.3**). Pulmonary MWCNT-7 cytotoxicity, as measured by LDH activity in the BALF, was similar between both WT and MMP9-/- mice (**Figure**

**3.7A**). In both dose groups, WT vessels treated with serum from MMP-9-/- mice achieved similar maximal relaxation compared with serum from DM-treated MMP-9-/- mice, with an average response of ~55% (**Figure 3.7B**). However, the dose-response curve revealed a significant right-shift in both dose groups relative to DM-control serum, which suggests that some residual bioactivity may be derived outside of MMP-9 activity. DM-control serum from the MMP-9-/- mice was actually more permissive of vasorelaxation that WT serum in this ex vivo assay, which further adds to the conjecture that MMP-9-derived degradation products may impair vascular function (Supplemental Figure 2). Serum-mediated constriction (**Figure 3.7C**) was unaltered between exposure groups in the MMP-9-/- animals. Collective maximal vasorelaxation outcomes for each permutation at the 4-h time point clearly show that pulmonary MWCNT-7 exposure leads to bioactivity in the serum that impairs vasorelaxation in a manner dependent on MMP-9 to generate the signal and CD36 to respond (Supplemental Figure 3).

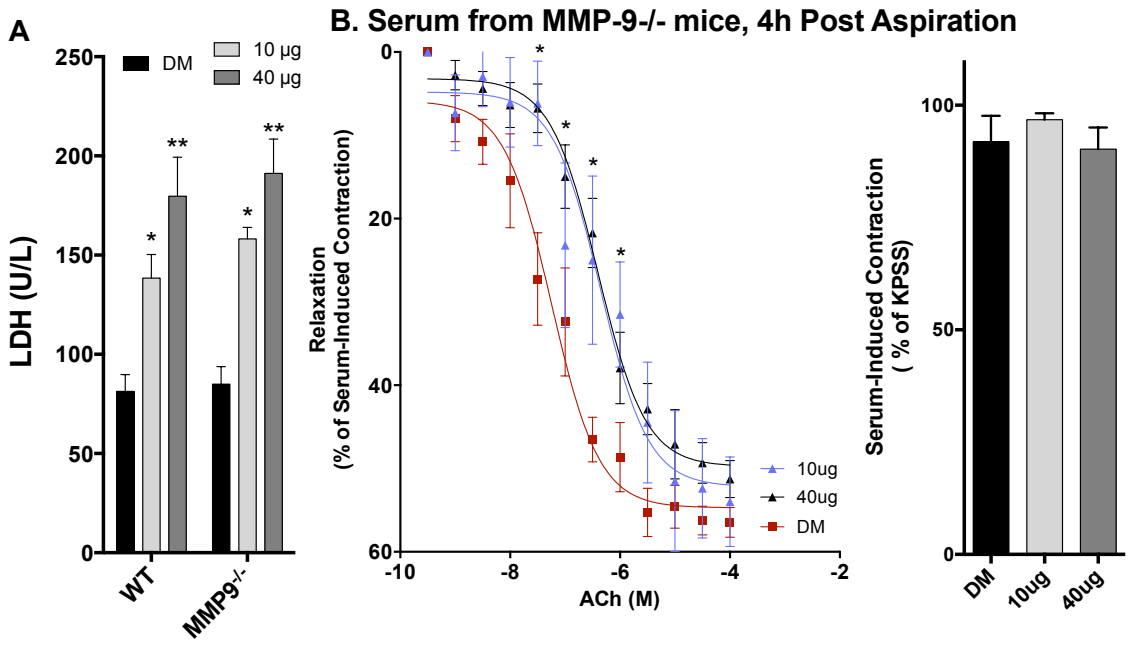


**Figure 3.7**

**A.** MMP-9$^{-/-}$ mice exhibit similar degree of lung injury at 4 h post MWCNT-7 aspiration, as measured by LDH from the BALF. Asterisks indicate significant difference from control by two-way ANOVA with Tukey's multiple comparison test (*p<0.01; **p<0.001). **B.** Serum from MMP-9$^{-/-}$ mice treated with 10 or 40 µg MWCNT-7 caused a modest right-shift effect on the concentration response to ACh-mediated vasorelaxation in WT vessels, compared to serum from the DM control mice, but did not reduce the overall magnitude of relaxation. Serum from the various groups exhibited a consistent contractile effect on all aortas. Asterisks indicate significant difference from control by two-way ANOVA with Tukey's multiple comparison test (*p<0.05; n=5-6 per group).

## 3.6 DISCUSSION

In this study we provide functional evidence for a mechanism by which MWCNT-7 exerts systemic endothelial dysfunction, which appears to be indirectly mediated by serum-borne components. Pulmonary exposure to MWCNT-7 led to the generation of bioactive factors in the serum that significantly impaired vascular function ex vivo. Furthermore, the principal components of the serum that confer abnormal vasorelaxation act through the vascular CD36 scavenger receptor and appear, at least acutely (4 h), to involve smaller biomolecules (<10 kDa) released into circulation. The effects of MWCNT-7-

induced serum biomolecules were not linearly associated with lung burden and may reflect induction of different biological responses at different doses. Within this study, we outline a plausible pathway by which ligands are derived from MMP-9 activity in the lung, access the circulation and interact with vascular CD36 receptors to reduced vasorelaxation. This overarching paradigm provides concrete mechanistic detail to theories of pulmonary "spillover" that explain the pathogenesis of extrapulmonary effects of inhaled particulates [30,162], although the biological complexity with potentially numerous metalloproteinases and pattern recognition receptors involved must be considered. Importantly, the observed vascular effects with serum from mice exposed to MWCNT-7 by a pulmonary route resolves issues inherent to direct-application nanomaterial research with cells or organs, offering an alternative and more anatomically sound approach to study mechanisms underlying the extrapulmonary toxicity of inhaled particulates.

The mechanism by which serum from MWCNT-7-exposed mice exerts its effects on vascular relaxation presumably involves impairment of eNOS and NO generation. Inhalation of pollutants such as diesel emissions can lead to uncoupling of eNOS and similar loss of dilatory function [163,164]. Nurkiewicz et al. found that TiO2 nanoparticles could directly scavenge NO [146], an effect that was eliminated in the presence of antioxidants. We recently observed that serum from ozone-exposed rats exhibited diminished serum levels of nitrites and nitrates, and there was some evidence for increased nitrosothiol formation in serum, suggesting that NO scavenging may occur [161]. In the present study, however, serum from MWCNT-7-exposed mice inhibited aortic vasorelaxation and

endothelial cell generation of NO, but did not scavenge spermine NONOate-donated NO. The outcomes from cell culture and isolated aortic rings suggest that a ligand-receptor interaction, and resultant intracellular signaling, mediated a loss of eNOS activity and diminished vasorelaxation.

One potential mechanism to explain how serum from MWCNT-7-exposed mice could impair eNOS is through the generation of CD36-interacting ligands [165]. Specific ligands to CD36 can adversely affect the lipid composition of caveole, interfering with eNOS and potentially causing eNOS to become uncoupled [121,166,167]. The present data, combined with recent studies of ozone-induced endothelial dysfunction [110], implicate an important role for CD36 in mediating the loss of aortic vasorelaxation caused by serum from MWCNT-7-treated mice. Notably, vessel relaxation in CD36-null aortas was more robust than in WT aortas when treated with control serum. CD36 has been implicated as a key inflammatory mediator in response to particulate matter exposure, an important component of the macrophage response to oxidized lipids [113] and thus may have broader implications for extrapulmonary effects than just endothelial dysfunction.

We propose that an additional crucial step required for the induction of eNOS-compromising bioactivity in serum from MWCNT-7-exposed mice involves the activation of pulmonary MMP-9, leading to the generation of protein fragments that can effect biological activity. MMP-9 plays a major role in the degradation of extracellular matrix in a large spectrum of physiological and pathophysiological process [118]. MMP-9 is secreted by a wide number of cell

types including neutrophils, macrophages and fibroblasts, creating the potential for a large amount of MMP-9 to be generated as a result of lung injury. Exposures to gasoline engine emissions in mice led to system-wide changes in MMP-9 concentrations and activity, including induction within atherosclerotic plaques [112]. Furthermore, serum MMP-9 was found to be elevated in both mice and humans exposed to diesel emissions [112]. Pulmonary MMP-9 expression has also been associated with vanadium [168], a vanadium-laden particulate [155] and metal fume [169] exposures. Few studies have examined the pathophysiological implications of MMP-9 activity in mediating pulmonary or extrapulmonary outcomes of inhaled particulates. Our study found that despite comparable acute (4-h) lung injury from MWCNT-7 exposure in WT and MMP-9-/- mice, MMP-9 deficiency resulted in diminished serum bioactivity after MWCNT-7 treatment compared to WT. Interestingly, serum from MMP-9 deficient mice treated with vehicle allowed for greater relaxation in aortic rings than did WT serum. MMP-9 has been shown to generate numerous vasoactive by-products from the degradation of extracellular matrix proteins, such as angiostatin [170,171], tumstatin [172], and β-dystroglycan [173]. MMP-9 may therefore be responsible for the generation of a number of vasoactive agents that help set baseline vascular tone.

Our study highlights the importance of pulmonary nanoparticle delivery in driving systemic vascular effects and the doses used in this study, based on numerous dosimetry analyses, represent an extreme but plausible scenario . It should be appreciated that more pronounced effects were achieved at lower depositions and a 1:100 dilution of serum from exposed mice nearly abolished

vascular relaxation. Mice have a blood volume of approximately 2 mL, depending on their body weight. Even if all of the MWCNT-7 left the lungs and stayed in the bloodstream – a gross exaggeration – the MWCNT-7 concentration in serum would be approximately 5 μg/mL, which would then be further diluted in the vascular bath to a maximal theoretical (yet still improbably high) concentration of 50 ng/mL, a concentration far below what has been reported to induce endothelial cell toxicity in vitro. The rationale for this extreme estimation of dose lies in how pulmonary exposure to particulates leads to a clear systemic vascular toxicity that cannot be reproduced with direct exposures of particles to the vessels. Furthermore, filtration of serum which would exclude molecules >10 kDa and certainly any trace of MWCNT-7, did not entirely abrogate vascular effects. Studies employing an oral gavage of carbon black were unable to induce substantial vascular dysfunction in rats [148], and studies using an intravenous injection of diesel exhaust particles, at similar concentrations to the current MWCNT-7 doses, in mice were unable to induce vascular dysfunction [174]. The lack of biological effect in these alternate exposure routes serves to highlight the importance of the pulmonary exposure in the pathogenesis of vascular outcomes.

In conclusion, serum obtained from mice exposed to MWCNT-7 has the capacity to impair vasorelaxation in naïve aortic rings ex vivo, an effect that persisted at least 24 h after exposure. Notably, the low dose of 10 μg induced even greater serum bioactivity at the 4-h time point than did the 40 μg dose. Results from the present study further highlight the role of smaller, <10 kDa

biomolecules, in addition to larger species, which appear to be generated by MMP-9 and may collectively act through the scavenger receptor CD36 to reduce responsiveness to ACh. These data further support the concept that pulmonary reactions lead to a spillover of secondary mediators from the lungs into the systemic circulation. Future work will need to further elucidate, via fractionation studies, which portions/components of the serum exhibit biological activity, as well as peptide sequencing to provide further insight into the enzymatic origins of the circulating peptides. Additionally, the use of serum from exposed mice in ex vivo assays offers a novel, more anatomically sophisticated and even translational approach for studying the systemic impact of inhaled substances.

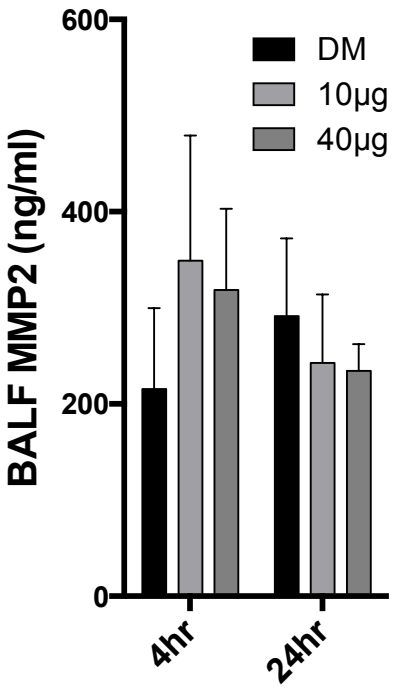


**Figure 3.8 (Supplemental Figure 1): BALF MMP2 levels were not altered by MWCNT-7 exposure.**

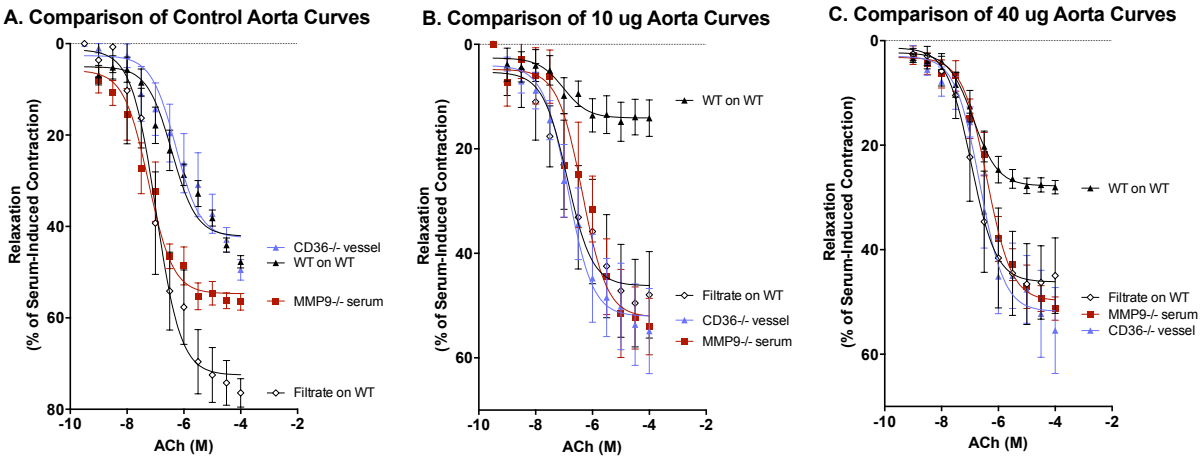


**Figure 3.9 (Supplemental Figure 2): Plotting acetylcholine relaxation curves for all DM, 10, and 40 µg groups at 4 h.**

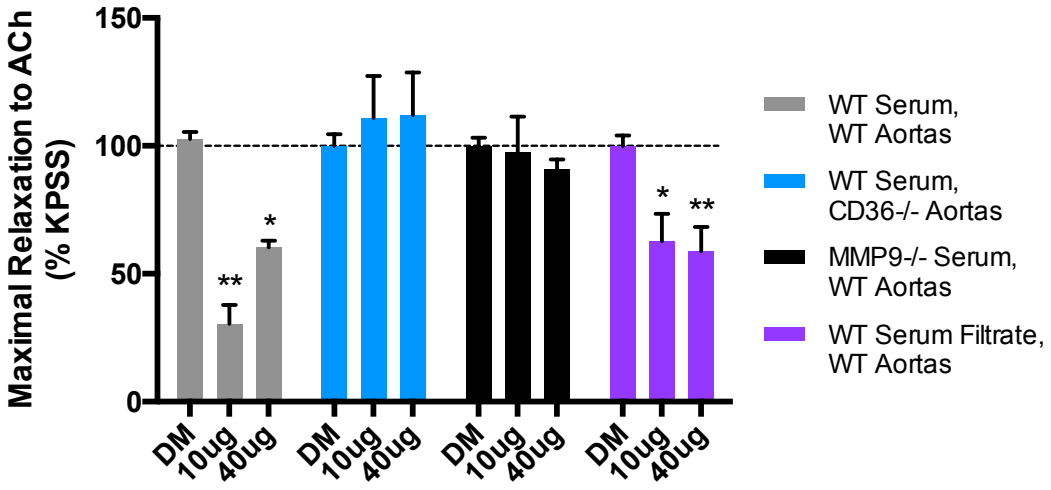


**Figure 3.10 (Supplemental Figure 3): Maximal ACh-induced relaxation for each group at 4 h, normalized to each control group.**

**Abbreviations**

ACh: Acetylcholine

BAL: Bronchoalveolar lavage

LDH: lactate dehydrogenase

CD36: Cluster of Differentiation 36

MWCNT: Multi-walled carbon nanotubes

ATP: Adenosine Triphosphate

NO: Nitric Oxide

eNOS: Endothelial Nitric Oxide Synthase

PM: Particulate Matter

mCECs: Mouse Cerebrovascular Endothelial Cells

FBS: Fetal Bovine Serum

EPR: Electron Paramagnetic Resonance

MGD: N-methyl-D-glutamindithiocarbamate

KPSS: Potassium Physiological Saline Solution

MMP: Matrix Metalloproteinase

Competing Interests

The authors declare that they have no competing interests.

**Authors Contributions**

MA conducted most facets of the study and data analysis and wrote the manuscript.

AE, along with RS, TE, LB, VK, and PZ-E, supported the overall study concept, exposed animals, analyzed parameters of pulmonary toxicity, and harvested serum samples.

JW developed and conducted EPR assays and assisted with writing.

AKO consulted on study design, provided fractionated serum, and conducted the LC/MS characterizations.

PH consulted on the study design, analysis of outcomes and provided CD36-null mice.

MJC designed the study, oversaw much of the conduct and analysis of data, and obtained funding, along with AE, for the project.

**Acknowledgements**

This study was funded by grants from the National Institute of Environmental Health Sciences (R01 ES014639), National Institute for Occupational Safety and Health (R21 OH010495; NTRC, 939ZXFL and 927ZKGW), National Heart Lung and Blood Institute (T32 HL007736) and the National Institutes of Health Center of Biomedical Research Excellence (P30GM103400). AKO thanks S. Tenzer from U. Mainz for customized beta release of Isoquant software for ion alignment of unidentified ions. AE thanks Diane Schwegler-Berry for the electron microscopy images of the MWCNT-7.

# 4. Serum-Borne Bioactivity Caused by Inhaled Multiwalled Carbon Nanotube Exposure Induces Neuroinflammation Via Increased Blood Brain Barrier Permeability

*In Preparation*

Mario Aragon (MJAragon@salud.unm.edu)[1], Lauren Topper (ltopper@unm.edu)[1], Bethany Sanchez (bsanchez@unm.edu)[1], Katherine Zychowski, Guy Herbert (gherbert@unm.edu)[1], Pamela Hall (Phall@unm.edu)[1], Aaron Erdely (efi4@cdc.gov)[2], Tracy Eye (tmh7@cdc.gov)[2], Patti Zeidler-Erdely (paz9@cdc.gov)[2], Jillian E. Stafflinger (jstafflinger@mymail.vcu.edu)[3], Andrew K. Ottens (akottens@vcu.edu)[3], Matthew J. Campen (mcampen@unm.edu)[1]

[1]Department of Pharmaceutical Sciences, University of New Mexico College of Pharmacy, Albuquerque, New Mexico 87131; [2]National Institute for Occupational Safety and Health, Morgantown, WV 26508; [3]Virginia Commonwealth University, Richmond, VA

**Corresponding Author:** Matthew J. Campen

MSC09 5360

1 University of New Mexico

Albuquerque, NM 87131

505 925-7778

mcampen@salud.unm.edu

**Running Header:** MWCNT-Induced BBB Dysfunction and Neuroinflammation

## 4.1 ABSTRACT

Multi-walled carbon nanotubes (MWCNT) are highly desired by manufacturers due to their mechanical properties, conductivity, and ability to withstand a high degree of functionalization. Previous studies have shown MWCNT exposure can cause cardiovascular effects such as systemic inflammation and acute phase protein expression. However, the mechanism for this, as well as potential inflammatory effects in other organs, such as the brain, is not yet known. MWCNTs translocate only minimally from the lungs into the systemic circulation. Therefore, their cardiovascular effects are most likely mediated by generation of circulating factors that spill over into the systemic circulation. It is possible that these factors can weaken blood brain barrier integrity. To test this, mice were exposed to varying doses (10 or 40 μg) of MWCNTs (Mitsui-7) via pharyngeal aspiration. Serum was collected at 4 and 24 h post-exposure, and applied to primary endothelial cells. Following exposure mice experienced massive pulmonary inflammation, characterized by increased gene expression of systemic pro-inflammatory cytokines. Systemic effects were also observed, categorized by increased expression of acute phase liver enzymes and immunohistochemical analysis of cerebellar and hippocampal regions noted enhanced GFAP staining, indicative of astrocyte activation in MWCNT-exposed mice. MWCNT exposure impaired blood brain barrier integrity, as noted by fluorescein uptake, which was associated with increased gene expression of IL-6 and CCL5 in the cortex and hippocampus. Pretreatment with the rho kinase inhibitor fasudil was able to prevent brain fluorescein uptake and neuroinflammation. Serum from MWCNT-7 exposed mice was able to induce

expression of adhesion molecules at both the gene and protein level in primary murine cerebrovascular endothelial cells. Treatment of endothelial cells with serum from MWCNT-7-exposed mice in a wound-healing assay resulted in decreased cell motility and cytokinesis, also consistent with mRNA expression patterns in microarray analysis. In conclusion, pulmonary exposure to MWCNT-7 alters circulating factors, which promotes endothelial cell inflammation, decreases in cellular tight junctions, and activation of inflammatory cells in the brain.

## 4.2 INTRODUCTION

Nanotechnology represents a broad interdisciplinary field of research and industrial activity involving particles less than 100 nanometers (nm) in at least one dimension. Nanoparticles are currently being incorporated into products in diverse fields of manufacturing; however, as a result of their unique size, nanoparticles exhibit novel physical, chemical, and biological effects in the body[46]. A subset of nanomaterials, multi-walled carbon nanotubes (MWCNT), has become increasingly desired due to the range of unique properties they exhibit. These properties include its conductivity, tensile strength, and ability to withstand a high degree of chemical manipulation[175,176]. As a result, hundreds of

tons of MWCNTs are manufactured every year, increasing the likelihood of occupational exposure in the manufacturing process[177-179].

Multiple studies demonstrate that inhalation of MWCNTs induces lung inflammation, indicated by infiltration of inflammatory cells from the periphery, increased lung permeability, and fibrosis[180]. The literature provides evidence of the systemic effects of MWCNTs[75,181], but their ability to translocate into the systemic circulation[182] is minimal. The inability of MWCNTs to translocate from the lung into the systemic circulation suggests a secondary mechanism through which MWCNTs induce systemic toxicity. Previously our lab has shown that pulmonary interactions can generate bioactive factors that spillover into the systemic circulation and dissipate throughout the body[109,110]. One consequence of these circulating factors is activation of the endothelium, characterized by the expression of adhesion molecules, extravasation of leukocytes, and activation of circulating inflammatory cells[19]. This combination of factors produces an inflammatory state in the wall of the blood vessel, a process central to the development of atherosclerosis. The nature and outcome of these effects is dependent on the vascular bed where the inflammation occurs and can include the aorta, mesentery, or cerebrovascular vessels.

Inflammation in the cerebrovascular vessels has been shown to increase permeability of the blood brain barrier (BBB)[183], a specialized structure composed of astrocytes, pericytes and endothelial cells that acts as a barrier between the brain and the rest of the body. Under normal conditions, the BBB prevents passage of undesired molecules from the bloodstream into the central

nervous system (CNS). However, under inflammatory conditions[184], the tight junctions between the endothelial cells can become destabilized resulting in a leaky BBB and allowing peripheral inflammatory molecules to invade the CNS and activate the brain's resident immune cells, specifically microglia[185] and astrocytes.

Presently there are few studies investigating the link between inhaled toxicants and neuroinflammation. Oppenheim and colleagues found that inhalation of mixed vehicle emissions was able to induce BBB permeability, as well as increase levels of inducible Nitric Oxide Synthase (iNOS) and IL-1β in the parenchyma[112]. Additionally, ozone exposure in rats has been associated with lipid peroxidation in the hippocampus[186]. To our knowledge, no studies currently exist exploring the role of engineered nanomaterials in induction of neuroinflammation or BBB permeability.

We hypothesize that, following MWCNT exposure, neuroinflammation arises due to increased BBB permeability caused by circulating factors. In this study, we demonstrate that MWCNT exposure induces the generation of circulating bioactive factors, leading to activation of the cerebrovasculature and inflammatory cells, as well as increased BBB permeability.

## 4.3 METHODS

### 4.3.1 Animals and Exposures

Specific pathogen-free, male C57BL/6J mice from Jackson Laboratory (Bar Harbor, ME) were used in this study. All mice housed in the AAALAC-approved NIOSH or University of New Mexico animal facility were provided food and tap water *ad libitum* in ventilated cages in a controlled humidity and temperature environment with a 12hr light/dark cycle. Animal care and use procedures were conducted in accordance with the "PHS Policy on Humane Care and Use of Laboratory Animals" and the "Guide for the Care and Use of Laboratory Animals" (NIH publication 86-23, 1996). These procedures were approved by the Institutional Animal Care and Use Committees of the University of New Mexico and the National Institute for Occupational Safety and Health.

C57BL/6J mice, 8 weeks of age, were treated with MWCNT (MWCNT-7) at 0, 10 μg, or 40 μg (n=12 for each group was needed to generate enough serum for all tests). The MWCNT were prepared in a dispersion media (DM) which served as the vehicle control. The DM consisted of mouse serum albumin (0.6 mg/ml) and 1,2-dipalmitoyl-sn-glycero-3-phosphocholine (DPPC; 10μ/ml). The MWCNT used in this study, MWCNT-7, have been extensively characterized previously [72,187]. The average diameter was 49 nm with a length of 3.86 μm (GSD 1.94). Purity was >99% carbon. Mice were euthanized at 4 and 24 h following pulmonary exposure. Serum was collected, and liver and the left lung lobe was removed and frozen to determine changes in relative mRNA expression.

4.3.2 Blood Brain Barrier Permeability

Animals were injected with 2% fluorescein sodium salt (Sigma-Aldrich F6377-100g, lot # MKBR1855V) 1 hour prior to sacrifice. Animals were transcardially perfused with ice cold saline prior to removal and dissection of the brain. Animals received Fasudil HCl (Selleckchem Catalog # S1573) formulated at 20mg/kg 2 hours before sacrifice.

4.3.3 Fluorescein Quantification

Brains were weighed and homogenized in 500µl of 50% Trichloroacetic acid. Following homogenization, supernatants were neutralized with 400µl of 5M Sodium Hydroxide. Neutralized homogenate was spun down for 10 minutes at 10,000g to pellet the tissue. A 200µl sample was placed in a 96 well optical bottom plate (Nagle Nunc International lot # 1019415) and read at 525/440nm in a spectrofluorophotometer.

4.3.4 Immunohistochemistry

Four animals from each group were anesthetized with isoflurane and transcardially perfused with saline followed by ice cold paraformaldehyde (PFA, 4% in PBS, pH 7.4). Brains were removed by decapitation, placed overnight in 4% PFA at 4°C, and then transferred to a 30% sucrose solution for ~48 hours at 4°C. Following cryoprotection, samples were rinsed with PBS and frozen in optimal cutting temperature compound. 16 µm sagittal sections were collected on a cryostat, dried, and stored at -20°C until use.

Sections were blocked and permeabilized with a PBS solution containing 1% bovine serum albumin, 5% goat serum, and 0.2% Triton X-100 for two hours at room temperature (RT). Primary antibodies were applied overnight at 4°C and were either rabbit anti-glial fibrillary acidic protein (GFAP, 1:500, Dako, Z0334) to label astrocytes, or rabbit anti-platelet endothelial cell adhesion molecule (PECAM-1, 1:100, Santa Cruz Biotechnology, sc-1506-R) to visualize cerebral blood vessels. The secondary antibody used was a donkey anti-rabbit Alexa Fluor 555 (1:1000, Life Technologies, A31572) and was applied for 2 hours at RT. All sections were stained with 4',6-diamidino-2-phenylindole (DAPI, 1:1000, Life Technologies, D3571) to label cell nuclei.

Imaging was performed by a blinded researcher on a Nikon TE2000 microscope with a nuance spectral camera (Quorum, model #N-MSI-FX) in the University of New Mexico Fluorescence Microscopy Shared Resource Center. Astrocytes were imaged in the hippocampus and cerebellar regions at 20X, and GFAP intensity was quantified as a marker of astrocyte activation using ImageJ software (NIH). In the cerebellum, three separate images were taken randomly throughout lobule regions and GFAP intensity was averaged. Cerebellar vasculature and fluorescein permeation were visualized using a 40X objective oil immersion lens.

4.3.5 Tissue relative mRNA expression:

RNA was isolated from frozen lung (left lobe) and liver using the RNeasy Mini Kit (Qiagen, Valencia, CA, USA). Evaluation of gene expression was

determined by standard 96-well technology using the StepOne™ (Applied Biosystems, Carlsbad, CA, USA) with pre-designed Assays-on-Demand™ TaqMan® probes and primers (Applied Biosystems). For lung *Il6* (Mn00446190_m1), *Ccl2* (Mn00441242_m1), and *Cxcl2* (Mn00436450_m1) were measured. For liver *Mt1* (Mn00496660_g1), *Mt2* (Mn00809556_s1), *Saa1* (Mn00656927_g1), *Hp* (Mn00516884_m1), and *Apcs* (Mn00488099_g1) were measured. Using 96 well plates, one µg of total RNA was reverse transcribed using random hexamers (Applied Biosystems) and Superscript III (Invitrogen, Carlsbad, CA). Nine µl of cDNA (1/10) was then used for gene expression determination. Hypoxanthine-guanine phosphoribosyltransferase was used as an internal reference. Relative gene expression was calculated using the comparative threshold method ($2^{-\Delta\Delta Ct}$) with vehicle-treated mice serving as the reference group[135].

4.3.6 Biometric analysis.

Sample: Labeled cRNA, from an input RNA of 375 ng, was prepared according to the manufacturer's protocol, using the illumina TotalPrep RNA Amplification Kit (Ambion, Catalog #IL1791) for hybridization to the arrays. The labeled cRNA samples were then assessed for quality and quantity. To ensure consistency for the array hybridization, all cRNA samples for each time point were quantified at the same time. The illumina RatRef-12 beadchip contains 22,523 probes and allows twelve samples to be interrogated in parallel. After a 20 h hybridization period at 58°C, the beadchips were scanned using an illumina BeadStation 500G - BeadArray Reader (Illumina, Inc., San Diego, CA, USA).

4.3.7 Microarray Analysis

Preparation of RNA. Total RNA was extracted and purified with Qiagen RNeasy kit from each sample (Qiagen, Valencia, CA). The total RNA concentrations were measured using the NanoDrop ND-1000 (ThermoScientific, Wilmington, DE), and RNA integrity was checked using Agilent 2100Bioanalyzer to assure sufficient quality before proceeding with microarray hybridization.

Microarray hybridization. Affymetrix GeneChip Mouse 430 2.0 arrays were used for gene expression analysis. All procedures were performed according to the manufactures instructions (Affymetrix, Santa Clara, CA). Briefly, 1.0μg of total RNA was used to generate double-stranded complementary DNA (cDNA) using an oligo dT-primer containing the T7 RNA polymerase promoter site and One-Cycle Target Labeling Kit (Affymetrix). cDNA was purified via column purifications using the GeneChip Sample Cleanup Module (Affymetrix), and biotinylated complementary RNA (cRNA) was synthesized by in vitro transcription using the GeneChip IVT Labeling Kit (Affymetrix). Biotin-labeled cRNA was purified and absorbance measured at 260 nm to determine yield (NanoDrop). Twenty micrograms of the labeled cRNA was fragmented and hybridized to the Affymetrix GeneChip Mouse 430 2.0 arrays for 16 h at 45_C following the Affymetrix protocol specific to the array type. Washing and staining were performed on the Affymetrix Fluidics 450 station according to the antibody amplification protocol (EukGE-Ws2v%;Fluidics Script). The GeneChips were scanned using the Affymetrix GeneChip Scanner 3000.

Statistical analysis procedures for whole microarray datasets have been extensively described. Briefly, samples were imported into illumina® Beadstudio 3.0.19.0 and reference, hybridization control, stringency and negative control genes were checked for proper chip detection. Beadarray expression data were then exported with mean fluorescent intensity across like beads and bead variance estimates into flat files for subsequent analysis. Illumina BeadArray expression data were analyzed in Bioconductor using the 'lumi' and 'limma' packages. Gene lists containing group means of expression, p-values and standard fold changes were utilized as input for subsequent bioinformatics analysis. The Downstream Effects Analysis were generated through the use of Ingenuity Pathway Analysis (Ingenuity® Systems, www.ingenuity.com). Whole datasets containing gene identifiers and corresponding expression values were uploaded into the application and a core analysis was done. Each identifier was mapped to its corresponding object in Ingenuity's Knowledge Base. In this study the following analysis criteria were utilized: log ratio of 0.5 and $p<0.01$. We have previously shown that a 1.1-1.3 fold change offered a reasonable number of molecules to evaluate responses (Erdely et al., 2014 – Type I interferon paper in P&FT). The log ratio of 0.5 used in this study corresponds to a 1.4 fold change. The differentially expressed genes were evaluated by the Downstream Effects Analysis which enables a visualization of biological trends in the dataset and predict the effect of gene expression changes on biological processes and disease or on toxicological functions. The analysis identifies functions that are expected to increase or decrease, given the observed gene expression changes.

The Downstream Effects Analysis is based on expected causal effects between genes and functions; the expected causal effects are derived from the literature compiled in the Ingenuity® Knowledge Base.

4.3.8 Serum-treated MCECs.

For the volume limited MWCNT exposure samples, exposed serum was added to the wells at a ratio of 1:9 (10%) with basal endothelial cell medium. Exposed serum was added in a similar manner from dispersion media controls in a 1:9 (10%). There was no FBS when exposed serum was mixed with basal endothelial cell medium. All treatments were done for 4 hours.

4.3.9 Cell Culture.

Mouse Cerebrovascular Endothelial Cells (MCECs) were obtained from a commercial vendor (Cell Biologics) and maintained according to manufactures recommendations at 37° and 5% $CO_2$ – 95% $O_2$ with complete endothelial cell medium supplemented with 10% Fetal Bovine Serum (FBS). All experiments were performed between passages 3-8. Upon final plating, approximately $2*10^4$ cells were added to each well of a 24-well plate (Beckon Dickinson) and grown to confluence to mimic the cell-cell environment found in the vasculature. Cells were serum starved for 12 hours prior to treatment with serum. Assays were batched by exposure to enhance consistency and comparability across samples.

4.3.10 RNA purification and quantitative PCR.

Following serum treatment, MCECs were washed with phosphate buffered saline (PBS), lysed, and collected for RNA purification. Total RNA was isolated

using RNeasy Mini Prep Kits (Qiagen) and RNA was reverse transcribed using High Capacity Reverse Transcriptase kits (Applied Biosystems, lot #-1307187) prior to quantitative real-time assessment of endothelial markers. Amplification of target message was performed in TaqMan Universal Master Mix following manufacturer's recommended conditions with TaqMan gene expression assays for TBP(Applied Biosystems Mm00446973), VCAM-1 (Applied Biosystems Mm01320970), eNOS (Applied Biosystems Mm00435217).

4.3.11 Flow Cytometry for Cell Surface Markers.

Following serum treatment, MCECs were washed with PBS, trypsonized, and collected in 12x75mm culture tubes (VWR). MCECs were then incubated with primary antibody for either VCAM-1 (BD Biosciences, Lot #-2117560, FITC conjugate) or ICAM-1 (BD Biosciences, Lot #-25775, PE conjugate), washed 3x with PBS, and suspended in 3% BSA. Samples were read on a BD Biosciences LSRFortessa.

4.3.12 Cell Migration Assay

MCECs were plated on 8-well chamber slides and allowed to come to confluence. Cells were then scratched with a p200 pipette tip and washed with PBS before exposed serum was applied to the cells. Chambers were then placed in a live cell imaging system (Olympus) and a digital image was taken every 15 minutes for 6 hours. Cell area was quantified with ImageJ and plotted over time.

## 4.4 RESULTS

### 4.4.1 Pulmonary Delivery of MWCNT Drives Lung and Systemic Transcriptional Responses

Representative transmission and scanning electron microscopy images of the MWCNT demonstrates the relative size and adequacy of dispersion (**Figure 4.1**). Following exposure to MWCNT multiple markers of inflammation were increased 10-15 fold in the lungs including systemic pro-inflammatory markers *Il6* and *Ccl2*, as well as *Cxcl2*; a chemokine secreted by macrophages that acts as a chemoattractant for neutrophils and stem cells (**Figure 4.1**). These effects persisted at 24 h in a primarily dose dependent manner.

Following exposure there was a 40-80 fold increase of liver enzyme gene expression, indicative of an acute inflammatory phase response. All responses were dose dependent with the 40μg dose eliciting a particularly strong response (**Figure 4.1**). Responses were elevated at both time points, however by the 24hr mark expression levels had significantly decreased when compared to 4hrs.

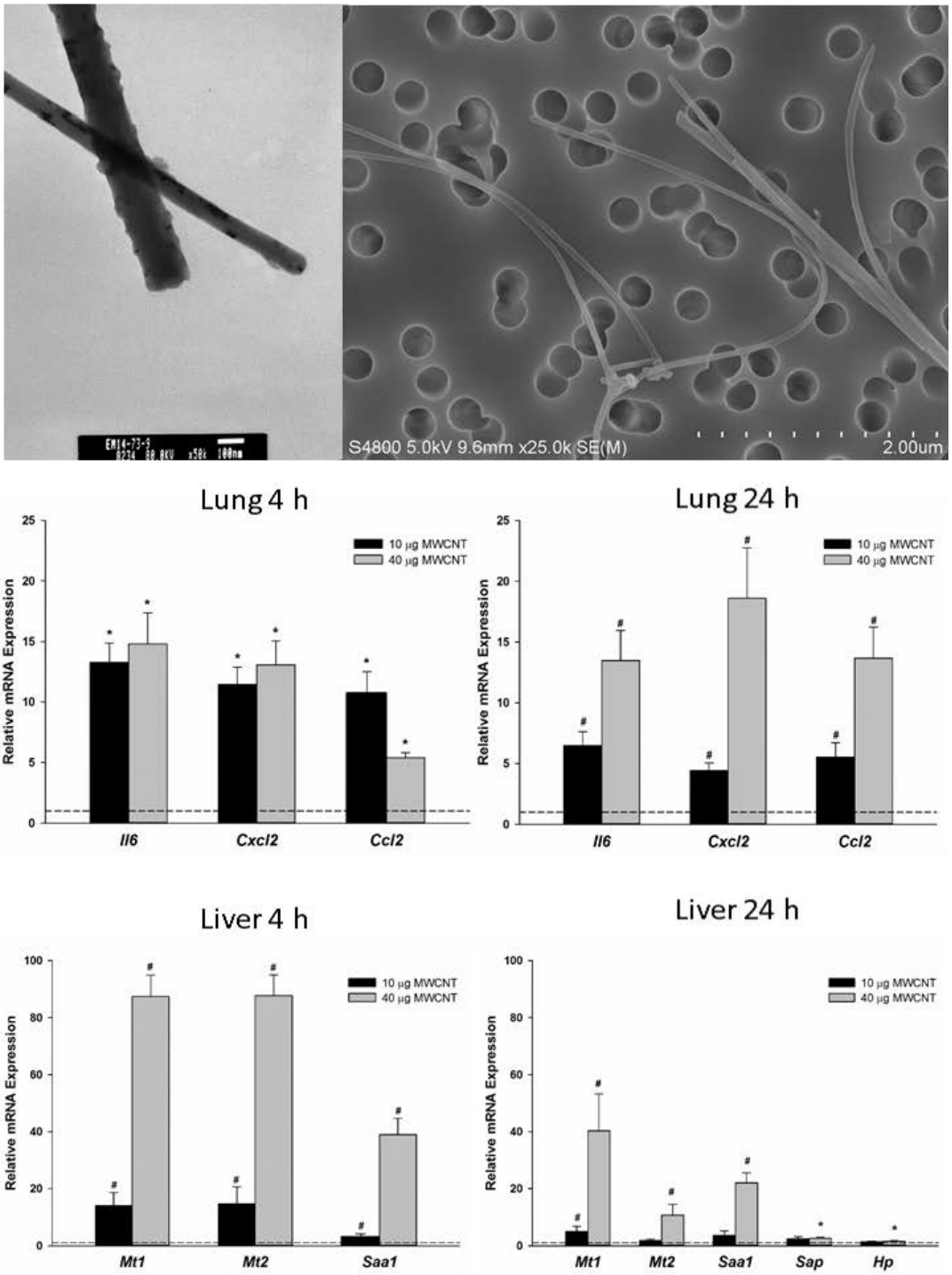


**Figure 4.1: MWCNT characterization by electron microscopy demonstrates the relative size and adequacy of dispersion.**

Markers of injury in the lung and liver were increased following exposure. ($^{\#}p<0.05$ vs all groups; *p<0.05 vs DM, N=6 per group).

### 4.4.2 Evidence of BBB Disruption and Neuroinflammation Following MWCNT Exposure

Immunohistochemistry of the cerebellum and hippocampus in mice 4h post-exposure to MWCNT revealed elevated GFAP staining, indicative of activated astrocytes, compared with DM-exposed control mice (**Figure 4.2**). Microglia were present, as indicated by IBA-1 staining, but were morphologically inactive (Supplemental figure 1). PECAM labeling of blood vessels identified fluorescein leaking in the animals that had been exposed to MWCNTs compared to DM-exposed controls. (**Figure 4.2**)

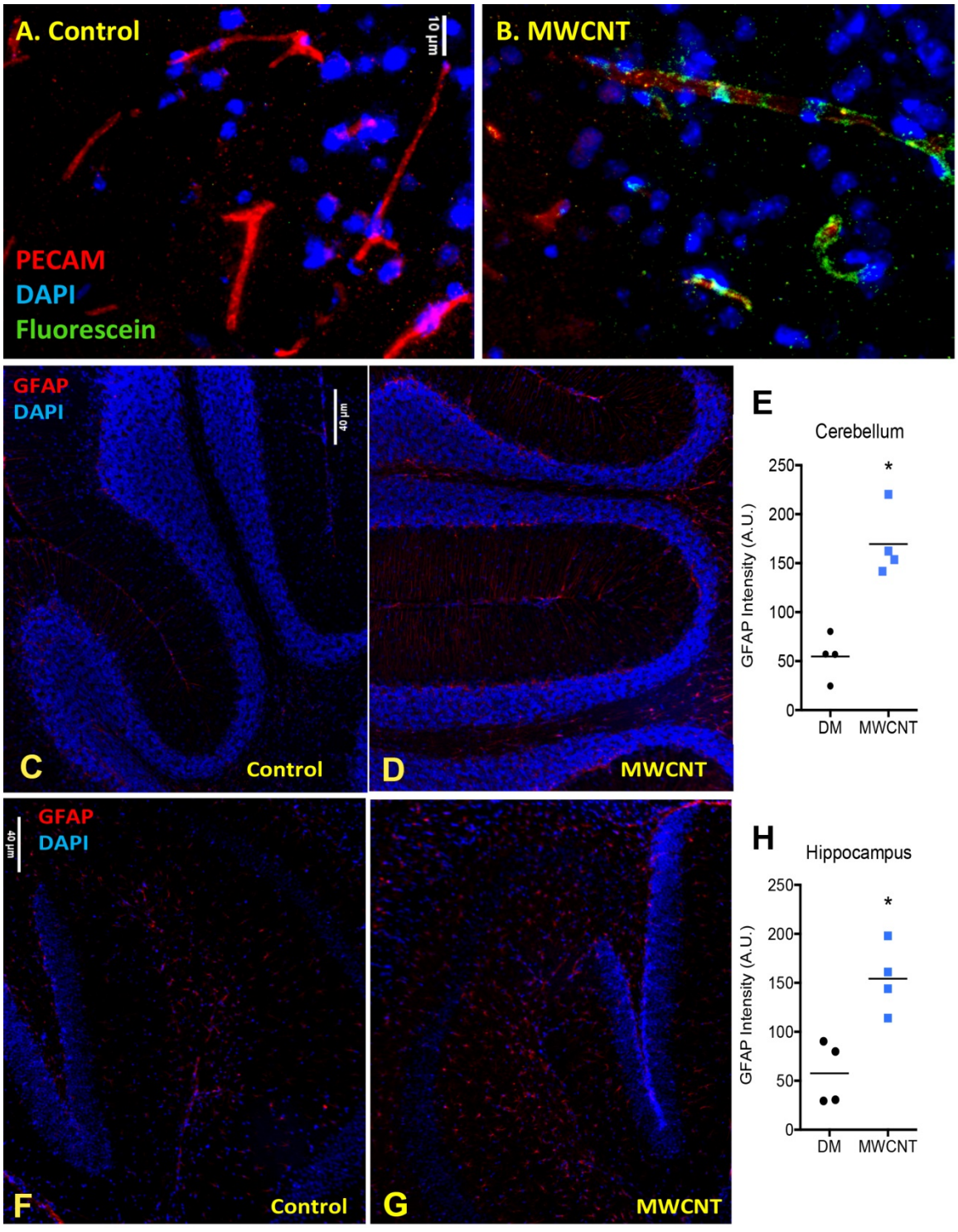


**Figure 4.2: MWCNT (10 ug) exposure acutely induces inflammatory responses in the brain.**

Figures **A-B**, fluorescein in the brain of exposed mice versus vehicle controls. Figures **C-H** visualization and quantification of astrocyte activation in the cerebellum and hippocampus. * indicates a p value of <0.05 by students t test.

4.4.3 Dependence of MWCNT-Induced Neuroinflammation on BBB Disruption

To specifically delineate whether the neuroinflammation was the result of loss of BBB integrity, mice were administered vehicle or the rho kinase inhibitor fasudil, which has been shown to improve BBB function and improve outcomes in stroke-related models [188,189]. Mice received fasudil either 2h after MWCNT aspiration, but before injection of the BBB tracer sodium fluorescein, or prior to MWCNT and again 2 hours later. The former permutation was designed to see if fluorescein uptake in the brain could be inhibited after exposure and neuroinflammation had occurred. The latter permutation was to prevent BBB disruption throughout the time course to test whether neuroinflammatory changes still occurred in the absence of BBB disruption.

Fluorescein uptake in the brain was significantly enhanced 4h after exposure to MWCNT (**Figure 4.3**). This pulmonary exposure was associated with increased Il6 and CcL5 mRNA expression in cortical regions, and increased CcL5 mRNA in the hippocampus (**Figure 4.3**). Treatment with fasudil at 2h post-exposure completely blocked fluorescein uptake in the brain, but had no effect on brain inflammatory outcomes.

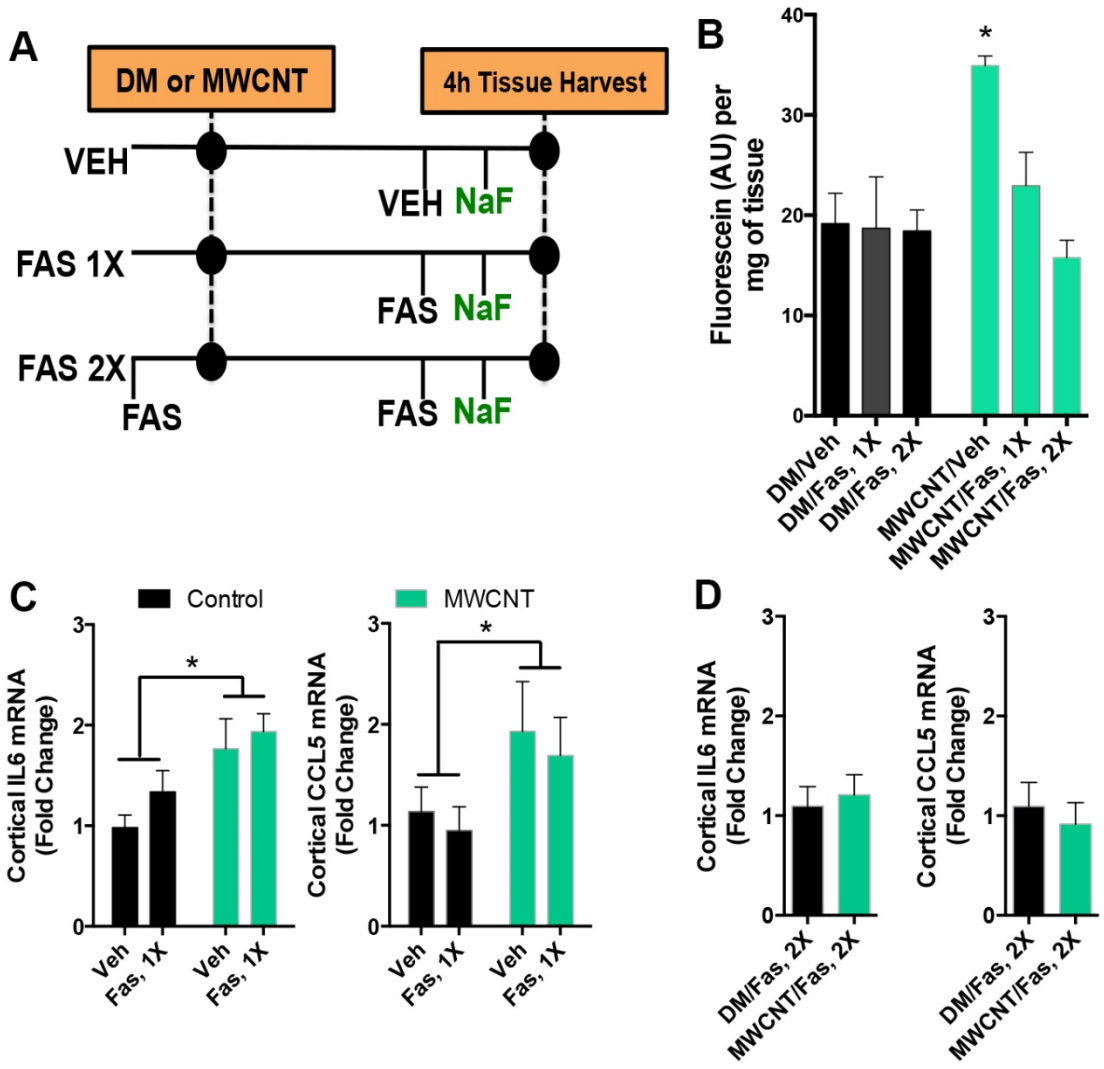


**Figure 4.3: MWCNT-induced neuroinflammatory responses are dependent on BBB disruption.**

**A**. General study design, incorporating a single (1X) fasudil treatment after MWCNT to reduce brain fluorescein uptake and a preventative (2X) fasudil treatment to prevent MWCNT-induced BBB disruption throughout the 4h timecourse. **B**. Fluorescein uptake in brains 4h following MWCNT aspiration with vehicle, 1X or 2X fasudil treatment. Asterisk indicates significant difference from control by ANOVA ($P<0.05$). **C**. Inflammatory markers IL-6, CCL5 mRNA in the cortex 4h following DM or MWCNT aspiration. Asterisks indicate a significant effect of MWCNT compared to control in a 2-way ANOVA ($P<0.05$) with no influence of the single post-MWCNT fasudil treatment. **D**. Preventative (2X) fasudil administration abrogated inflammatory marker mRNA expression (IL-6, CCL5) in the cortex.

4.4.4 Dependence of MWCNT induced Neuroinflammation dependent on BBB disruption

CD36 is a class II scavenger receptor involved in a wide range processes including fatty acid metabolism[190], heart disease, and atherosclerosis[191]. CD36$^{-/-}$ mice showed no increases in fluorescein or pro-inflammatory gene expression in the cortex or hippocampus 4h following 10µg MWCNT aspiration. **(Figure 4.4)**

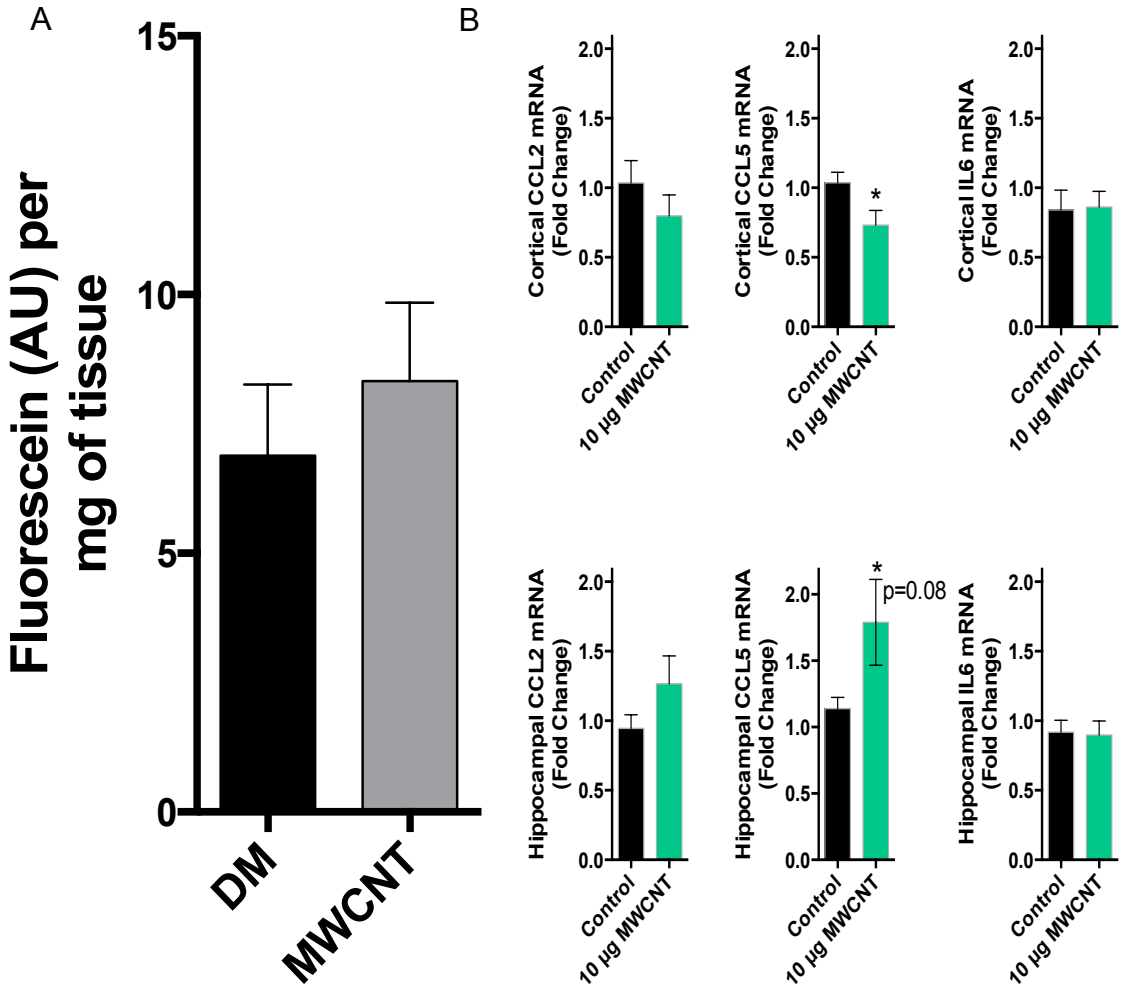


**Figure 4.4: CD36 mice are largely protected from the BBB disruption and neuroinflammatory effects of pulmonary MWCNT exposure.**

**A.** Fluorescein uptake in the brain of CD36$^{-/-}$ mice 4h following treatment with DM or MWCNT. **B.** Neuroinflammatory markers in the cortex and hippocampus of CD36$^{-/-}$.

4.4.5 Bioactivity of MWCNT-Induced, Serum-Borne Factors: Endothelial Inflammatory Responses

Microarray analysis was performed on mRNA isolated from endothelial cells after they had been treated with serum collected from MWCNT-exposed serum. The results of the microarray revealed induced disease or functional categories associated with inflammation, immune response, and chemoattraction / recruitment of leukocytes. The effect was more prominent in endothelial cells challenged with serum collected from mice exposed to 40 μg MWCNT. (**Figure 4.5**).

Application of 10% serum from MWCNT-treated mice on primary murine cerebrovascular endothelial cells for 4h resulted in a 50% increase in vascular cell adhesion molecule-1 (Vcam-1) and approximately 3-fold increases in relative mRNA expression of C-C motif ligand-2 (Ccl-2) and C-C motif ligand-5 (Ccl-5) pro-inflammatory cytokines in the 40μg dose at the 4hr time point (**Figure 4.5A-C**). The 10μg caused slight increases in Ccl-2 and Ccl-5, but was not statistically significant.

Similarly, treatment of primary murine cerebrovascular endothelial cells with serum from MWCNT-treated mice elicited small, but significant up-regulation of both VCAM-1 and intercellular adhesion molecule-1 (ICAM-1) on the cell surface, as assessed by flow cytometry (**Figure 4.5D,E**). By 24hrs the effects had returned to baseline. These data taken in conjunction with the gene expression are consistent with activation of the endothelium via canonical NFkB intracellular signaling pathways.

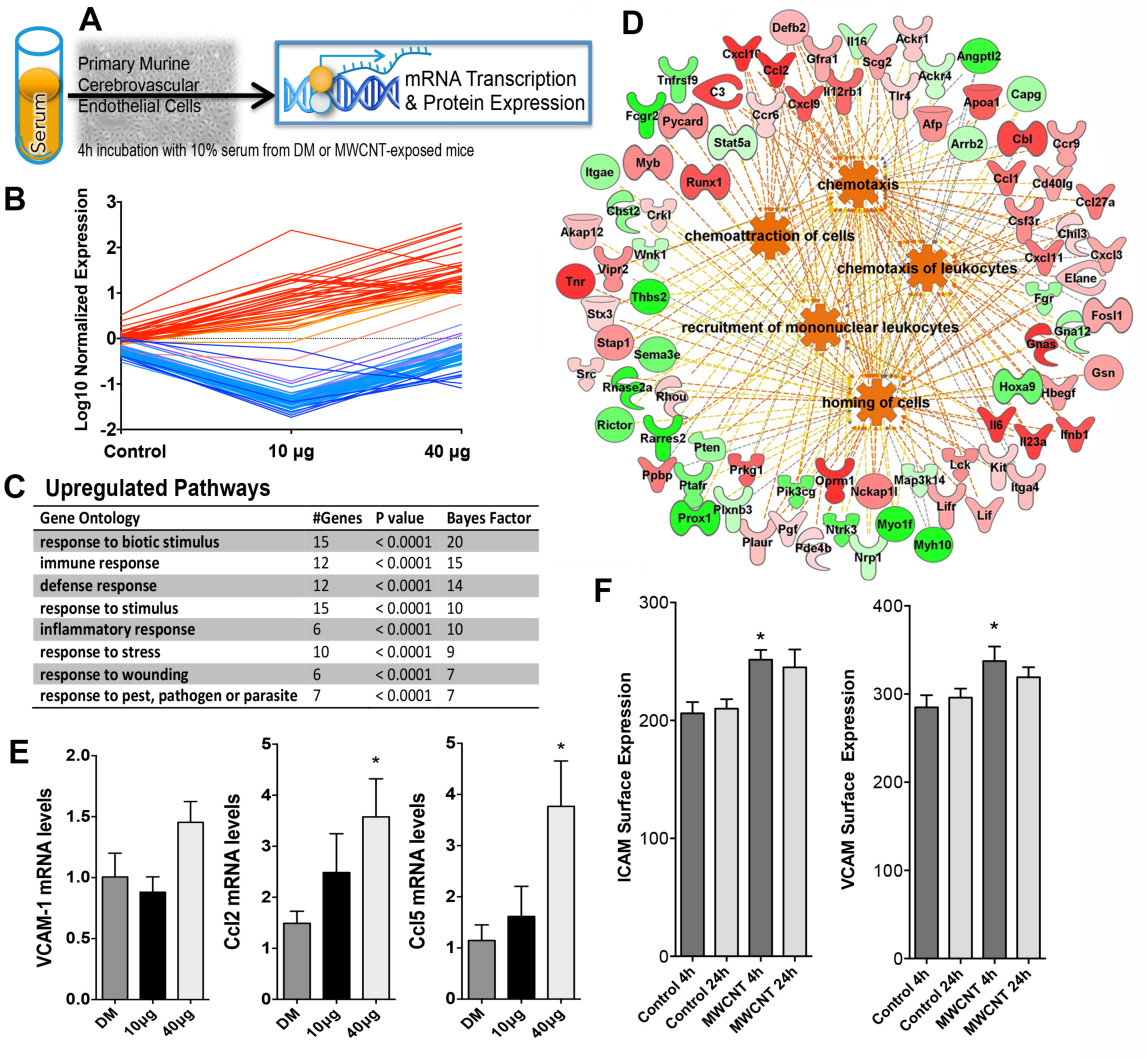


**Figure 4.5: Inflammatory responses of cerebrovascular endothelial cells treated with serum from MWCNT-exposed mice.**

**A.** General depiction of assay protocol, with serum from exposed mice incubated on primary murine cerebrovascular endothelial cells. **B**. Microarray results indicate numerous transcripts (60) from serum-treated endothelial cells were elevated in a dose-dependent manner; elevated transcripts were ontologically related inflammatory and/or cellular defense response. **C**. Specific inflammatory genes responses from microarray results. **D**. Gene ontology graphs showing the relationships between up-regulated inflammatory genes. **E**. Confirmation of key inflammatory mRNA responses by PCR finds that endothelial VCAM-1, Ccl-2, and Ccl-5 mRNA were all significantly up regulated by serum from MWCNT-treated mice. **F.** Endothelial cell surface ICAM-1 and VCAM-1 protein expression were both elevated by serum from mice exposed to the 40µg dose of MWCNT as compared to control. Asterisks denote significant difference from DM control serum ($P<0.05$).

### 4.4.6 Bioactivity of MWCNT-Induced, Serum-Borne Factors: Endothelial Cell Regrowth and Motility

A scratch assay was employed to assess the functional effects of serum collected from MWCNT-exposed serum. Serum was applied to confluent endothelial cells that had been "scratched" with a sterile pipette tip and allowed to grow back over the course of 6 h. During the regrowth, images were taken every 15 minutes and total cell area was quantified. At the 6 h mark, the controls had achieved 100 μm of cell growth when compared to 60 μm of growth for the 40 μg group and 50 μm of growth for the 10μg group. (**Figure 4.6**) These results were in complement to the microarray results indicating significantly decreased gene expression related to cell cycle, mitosis, and cytokinesis which was more prevalent in endothelial cells incubated with serum collected from mice exposed to 10 μg of MWCNT (**Figure 4.6**)

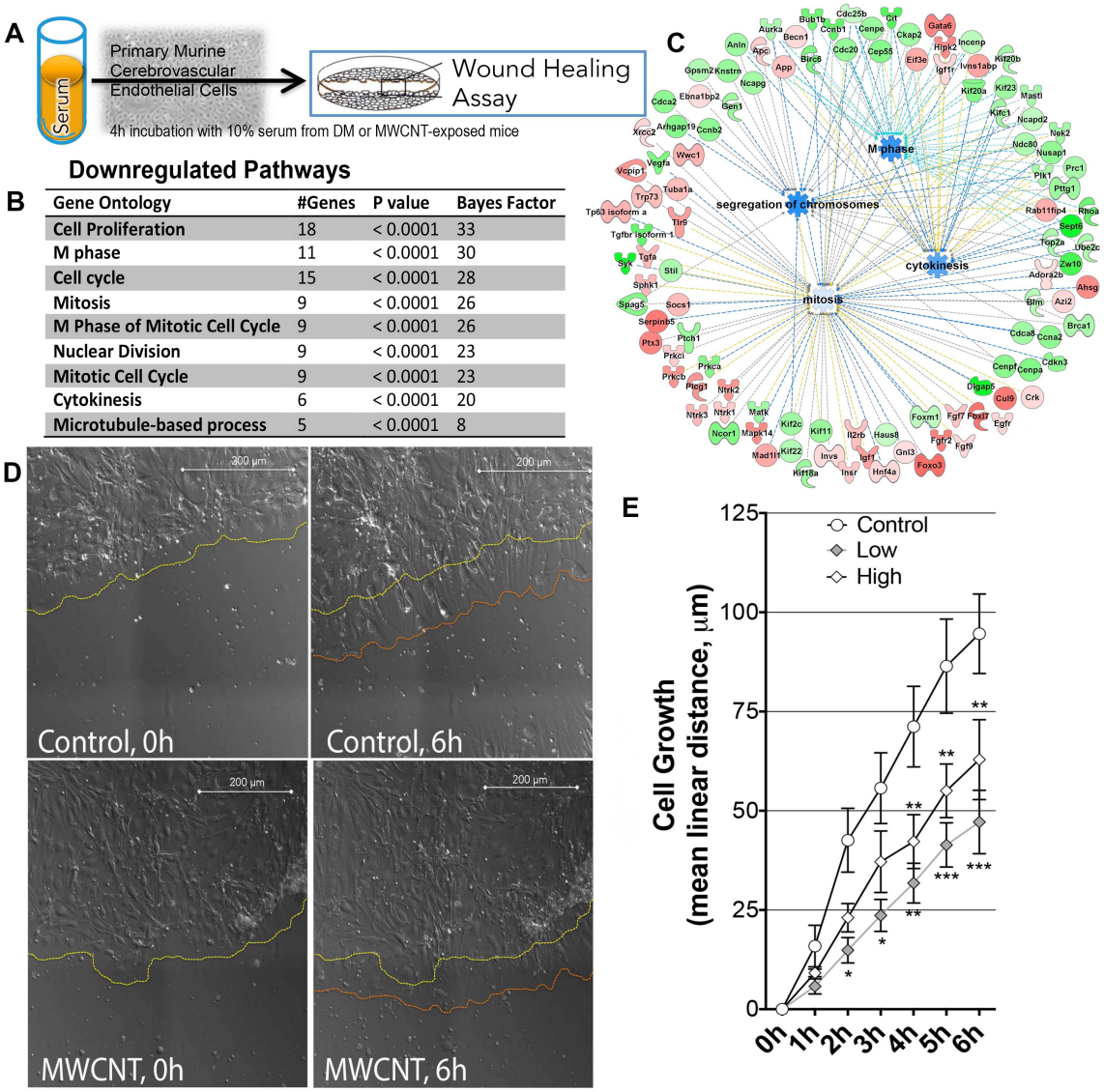


| Gene Ontology | #Genes | P value | Bayes Factor |
|---|---|---|---|
| Cell Proliferation | 18 | < 0.0001 | 33 |
| M phase | 11 | < 0.0001 | 30 |
| Cell cycle | 15 | < 0.0001 | 28 |
| Mitosis | 9 | < 0.0001 | 26 |
| M Phase of Mitotic Cell Cycle | 9 | < 0.0001 | 26 |
| Nuclear Division | 9 | < 0.0001 | 23 |
| Mitotic Cell Cycle | 9 | < 0.0001 | 23 |
| Cytokinesis | 6 | < 0.0001 | 20 |
| Microtubule-based process | 5 | < 0.0001 | 8 |

**Figure 4.6: Serum from MWCNT-exposed mice inhibits endothelial cell growth and motility.**

**A**. General depiction of assay protocol, with serum from exposed mice incubated on primary murine cerebrovascular endothelial cells. **B.** Ontological classifications of 86 significantly down regulated genes (noted in Figure 4.5B) suggest loss of cell motility and growth pathways. **C**. Gene ontology charts showing the relationship between genes that are down regulated **D**.Live cell images of wound recovery, showing the initial edge of endothelial cells (yellow dashed line) and the edge after 6 h (orange dashed line). **E**. Mean cell regrowth following wounding in primary cerebrovascular endothelial cells incubated with serum from DM or MWCNT-exposed mice. Asterisks denote significant difference from DM control serum effects using a 2-way Repeated Measures ANOVA (*P<0.05; **P<0.01; ***P<0.001).

## 4.5 DISCUSSION

Neurological effects of inhaled particulates have been reported but considerable uncertainty exists regarding the pathway by which toxic effects transfer from the lung to the brain. The present study establishes that a circulating signal arises after pulmonary exposure to MWCNT that leads to a BBB-dependent neuroinflammatory response. Serum from MWCNT-exposed mice upregulated adhesion molecules and pro-inflammatory cytokines in primary cerebrovascular endothelial cells at both the gene and protein level. Serum from exposed mice also adversely affected the ability of endothelial cells to migrate in a wound-healing assay. Collectively, these findings implicate a modified serum composition stemming from pulmonary interactions with MWCNT as a source of diminished BBB integrity and neural effects.

Severe disruption of BBB integrity has been documented in major cerebrovascular events or neurological diseases, and BBB permeability has been directly linked to neuroinflammation. Ischemia/Reperfusion in spontaneously hypertensive rats has been associated with increased BBB permeability[192]. MRI imaging showed increased BBB permeability in people with multiple sclerosis[193]. Mouse models of Alzheimer's disease have found BBB permeability to precede the formation of the β-amyloid plaques that are the hallmark of the disease[194].

Rho kinase inhibition has been shown to reduce neuropathology in scenarios where BBB is otherwise dysfunctional. Fasudil treatment in a mouse ischemia model was found to prevent BBB permeability as well as the formation of oxidative stress[189]. Rho kinase inhibition with fasudil has been shown to

accelerate functional recovery in different mouse and rat spinal cord injury models, with fasudil given locally or systemically after injury[195-197]. Autoimmune demyelinating disorders, such as multiple sclerosis, have been treated with Rho kinase inhibitors with great success. It is thought that Rho kinase inhibition in these disorders prevents the leukocyte migration into the central nervous system[198].

The class B scavenger receptor CD36 mediates free radical production and brain injury in cerebral ischemia[199]. It has also been shown to activate the Rho/Rho kinase pathway[200]. Our lab has found CD36 to play a key role in mediating vasorelaxation as a result of ozone exposure[110]. Loss of CD36 prevented both the BBB permeability and neuroinflammation that was associated with MWCNT exposure, suggesting an important role for CD36 activation.

Inhalation of PM has been associated with neuroinflammation and BBB integrity deficits [201,202], but this is the first study to show a mechanistic link between the two outcomes. Oppenheim et al identified significant increases in brain fluorescein uptake resulting from long-term exposure (50d) to a mixture of gasoline and diesel emissions in ApoE$^{-/-}$ mice [203]. These findings were similarly associated with increased cerebrovascular gelatinase levels and reduced occludin and claudin-5 expression and, in parallel, increased inducible nitric oxide synthase expression in the brain parenchyma. Rats exposed to diesel emissions for 6 months demonstrated significant increases in cortical TNFα, α-synuclein, and Aβ42 expression [204]. Importantly, all of these studies involved

long-term exposures, while the present study reveals effects within 4h of pulmonary MWCNT exposure.

Unique to this study is the idea that serum is able to drive disparate endothelial responses at multiple levels, consistent with a complex activation of multiple homeostatic responses at varying dose-response relationships. Due to the nature of the modifications in the serum there exists the possibility of activating multiple endothelial cell surface receptors, thereby eliciting a wide range of cellular responses. Our lab and others have shown that immunomodulatory scavenger receptors, such as CD36[110,113], TLR4[114], and LOX-1[115] play a major role in eliciting endothelial inflammatory and antidilatory responses following exposure to various inhaled toxicants. Further study will be required to elucidate the principal ligand/receptor interactions responsible for activating the inflammatory responses.

Alternate pathways, such as direct delivery of inhaled particulates and CNTs have been hypothesized, but limited evidence exists demonstrating substantive transference of CNTs across the BBB, and no evidence for a direct biological effect has been mechanistically established in such studies. MWCNTs, specifically, accumulate in the brain in only small fractions of the original pulmonary dosage (0.001% of the lung burden at day 1 post-inhalation for 12 d), and specific confirmation that the material has penetrated beyond the capillary wall is often lacking in distribution studies, *i.e.,* much of the residual mass of CNTs may simply reside in the cerebrovascular compartment and not the brain tissue. CNTs, and specifically MWCNTs, have many characteristics

that make them highly desirable as drug delivery platforms. The ability to withstand a high degree of functionalization is perhaps their most desirable feature. Many labs have employed MWCNTs as the basis for the targeted delivery of numerous compounds to different organs. MWCNTs were used to deliver Doxorubicin to brain glioma cells. The MWCNTs were PEGylated with angiopep-2 in BALB/c mice engrafted with C6 glioma cells. While the authors were able to discern a statistically significant amount of doxorubicin in the brain when compared to controls, they were unable to conclude that this route of delivery would be clinically relevant[205], despite extensive engineering efforts to target the brain[206].

MWCNTs are able to withstand a high degree of functionalization, including surface coating, attachment of fluorescent linkers, and drug delivery insertion[207]. These manipulations are able to decrease the amount of toxicity that MWCNTs can induce[208], as well as allowing for less aggregation[209] and better clearance by the body[210]. However targeting of CNTs to specific locations in the body is still very difficult[205,211,212]. Targeting CNTs to the brain adds an extra layer of complexity when the BBB is taken into account. This specialized structure has proven to be especially adapt at keeping functionalized MWCNTs out of the brain[213]. Other labs have investigated both the *in vivo* biodistribution and pharmacokinetics of various permutations of drug delivery systems that were built on a MWCNT platform. Singh et al found that MWCNT-GEM complex with FA targeting in rats accumulated in major organs including the liver, lung, kidney and spleen[214]. Moore et al investigated the biodistribution pattern of PLA-PEG-

coated MWCNT loaded with PTX. Intravenously (IV) injected CNTs in mice showed accumulation in the lungs, liver, and spleen. These particular CNTs did show a lack of an inflammatory response when compared to controls[215].

Future analysis of the serum will be required to better understand the nature of the systemic effects that occur as a result of MWCNT exposure. While our proteomics data denotes a number of modified proteins following exposure (personal communication with Dr. Andrew Ottens), it is important to keep in mind that the analysis was only conducted on the fraction of the serum that was <5Kd, creating the possibility that larger proteins could also be affected. Lipidomic analysis could also provide information on the nature of the serum due to the potential for MWCNTs to interact with lipids in the lung.

In conclusion acute, occupationally relevant doses of MWCNTs are able to induce neuroinflammation dependent on BBB permeability. These effects seem to be driven in part by an as yet identified serum signal that is able to drive inflammatory outcomes in naïve endothelial cells.

## Abbrevations

MWCNT – Multiwalled Carbon Nanotube

BBB – Blood Brain Barrier

CNS – Central Nervous System

MVE – Mixed Vehicle Emissions

iNOS – inducible Nitric Oxide Synthase

DM – Dispersion Media

BAL – Bronchoalveolar Lavage

mCEC – mouse Cerebrovascular Endothelial Cells

PBS – Phosphate Buffered Saline

LPS – Lipopolysacchride

VCAM -1 – Vascular Adhesion Molecule

ICAM-1 – Intercellular Adhesion Molecule

## Competing Interests

The authors declare they have no competing interests.

## Authors Contributions

MA conducted most facets of the study and data analysis and wrote the manuscript.

MC contributed substantially to the overall design of the study, the write-up, and provided funding.

LT performed immunohistochemistry and contributed to the conduct of exposures and overall study design

BS performed biochemical assays and analyzed data and contributed to writing.

**Acknowledgements**

This study was funded by grants from the National Institute of Environmental Health Sciences (R01 ES014639, MJC), National Institute for Occupational Safety and Health (R21 OH010495, MJC; NTRC, 939ZXFL and 927ZKGW, AE), National Heart Lung and Blood Institute (T32 HL007736) and the National Institutes of Health Center of Biomedical Research Excellence (P30GM103400). AKO thanks S. Tenzer from U. Mainz for customized beta release of Isoquant software for ion alignment of unidentified ions. AE thanks Diane Schwegler-Berry for the electron microscopy images of the MWCNT.

# Discussion

Epidemiological studies established the adverse cardiovascular health effects of air pollution in the early 90's[216]. Increasing evidence found that particulate matter, specifically $PM_{2.5}$, was able to drive a wide range of cardiovascular effects including chronic cardiovascular disease progression[217] to increased incidence of myocardial infarction[218] and even death[219]. With these effects established, researchers began to investigate the mechanisms through which inhaled particulates were able to induce systemic cardiovascular effects. While no single mechanism was identified, it soon became clear that smaller particles were significantly more toxic than larger particles.

The advent of nanotechnology created a new field of toxicology focused on particles that were <100 nm in any dimension. The size of these particles gave them unique physiochemical properties that required investigation into both their local and systemic effects. Several studies were able to establish both the time course and magnitude of pulmonary toxicity resulting from inhaled nanoparticles; however, their systemic extrapulmonary effects and underlying mechanisms have only recently come under investigation.

## 4.6 Novel Methodology to Assess "Spillover" Hypothesis

As evidence accumulated indicating that CNTs were unable to directly translocate from the lungs into the systemic circulation in significant amounts, other mechanisms began to receive more attention. More focus was placed on the spillover mechanism. Our lab embraced this idea with a focus on the serum

component of the blood carrying an “inflammatory signal.” This relatively unbiased approach is advantageous on many levels. It allows for a more holistic assessment of the serum, as opposed to focusing on individual serum components and trying to draw broad conclusions. It also allows for a more anatomically appropriate approach as serum (but not particles) comes in direct contact with endothelial cells. Utilization of the serum allows for the almost complete removal of any particles that may make their way into the circulation, with the filtration of anything >10 kDa (as in Chapter 3) ensuring that there are neither particles nor even cytokines driving the observed vascular effects. This approach, however, did enable us to assess the potential for MMP9 degradation products that entered the circulation to mediate serum bioactivity.

This approach does have important drawbacks, however. The complex nature of the serum makes it difficult to identify individual molecules with biological activity that drives adverse outcomes. Despite removal of large serum components, many small molecules, lipids, lipoprotein particles, proteins, cells and subcellular material remain. It is clear from our studies that particles, especially MWCNTs, create an altered bioactivity that is pro-inflammatory and anti-dilatory. Nonetheless, the molecular mechanism(s) by which the circulation becomes bioactive likely involves complex pathway arising from particle interactions in the lungs. Future –omic approaches will be necessary to provide insight into those complex, pathways and to identify the specific molecules that are modified.

## 4.7 Analysis of the Lung response to MWCNTs

The lungs have the largest surface area of any organ in the body. This makes them especially vulnerable to the effects of airborne pollutants. They are not, however, without their own defense systems that facilitate clearance or metabolism to mitigate the adverse effects of inhaled toxicants.

Due to their size, MWCNTs are able to reach and deposit in the alveolar regions of the lungs[180]. Deeply deposited particles cannot be easily or rapidly cleared via the mucociliary escalator and instead must be cleared through the activation of alveolar macrophages, which effectively phagocytize PM to remove them from the lungs. As a result of activation, the macrophages secrete pro-inflammatory cytokines and other enzymes. Analysis of the BALF has found that there is also an increase in neutrophil infiltration following MWCNT exposure. Neutrophils clear pathogens in part via generation of ROS[220]. This process is not well controlled and can result in damage to the surrounding tissue. Combined with the increased endothelia-epithelial permeability (as observed by an influx of albumin) and edematous changes, MWCNT exposure creates a very pro-inflammatory environment in the lung.

At present, the chemical changes in the lung resulting from this pro-inflammatory environment are not sufficiently well understood to draw conclusions related to functional systemic outcomes. Nanoparticle exposure creates the potential for modified proteins and lipids in the epithelial lining fluid, as well as pro-inflammatory cytokines and oxidative stress. Because such reactive intermediates form in the alveolar region of the lung, it creates the

potential for some spillover into the systemic or lymphatic circulation, although specific pathways by which reactive intermediates gain access to these compartments is unclear. Furthermore, which intermediates and the concentrations, thereof, actually attaining access to the systemic circulation is currently unknown. Proteomics analysis by Dr. Andrew Ottens (VCU; personal communication) has found that a large number of fragmented proteins are found in the serum component of the blood following exposure to MWCNTs. While this is consistent with outcomes related to MMP activation, it does not preclude the possibility that modified lipids, adducted/modified proteins or secreted peptides from activated macrophages are being generated and making their way into the systemic circulation. Dr. Ottens found approximately 1500 modified proteins in the serum following exposure of mice to MWCNTs and the findings were consistent with serum changes following ozone exposure. Identifying the proteins of pathological relevance remains to be determined, and it would be valuable to examine proteomic signatures in the lung to examine whether serum molecules arise from the airways. Dr. Ottens removed all the proteins in the serum that were larger than 10 kDa to focus on those factors most likely to penetrate a disrupted BBB. This suggests that any effects observed with this fractioned serum are independent of any MWCNTs that may have translocated directly from the lungs into the systemic circulation.

## 4.8 Analysis of the Systemic Vasculature following MWCNT exposure

The reactive intermediates that were generated in the lungs and spilled over into the systemic circulation have the potential to create a wide range of

adverse effects. One possible effect is the disruption of endothelial homeostasis. Under normal conditions the endothelium functions to maintain an anti-inflammatory environment and regulate blood flow to peripheral organs. Once the endothelium is “injured” or adversely perturbed, it becomes activated and begins to mount a response[221].

Initial activation of the endothelium involves two key outcomes. First the endothelial cells begin to upregulate the expression of adhesion molecules, such as ICAM-1, VCAM-1, and p-selectin. By interacting with EC adhesion molecules, circulating leukocytes are able to adhere, roll, firmly tether, and eventually transmigrate into the tunica intima. In the case of monocytes, this transmigration into the tunica intima causes them to transform into macrophages, significantly increasing their ability to phagocytize cellular debris or other macromolecules and activate $T_H1$ cells[222]. Macrophages in the vascular wall are central to the progression of atherosclerosis[223].

The second consequence of the activation of the endothelium is the loss of eNOS function. eNOS is very cardioprotective, exerting anti-inflammatory, anti-coagulatory, and anti-migratory effects. It is also one of the chief proteins responsible for vascular smooth muscle cell relaxation and vasodilation. Under normal conditions, eNOS exists as a dimer, with tetrahydrobiopterin ($BH_4$) acting as a key cofactor that facilitates electrochemical coupling. It is important to note that $BH_4$ is also an excellent scavenger of superoxide anion[224]. When intracellular oxidative stress increases, eNOS can be “uncoupled” due of a loss of $BH_4$ and transformed into a superoxide anion-generating monomer[225]. This

uncoupling and superoxide anion generation further contributes to the pro-oxidative and pro-inflammatory environment.

The combination of an activated endothelium and a loss of eNOS functionality is central to the early stages of vascular disease pathogenesis. Protein and lipid components of low-density lipoprotein can be oxidized leading to stimulation of CD36[226] and enhancing lipoprotein phagocytosis by macrophages, which then differentiate into foam cells. Foam cells reside at the site of injury and continue to secrete chemoattractant cytokines[227]. The activity and accumulation of the resultant foam cells help determine the behavior of the plaque. MMPs can also become secreted and induce rupture of the plaque.

Over time, plaques form as a result of this vascular injury and endothelial activation. Lesions can be either stable or unstable, depending on the nature and composition of the plaque. Other factors outside of environmental PM exposures can have a large influence the pathogenesis of plaques, such as age, diet, lifestyle, and genetics. Plaque stability determines long-term health effects. Stable plaques lead to cardiac symptoms when oxygen demand rises[228]. Unstable plaques can rupture and contribute to vessel occlusion, which can result in thrombosis[229], stroke[230], or myocardial infarction[231], depending on the affected vessel bed. This process of atheroma formation and destabilization takes a long time to develop and is generally asymptomatic until a major health event occurs.

Several studies have examined the ability of nanomaterials to induce atherosclerosis. Cao et al. showed that two different types of MWCNTs were able to provoke progression of atherosclerosis in the aorta when compared to control. The model used in this study was an ApoE$^{-/-}$ mouse on a high fat diet, where cholesterol levels in excess of 1000 mg/dl can be achieved and atheromatous lesions develop over the course of several weeks, progressing to advanced lesions in a year. Wild type mice on normal chow diets do not develop aortic plaques in their aorta due to their ability to rapidly remove LDL. This study also employed two different kinds of MWCNTs. The MWCNTs in this study were from Nanocyl with a diameter of 30 nm, slightly smaller than the more commonly used Mitsui-7[74]. Mice were dosed with 25.6 μg of MWCNTs once a week for 5 weeks via ITI dosing. Total plaque area in the aortic root was increased compared to controls, which was associated with increased pulmonary inflammation. Interestingly, circulating cytokines were not changed compared to control. An earlier study by Li et al. investigated the cardiovascular effects of SWCNTs. They also utilized an ApoE$^{-/-}$ mouse model and exposed mice to four doses of SWCNTs at 20 μg/dose of particles via pharyngeal aspiration. Thoracic aorta was formalin fixed and total plaque area was quantified. Histological assessment of lesions in mice confirmed that SWCNT were able to significantly increase lesion progression when compared to controls[74]. Thus, chronic, repeated exposures to nanomaterials can promote vascular disease. Despite the short-term study design employed in the present research, our outcomes are

consistent with the idea that, over time, the serum factor-induced endothelial activation may exacerbate vascular disease.

It is not presently known what components of the serum are interacting with the endothelial cells, and which receptors are being activated. Evidence from our lab and others implicates a strong role for scavenger receptors. These receptors, such as LOX-1[115], toll-like receptors[232], and various clusters of differentiation markers[113], bind a wide range of peptides in addition their native ligands. Our lab in particular has found LOX-1 and CD36 in the vasculature play important roles. These studies bolster the concept that serum-borne ligands drive endothelial cell activation following pulmonary exposure to particles. Given the overlap in findings, it remains to be seen how such multiligand receptors may cooperate or interact on the cell surface to promote intracellular responses.

## 4.9 Analysis of the BBB following MWCNT exposure

At present, few studies have mechanistically examined neurological effects related to inhaled pollutants. Studies that have investigated neuroinflammation following exposure have reported inconsistent effects. Ozone exposure at 1 ppm for 60 and 90 days was shown to result in pro-inflammatory gene expression in the hippocampus of adult rats[186]. Diesel exhaust exposure across a range of concentrations ranging from 0-1.0 mg/m$^3$ for 6 months was found to increase pro-inflammatory protein expression and increase signs of Alzheimers in rats[204]. No clear mechanism has been established for these

effects, but the present study highlights the potential for BBB deficits to be a central player.

Because we hypothesize that translocated particles are not the direct driver of neuroinflammation, we addressed the more proximal interaction between serum and the BBB. This study focused on the permeability of the BBB following a bolus exposure to 10 μg MWCNT-7. This dose was chosen due to ability of MWCNT-7 to induce a greater vascular dysfunction in numerous assays as compared to a dose of 40 μg. The scavenger receptor CD36 and modulation of BBB permeability were chosen to identify potential mechanisms responsible for the neuroinflammation found in our model.

### 4.9.1 BBB permeability

Following nanotube exposure, evidence of neuroinflammation was found in the brain, as characterized by increased pro-inflammatory gene expression in the cortex and hippocampus and activation of astrocytes. BBB impairment was also noted by the increased brain uptake of the fluorescent tracer fluorescein. A single dose of fasudil 2 hr after MWCNT exposure prior to fluorescein injection was able to mitigate the uptake of fluorescein in the brain, but inflammatory gene expression was still modestly elevated. However, prophylactic treatment with fasudil maintained BBB integrity after MWNT exposure and blocked cortical and hippocampal Il6 and CcL-5 mRNA induction.

Aside from its high affinity for ox-LDL, CD36 has also been shown to activate the Rho kinase pathway and tyrosine kinases associated with

constriction in a $Ca^{2+}$ independent manner[200]. Fasudil works to inhibit the Rho kinase pathway, allowing the actin cytoskeleton to relax and effectively maintain BBB permeability. Loss of CD36 or inhibition of Rho kinase via administration of fasudil both effectively maintained the tight junctions of the cerebrovascular endothelium and prevented neuroinflammation after MWCNT exposure. Consistent with our findings, inhibition of Rho kinase has been found to prevent ischemia induced injury[189]. **(Figure 5.1)**

Astrocytes are the most abundant cell type in the brain and have been associated with a wide range of processes including BBB modulation, maintenance of neurons, and regulation of ion gradients. Their activation as a result of nanotube exposure appeared dependent on the increased BBB permeability also observed, and is possibly a sentinel effect of further neuropathologies that could emerge from nanoparticle exposure. Due to their multitude of functions it is difficult to determine what other roles astrocytes might be playing aside from their role in providing support to the BBB. Further efforts to characterize a range of doses and time course of exposure would be informative as to the potential that astrocyte activation promotes adverse neurological outcomes.

### 4.10 MMP-9 Activation in the Lungs

The origin of bioactive ligands that activate EC scavenger receptors is postulated to be particle interactions in the lung microenvironment. Several lines of evidence, including gene and protein expression in the lung, suggested that

MMP-9 might be playing a major role in the generation of such ligands. Proteomic analysis by Dr. Andy Ottens **(personal communication)** identified a wide array of modified proteins in the serum following nanotube exposure.

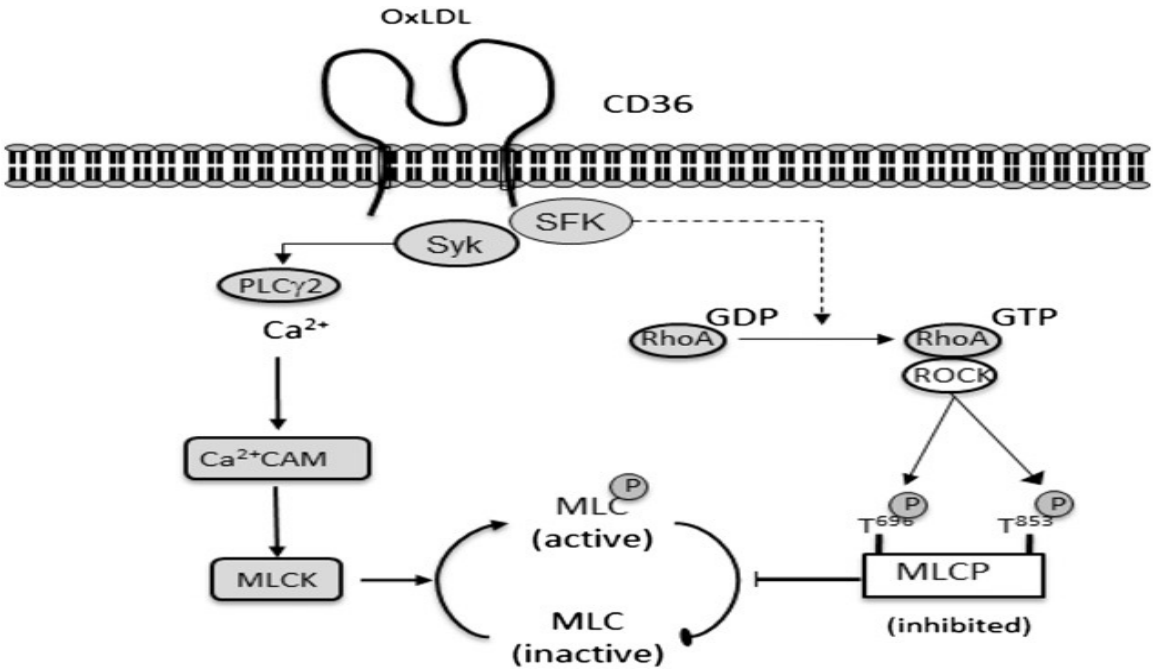


**Figure 5.1: Ox-LDL can induce CD-36 signaling pathways leading to phosphorylation of MLCP and MLCK.**

Peptide sequencing of the smaller fraction (<10 kDa) of these proteins led to the realization that many originated from ECM substrates, suggesting a role for MMP-associated proteolysis. It is important to remember that even under homeostatic conditions, MMPs generate numerous protein fragments that can possess biological activity. Activation of MMPs as a result of nanotube exposure could result in prolonged MMP production/secretion and continued generation of novel, circulating fragments with unknown biological activity.

4.10.1 MMP-9 Activation

Macrophages are a major source of MMP-9 secretion[233]. Analysis of the bronchoalveolar lavage fluid following nanotube exposure found increased alveolar macrophage activation, opening the door for significant MMP-9 secretion as a result. It is important to note that protein fragments that are generated by MMP-9 as a result of nanotube exposure may be novel, and as such may contain unknown structures. These novel protein fragments carry the potential for further modifications, depending on their structures, which could result in greater levels of biological activity than protein fragments that are generated under baseline conditions. **(Figure 5.2)**

Measurement of MMP protein or gene expression is insufficient to demonstrate functional changes; rather, the activity of the MMP enzyme must be assessed. This can be accomplished through the use of zymography (either in situ or electrophoresis gel-based) to assess an active MMP. MMP activation can be mediated through multiple mechanisms including xanthine oxidase activity[234], convertases[235], or reaction with the cysteine switch, leading to activation[236]. This required cleavage of the pro-MMP for activation suggests a role for other MMPs as well. While the focus of this study was MMP9, there was no assessment of its activity level, which remains a significant gap in the present research. Other MMPs, such as MMP2, were not highly expressed following MWCNT exposure, but their activity level could have been altered, potentially contributing to systemic serum bioactivity. Like MMP9, the prototypical substrate of MMP2 is gelatin making it the most likely alternate MMP to be playing a role.

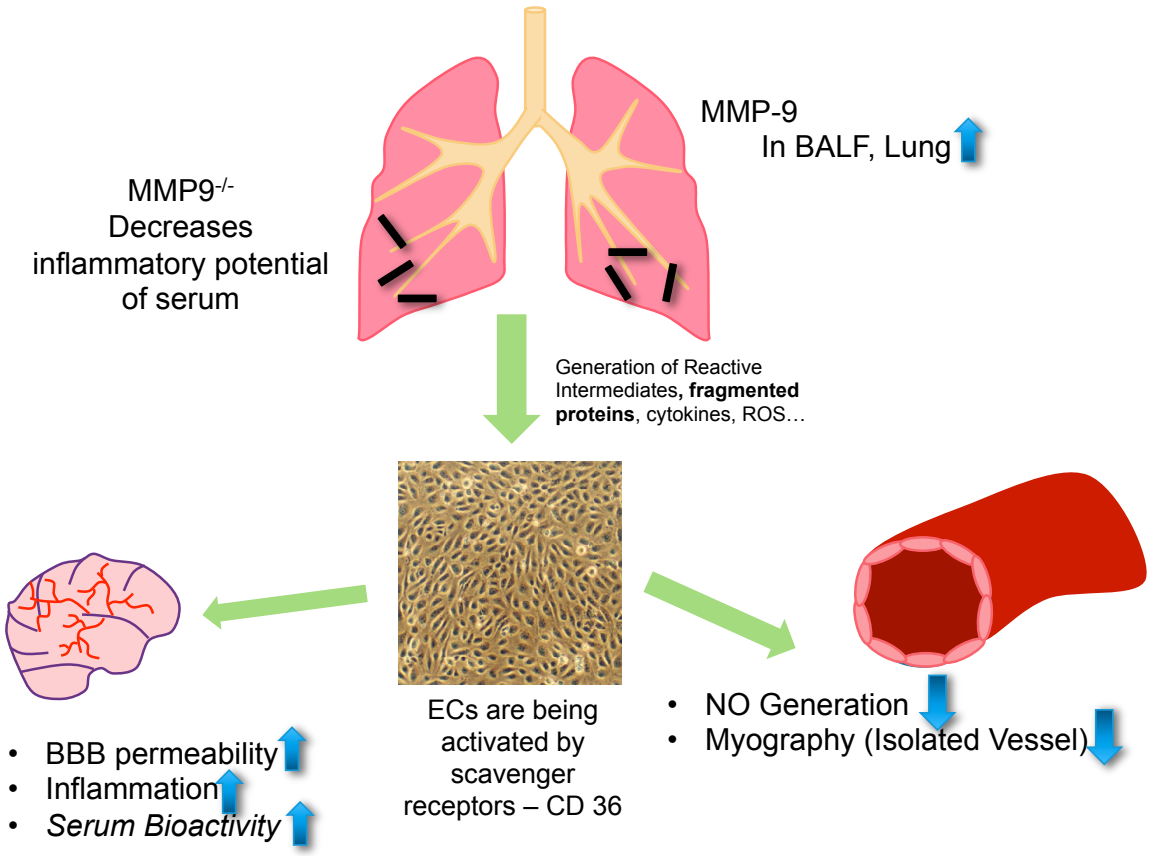


**Figure 5.2: Schematic Representation of Experimental Results.**

## 4.11 Pathological Outcomes of Novel Protein Fragments

Novel protein fragments that are generated as a result of MMP-9 activation and nanotube exposure create the potential for different pathological outcomes. Damage Associated Molecular Patterns (DAMPs) are molecules that can initiate and perpetuate immune response in the noninfectious inflammatory response[237]. Protein DAMPS include heat shock proteins[238], High Mobility Group Box 1 (HMGB1)[239], and extracellular matrix fragments including hyaluronan fragments[240]. There exists the potential for the formation of protein-based extracellular fragments that can bind TLR2, TLR4, and Receptor for Advanced Glycation Endproducts (RAGE) resulting in pro-inflammatory cytokine secretion

(IL-6, IL-1, IL-8) as well as up-regulation of adhesion molecules (ICAM-1, VCAM-1) on endothelial cells.

A second pathological outcome involves the formation of a neoantigen and autoimmunity. This would likely be mediated by a T cell response, with a $T_H17$ response being the most likely outcome. $T_H17$ overaction against an autoantigen will cause type 3 immune complex and complement mediated hypersensitivity. In the case of novel protein fragment generation, a neoantigen may be formed that would then be processed by antigen presenting cells (APCs) allowing for activation of $T_H17$ cells and an autoimmune response.

## 4.12 Health Outcomes

### 4.12.1 Acute

The results of this work highlight the possibility for myriad adverse cardiovascular and neurological health outcomes, both acute and chronic, resulting from MWCNT exposure. The myography data suggest the potential for aortic stiffness and vasoconstriction, which could lead to increased blood pressure, and/or impaired perfusion to specific (or vulnerable) vascular beds. Vascular inflammatory outcomes may predispose to more serious sequelae following exposure, include stroke or myocardial infarction. Localized vascular activation of MMP9 could act to degrade/destabilize vulnerable plaques. These outcomes would depend on several factors including an individual's disease state, lifestyle, genetics, and diet[112].

Chronically, the most likely outcome of concern related to MWCNT exposure outside of the lung is the development and progression of atherosclerosis. Because atherosclerosis is a disease that can manifest in several different ways over a long period of time, the impact of inhaled nanomaterials would largely influence existing pathologies. Plaques may be stable and have few health consequences, or the plaque could rupture leading to major health complications. It is heavily dependent on a combination of factors and time that vary from person to person.

The increased BBB permeability and resultant neuroinflammation also create the potential for neural pathologies. Alzheimer's disease, in particular, has been hypothesized to involve a breakdown in the BBB and death of astrocytes, resulting in formation/accumulation of insoluble plaques. Because Alzheimer's is not well understood, it is unclear whether increased BBB permeability drives disease progression or if it exacerbates symptoms as a result of activation of resident immune cells in the brain[241]. Multiple Sclerosis, an autoimmune disorder, has also been associated with increased BBB permeability. In the case of MS, the increased permeability of the BBB results in an influx of T cells that attack the myelin sheath of neurons, rendering them incapable of transmitting nerve impulses[242]. Importantly, the serum-based functional assays employed in the present research offers a unique and translational means of confirming the contributions of nanotube-induced blood-borne factors to driving chronic disease outcomes.

## 4.13 Integration and Synthesis of Findings

### 4.13.1 Modified Endogenous Lipids, Proteins, and Scavenger Receptor Signaling

This work highlights the importance of scavenger receptors, particularly CD36, and the role they play in mediating systemic effects following MWCNT exposure. Thrombospondin-1 (TSP-1) is the endogenous ligand for CD36[243]. TSP-1 is a very large protein, but its binding sequence consists of 30 amino acids that are acidic in nature and common to other proteins, especially those in the extracellular matrix. Serum compositional analysis is needed, specifically peptide sequencing of the protein fragments that arise from nanotube exposure, to facilitate comparison with the TSP-1 binding sequence. Such sequencing will help to confirm whether consensus sequences for CD36 binding are elevated in the serum after MWCNT exposure, and the degree to which MMP-9 is a key mediator generating those peptide fragments.

Ox-LDL binds CD36 with a very high affinity[244]. Classic lipid panels do not measure circulating ox-LDL levels, but with mounting evidence implicating the inflammatory effects of ox-LDL, extra effort to assess the protein/lipid modifications of LDL would be valuable given the role for CD36 in driving environmental effects. Circulating ox-LDL levels could be measured and compared between control and experimental groups; previous studies of engine emissions show increased ox-LDL in mice and humans. If ox-LDL is elevated, a neutralizing antibody could be used against ox-LDL[115] and eNOS mediated relaxation could be assessed to determine the inflammatory potential of the serum.

4.13.2 T cells

As evidence mounts implicating the role of inflammation in atherosclerosis, recent studies have begun to support a role for T cells. T cells control the adaptive arm of the immune system, and as such their activation is tightly regulated. Aberrant activation of T cells has been implicated in many systemic autoimmune diseases including rheumatoid arthritis[245], type I diabetes[246], atherosclerosis[247], and systemic lupus erythematosus[248]. A study by Lim et al investigated the relationships between proatherogenic factors and autoimmunity. The authors used LDb mice, mice that lack both the LDL receptor and apolipoprotein B receptor develop atherosclerosis on a normal chow diet, which created an environment that was favorable for Th17 cell polarization of autoreactive T cells. Moreover, when dendritic cells took up ox-LDL it resulted in secretion of IL-6 Th17 cell polarization[249].

Evidence from our model provides indirect evidence for T cell activation, namely the ability of the serum to up-regulate the expression of CcL-5 when incubated on naïve endothelial cells, and up-regulation of CcL-5 in the brain following exposure to MWCNTs. CcL-5 is chemotactic for T cells and plays an active role in recruiting leukocytes to inflammatory sites. The BBB is an area of intense research. It was generally thought that the only factors that were able to cross the BBB were water, oxygen, and vitamins/nutrients. However, recent studies have discovered the ability of T cells to cross the BBB[250]. **(Figure 5.3)**

At present there are three main mechanisms through which the BBB can be compromised: the BBB contains a limited number of transporters that can be

used to transport cytokines; certain cytokines have shown the ability to destroy the tight junctions of the endothelial cell layer of the BBB; and there also exists certain regions of the brain where the BBB is not full developed[250].

Kipnis et al. recently established the unique lymphatic system associated with the BBB. The authors found functional lymphatic vessels lining the dural sinuses. These structures express all of the molecular hallmarks of lymphatic endothelial cells, are able to carry both fluid and immune cells from the cerebrospinal fluid, and are connected to the deep cervical lymph nodes. Their discovery allows for a reassessment into the processes of neuroimmunology and neuroinflammation[251]. This system allows for one potential mechanism through which T cells could bypass the BBB.

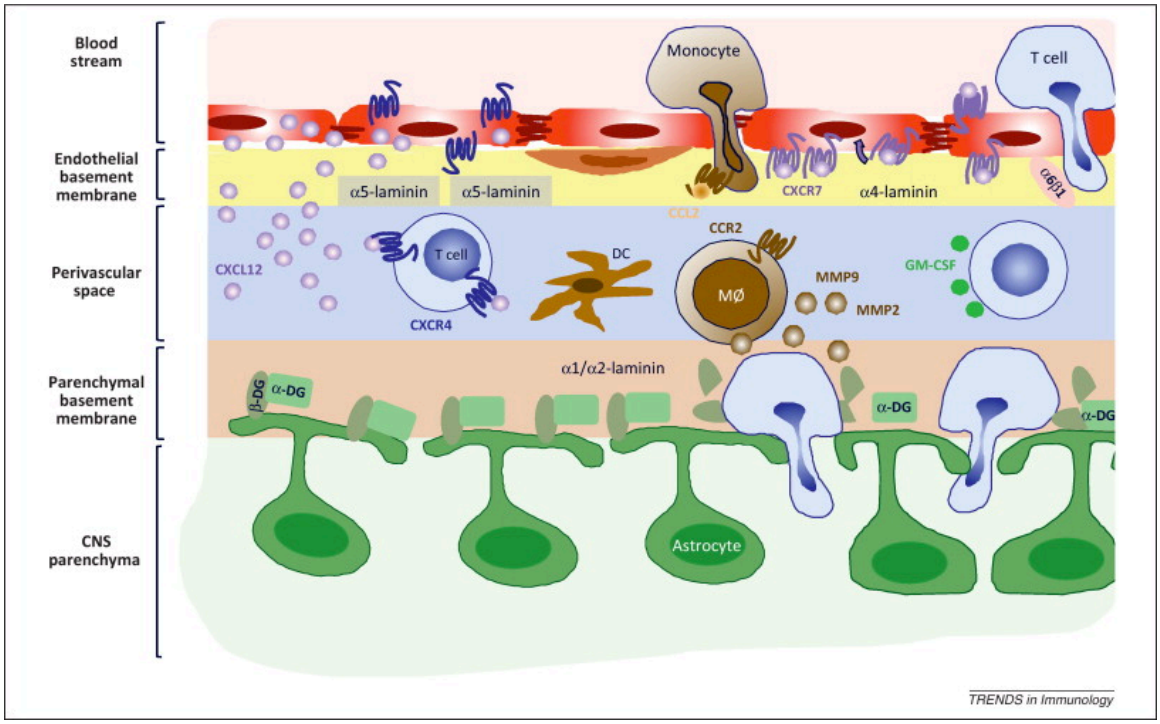


**Figure 5.3: Potential Mechanism for T cell migration into the Brain[252]**

T cells cross the first layer of the BBB in manner similar to the periphery. There exists a second layer they must cross that requires activation of MMP9.

In addition to crossing the BBB, circulating inflammatory cells need to cross a second layer composed almost entirely of astrocytes. The process by which T cells traverse this layer is not well understood. There does seem to be a role for MMPs, specifically the gelatinases (MMP-2,9), but more work is needed to understand the interactions that are occurring at this junction[253,254]. MMP-9 is thought to play an essential role in destroying the tight junctions at this second layer, suggesting the loss of MMP-9 in our model would result in a neuroprotective effect.

To assess the potential for T cell involvement following particle exposure, T cell populations in the circulation could be measured by flow cytometry. T cell function could also be assessed if T cell populations are unchanged between groups. Staining for the presence of T cells in the brain following exposure would help substantiate the purported role for CcL-5. The presence of T cells in the brain following nanotube exposure would be interesting and simultaneously raise several questions related to the mechanism of recruitment and their functional/pathological role in the brain.

## 4.14 Study Caveats

All studies have their shortcomings. The present work relies on bolus doses of nanotubes delivered to the lungs and short time courses for health outcome assessment. Even though studies have shown that PA and inhalation result in similar effects[255], inhalation studies would allow for a more accurate assessment of the effects of nanotube exposure. In pilot studies, we did show

some consistency of bioactivity in serum from mice exposed to 5 mg/m$^3$ MWCNT for 6 h/d x 19 days. This work was developmental, though, and follow-up is required to better understand the severity of effects and establish a no-effect level.

Similarly controlled human studies would also provide more insight into the acute and chronic effects of nanotube exposure. Current workplace exposure results in a wide range of doses and particle configurations. Controlled studies would provide greater insight as to the dose, time course, and particle forms are most likely to cause adverse health effects. Additionally, the substantial variability in health, genetics, and lifestyle may impact the outcomes of pulmonary MWCNT exposure and the impact of these factors was not addressed in the present study. Thus, future human studies would help to establish the variability in biological responses that occur as a result of these variables.

Lastly, this study relies on acute exposure periods. Long-term studies are needed to determine if chronic inflammatory diseases or adaptive immune changes result from repeated exposure or a longer period before sacrifice. The development of atherosclerosis requires many weeks, sometimes months, even in specially engineered mouse models. Longer-term studies would provide more concrete evidence as to the ability of the body to adapt to such exposure challenges, or if it is unable to overcome the repeated acute effects of vascular inflammation, endothelial dysfunction, and BBB impairment.

## 4.15 Conclusions

This work establishes the serum-borne bioactivity as a key mediator of the systemic effects that can occur as a result of particle exposure. Endothelial cells are particularly sensitive due to their anatomical location and their role in maintaining homeostasis in the blood vessels. Under basal conditions MMP-9 generates ligands with known bioactivity. MWCNT exposure causes enhanced MMP-9 levels presumably resulting in the generation of new/altered ligands, some of which are potentially unknown structures, which further contribute to the bioactivity of the serum. The altered composition of the serum is able to adversely affect vessel relaxation, as well as induce cerebrovascular/neural inflammation both *in vitro* and *in vivo*.

The results of this study highlight the importance of the scavenger receptor CD36. The ability of CD36 to bind a wide range of ligands and activate a myriad of responses with other cell-surface proteins further confirms its importance. Loss of CD36 in the vasculature and the BBB was protective against the effects of inhaled MWCNTs. The BBB is specialized region of the brain that contains a high number of tight junctions between the endothelial cells. This work ascertains the ability of nanotubes to induce BBB permeability, resulting in neuroinflammation in the cortex, and cerebellum. Serum from exposed animals was able to up-regulate adhesion molecules and pro-inflammatory cytokines when incubated on naïve cerebrovascular endothelial cells. Taken together, nanotube exposure induces serum compositional changes that destabilize the

BBB and stimulate neuroinflammation, potentially explaining cardiovascular and neurological impacts of inhaled PM.

# 5. References


1. Samet, J. & Krewski, D. Health effects associated with exposure to ambient air pollution. *J Toxicol Environ Health A* **70**, 227-242 (2007).
2. Nawrot, T.S., Perez, L., Kunzli, N., Munters, E. & Nemery, B. Public health importance of triggers of myocardial infarction: a comparative risk assessment. *Lancet* **377**, 732-740 (2011).
3. Rubanyi, G.M. The role of endothelium in cardiovascular homeostasis and diseases. *J Cardiovasc Pharmacol* **22 Suppl 4**, S1-14 (1993).
4. Jonasson, L., Holm, J., Skalli, O., Bondjers, G. & Hansson, G.K. Regional accumulations of T cells, macrophages, and smooth muscle cells in the human atherosclerotic plaque. *Arteriosclerosis* **6**, 131-138 (1986).
5. Frostegard, J.*, et al.* Cytokine expression in advanced human atherosclerotic plaques: dominance of pro-inflammatory (Th1) and macrophage-stimulating cytokines. *Atherosclerosis* **145**, 33-43 (1999).
6. Nahrendorf, M.*, et al.* The healing myocardium sequentially mobilizes two monocyte subsets with divergent and complementary functions. *J Exp Med* **204**, 3037-3047 (2007).
7. Hansson, G.K. Atherosclerosis--an immune disease: The Anitschkov Lecture 2007. *Atherosclerosis* **202**, 2-10 (2009).
8. Levitan, I., Volkov, S. & Subbaiah, P.V. Oxidized LDL: diversity, patterns of recognition, and pathophysiology. *Antioxid Redox Signal* **13**, 39-75 (2010).
9. Steinberg, D. Low density lipoprotein oxidation and its pathobiological significance. *J Biol Chem* **272**, 20963-20966 (1997).
10. Nakashima, Y., Raines, E.W., Plump, A.S., Breslow, J.L. & Ross, R. Upregulation of VCAM-1 and ICAM-1 at atherosclerosis-prone sites on the endothelium in the ApoE-deficient mouse. *Arterioscler Thromb Vasc Biol* **18**, 842-851 (1998).
11. Stanley, E.R., Berg, K.L., Einstein, D.B., Lee, P.S. & Yeung, Y.G. The biology and action of colony stimulating factor-1. *Stem Cells* **12 Suppl 1**, 15-24; discussion 25 (1994).
12. Lin, S.J., Jan, K.M., Schuessler, G., Weinbaum, S. & Chien, S. Enhanced macromolecular permeability of aortic endothelial cells in association with mitosis. *Atherosclerosis* **73**, 223-232 (1988).
13. Friedman, M. & Byers, S.O. Endothelial permeability in atherosclerosis. *Arch Pathol* **76**, 99-105 (1963).
14. Dejana, E. Endothelial cell-cell junctions: happy together. *Nat Rev Mol Cell Biol* **5**, 261-270 (2004).
15. Persidsky, Y., Ramirez, S.H., Haorah, J. & Kanmogne, G.D. Blood-brain barrier: structural components and function under physiologic and pathologic conditions. *J Neuroimmune Pharmacol* **1**, 223-236 (2006).
16. McDonald, D.M., Thurston, G. & Baluk, P. Endothelial gaps as sites for plasma leakage in inflammation. *Microcirculation* **6**, 7-22 (1999).

17. Carman, C.V. & Springer, T.A. A transmigratory cup in leukocyte diapedesis both through individual vascular endothelial cells and between them. *J Cell Biol* **167**, 377-388 (2004).
18. Moncada, S. & Higgs, A. The L-arginine-nitric oxide pathway. *N Engl J Med* **329**, 2002-2012 (1993).
19. Harrison, D.G. Endothelial dysfunction in atherosclerosis. *Basic Res Cardiol* **89 Suppl 1**, 87-102 (1994).
20. Kubes, P., Suzuki, M. & Granger, D.N. Nitric oxide: an endogenous modulator of leukocyte adhesion. *Proc Natl Acad Sci U S A* **88**, 4651-4655 (1991).
21. Alheid, U., Frolich, J.C. & Forstermann, U. Endothelium-derived relaxing factor from cultured human endothelial cells inhibits aggregation of human platelets. *Thromb Res* **47**, 561-571 (1987).
22. Forstermann, U., Pollock, J.S., Schmidt, H.H., Heller, M. & Murad, F. Calmodulin-dependent endothelium-derived relaxing factor/nitric oxide synthase activity is present in the particulate and cytosolic fractions of bovine aortic endothelial cells. *Proc Natl Acad Sci U S A* **88**, 1788-1792 (1991).
23. Chen, P.F. & Wu, K.K. Characterization of the roles of the 594-645 region in human endothelial nitric-oxide synthase in regulating calmodulin binding and electron transfer. *J Biol Chem* **275**, 13155-13163 (2000).
24. Goetz, R.M.*, et al.* Estradiol induces the calcium-dependent translocation of endothelial nitric oxide synthase. *Proc Natl Acad Sci U S A* **96**, 2788-2793 (1999).
25. Fleming, I., Fisslthaler, B., Dimmeler, S., Kemp, B.E. & Busse, R. Phosphorylation of Thr(495) regulates Ca(2+)/calmodulin-dependent endothelial nitric oxide synthase activity. *Circ Res* **88**, E68-75 (2001).
26. Michell, B.J.*, et al.* Coordinated control of endothelial nitric-oxide synthase phosphorylation by protein kinase C and the cAMP-dependent protein kinase. *J Biol Chem* **276**, 17625-17628 (2001).
27. Fulton, D., Gratton, J.P. & Sessa, W.C. Post-translational control of endothelial nitric oxide synthase: why isn't calcium/calmodulin enough? *J Pharmacol Exp Ther* **299**, 818-824 (2001).
28. Wohlfahrt, G.*, et al.* An ecosystem-scale perspective of the net land methanol flux: synthesis of micrometeorological flux measurements. *Atmos Chem Phys* **15**, 2577-2613 (2015).
29. Carvalho, T.C., Peters, J.I. & Williams, R.O., 3rd. Influence of particle size on regional lung deposition--what evidence is there? *Int J Pharm* **406**, 1-10 (2011).
30. Brook, R.D.*, et al.* Particulate matter air pollution and cardiovascular disease: An update to the scientific statement from the American Heart Association. *Circulation* **121**, 2331-2378 (2010).
31. Williams, R., Rankin, N., Smith, T., Galler, D. & Seakins, P. Relationship between the humidity and temperature of inspired gas and the function of the airway mucosa. *Crit Care Med* **24**, 1920-1929 (1996).

32. Sleigh, M.A., Blake, J.R. & Liron, N. The propulsion of mucus by cilia. *Am Rev Respir Dis* **137**, 726-741 (1988).
33. Raunio, H.*, et al.* Expression of xenobiotic-metabolizing CYPs in human pulmonary tissue. *Exp Toxicol Pathol* **51**, 412-417 (1999).
34. Gram, T.E. Chemically reactive intermediates and pulmonary xenobiotic toxicity. *Pharmacol Rev* **49**, 297-341 (1997).
35. Fridovich, I. Superoxide dismutases. *Adv Enzymol Relat Areas Mol Biol* **41**, 35-97 (1974).
36. Deisseroth, A. & Dounce, A.L. Catalase: Physical and chemical properties, mechanism of catalysis, and physiological role. *Physiol Rev* **50**, 319-375 (1970).
37. Rahman, I. & MacNee, W. Oxidative stress and regulation of glutathione in lung inflammation. *Eur Respir J* **16**, 534-554 (2000).
38. Postlethwait, E.M., Langford, S.D. & Bidani, A. Reactive absorption of nitrogen dioxide by pulmonary epithelial lining fluid. *J Appl Physiol (1985)* **69**, 523-531 (1990).
39. Sibille, Y. & Reynolds, H.Y. Macrophages and polymorphonuclear neutrophils in lung defense and injury. *Am Rev Respir Dis* **141**, 471-501 (1990).
40. Lambrecht, B.N. Alveolar macrophage in the driver's seat. *Immunity* **24**, 366-368 (2006).
41. Pouliot, P., Turmel, V., Gelinas, E., Laviolette, M. & Bissonnette, E.Y. Interleukin-4 production by human alveolar macrophages. *Clin Exp Allergy* **35**, 804-810 (2005).
42. Paul, W.E. Interleukin-4: a prototypic immunoregulatory lymphokine. *Blood* **77**, 1859-1870 (1991).
43. Hamilton, R.F., Iyer, L.L. & Holian, A. Asbestos induces apoptosis in human alveolar macrophages. *Am J Physiol* **271**, L813-819 (1996).
44. Cooke, W.E. Fibrosis of the Lungs Due to the Inhalation of Asbestos Dust. *Br Med J* **2**, 147-140 142 (1924).
45. Gasser, M.*, et al.* Pulmonary surfactant coating of multi-walled carbon nanotubes (MWCNTs) influences their oxidative and pro-inflammatory potential in vitro. *Part Fibre Toxicol* **9**, 17 (2012).
46. Stoner, B.R., Brown, B. & Glass, J.T. Selected Topics on the Synthesis, Properties and Applications of Multiwalled Carbon Nanotubes. *Diam Relat Mater* **42**, 49-57 (2014).
47. Yu, M.F.*, et al.* Strength and breaking mechanism of multiwalled carbon nanotubes under tensile load. *Science* **287**, 637-640 (2000).
48. Lu, X. & Chen, Z. Curved pi-conjugation, aromaticity, and the related chemistry of small fullerenes (< C60) and single-walled carbon nanotubes. *Chem Rev* **105**, 3643-3696 (2005).
49. Kim, D.H. & Waki, K. Crystal defects on multi-walled carbon nanotubes by cobalt oxide. *J Nanosci Nanotechnol* **10**, 2375-2380 (2010).
50. Thess, A.*, et al.* Crystalline Ropes of Metallic Carbon Nanotubes. *Science* **273**, 483-487 (1996).

51. Chakraborty, S.*, et al.* Surface area measurement of functionalized single-walled carbon nanotubes. *J Phys Chem B* **110**, 24812-24815 (2006).
52. Park, S.J., Schmidt, A.J., Bedewy, M. & Hart, A.J. Measurement of carbon nanotube microstructure relative density by optical attenuation and observation of size-dependent variations. *Phys Chem Chem Phys* **15**, 11511-11519 (2013).
53. Zanello, L.P., Zhao, B., Hu, H. & Haddon, R.C. Bone cell proliferation on carbon nanotubes. *Nano letters* **6**, 562-567 (2006).
54. Choi, H.J., Zhang, K. & Lim, J.Y. Multi-walled carbon nanotube/polystyrene composites prepared by in-situ bulk sonochemical polymerization. *J Nanosci Nanotechnol* **7**, 3400-3403 (2007).
55. Kateb, B.*, et al.* Multi-walled carbon nanotube (MWCNT) synthesis, preparation, labeling, and functionalization. *Methods Mol Biol* **651**, 307-317 (2010).
56. Donaldson, K.*, et al.* Carbon nanotubes: a review of their properties in relation to pulmonary toxicology and workplace safety. *Toxicol Sci* **92**, 5-22 (2006).
57. Schubauer-Berigan, M.K., Dahm, M.M. & Yencken, M.S. Engineered carbonaceous nanomaterials manufacturers in the United States: workforce size, characteristics, and feasibility of epidemiologic studies. *J Occup Environ Med* **53**, S62-67 (2011).
58. Evans, D.E., Ku, B.K., Birch, M.E. & Dunn, K.H. Aerosol monitoring during carbon nanofiber production: mobile direct-reading sampling. *Ann Occup Hyg* **54**, 514-531 (2010).
59. Dahm, M.M., Evans, D.E., Schubauer-Berigan, M.K., Birch, M.E. & Deddens, J.A. Occupational exposure assessment in carbon nanotube and nanofiber primary and secondary manufacturers: mobile direct-reading sampling. *Ann Occup Hyg* **57**, 328-344 (2013).
60. Maynard, A.D.*, et al.* Exposure to carbon nanotube material: aerosol release during the handling of unrefined single-walled carbon nanotube material. *J Toxicol Environ Health A* **67**, 87-107 (2004).
61. Birch, M.E., Ku, B.K., Evans, D.E. & Ruda-Eberenz, T.A. Exposure and emissions monitoring during carbon nanofiber production--Part I: elemental carbon and iron-soot aerosols. *Ann Occup Hyg* **55**, 1016-1036 (2011).
62. Driscoll, K.E.*, et al.* Intratracheal instillation as an exposure technique for the evaluation of respiratory tract toxicity: uses and limitations. *Toxicol Sci* **55**, 24-35 (2000).
63. Sabaitis, C.P., Leong, B.K., Rop, D.A. & Aaron, C.S. Validation of intratracheal instillation as an alternative for aerosol inhalation toxicity testing. *J Appl Toxicol* **19**, 133-140 (1999).
64. Lam, C.W.*, et al.* Pulmonary toxicity of simulated lunar and Martian dusts in mice: I. Histopathology 7 and 90 days after intratracheal instillation. *Inhal Toxicol* **14**, 901-916 (2002).
65. Lam, C.W., James, J.T., Latch, J.N., Hamilton, R.F., Jr. & Holian, A. Pulmonary toxicity of simulated lunar and Martian dusts in mice: II.

Biomarkers of acute responses after intratracheal instillation. *Inhal Toxicol* **14**, 917-928 (2002).
66. Henderson, R.F.*, et al.* A comparison of the inflammatory response of the lung to inhaled versus instilled particles in F344 rats. *Fundam Appl Toxicol* **24**, 183-197 (1995).
67. Rao, G.V.*, et al.* Efficacy of a technique for exposing the mouse lung to particles aspirated from the pharynx. *J Toxicol Environ Health A* **66**, 1441-1452 (2003).
68. Ma-Hock, L.*, et al.* Inhalation toxicity of multiwall carbon nanotubes in rats exposed for 3 months. *Toxicol Sci* **112**, 468-481 (2009).
69. Pauluhn, J. Subchronic 13-week inhalation exposure of rats to multiwalled carbon nanotubes: toxic effects are determined by density of agglomerate structures, not fibrillar structures. *Toxicol Sci* **113**, 226-242 (2010).
70. Ryman-Rasmussen, J.P.*, et al.* Inhaled carbon nanotubes reach the subpleural tissue in mice. *Nat Nanotechnol* **4**, 747-751 (2009).
71. Muller, J.*, et al.* Respiratory toxicity of multi-wall carbon nanotubes. *Toxicol Appl Pharmacol* **207**, 221-231 (2005).
72. Porter, D.W.*, et al.* Mouse pulmonary dose- and time course-responses induced by exposure to multi-walled carbon nanotubes. *Toxicology* **269**, 136-147 (2010).
73. Mercer, R.R.*, et al.* Distribution and persistence of pleural penetrations by multi-walled carbon nanotubes. *Part Fibre Toxicol* **7**, 28 (2010).
74. Cao, Y.*, et al.* Vascular effects of multiwalled carbon nanotubes in dyslipidemic ApoE-/- mice and cultured endothelial cells. *Toxicol Sci* **138**, 104-116 (2014).
75. Erdely, A.*, et al.* Cross-talk between lung and systemic circulation during carbon nanotube respiratory exposure. Potential biomarkers. *Nano letters* **9**, 36-43 (2009).
76. Li, Z.*, et al.* Cardiovascular effects of pulmonary exposure to single-wall carbon nanotubes. *Environ Health Perspect* **115**, 377-382 (2007).
77. Mitchell, L.A.*, et al.* Pulmonary and systemic immune response to inhaled multiwalled carbon nanotubes. *Toxicol Sci* **100**, 203-214 (2007).
78. Mitchell, L.A., Lauer, F.T., Burchiel, S.W. & McDonald, J.D. Mechanisms for how inhaled multiwalled carbon nanotubes suppress systemic immune function in mice. *Nat Nanotechnol* **4**, 451-456 (2009).
79. Brook, R.D.*, et al.* Insights into the mechanisms and mediators of the effects of air pollution exposure on blood pressure and vascular function in healthy humans. *Hypertension* **54**, 659-667 (2009).
80. Brown, J.S., Zeman, K.L. & Bennett, W.D. Ultrafine particle deposition and clearance in the healthy and obstructed lung. *Am J Respir Crit Care Med* **166**, 1240-1247 (2002).
81. Steiner, S.*, et al.* Technosphere/Insulin--proof of concept study with a new insulin formulation for pulmonary delivery. *Exp Clin Endocrinol Diabetes* **110**, 17-21 (2002).

82. Nemmar, A.*, et al.* Inflammatory effect of intratracheal instillation of ultrafine particles in the rabbit: role of C-fiber and mast cells. *Toxicol Appl Pharmacol* **160**, 250-261 (1999).
83. Kreyling, W.G.*, et al.* Translocation of ultrafine insoluble iridium particles from lung epithelium to extrapulmonary organs is size dependent but very low. *J Toxicol Environ Health A* **65**, 1513-1530 (2002).
84. Oberdorster, G.*, et al.* Extrapulmonary translocation of ultrafine carbon particles following whole-body inhalation exposure of rats. *J Toxicol Environ Health A* **65**, 1531-1543 (2002).
85. Takenaka, S.*, et al.* Pulmonary and systemic distribution of inhaled ultrafine silver particles in rats. *Environ Health Perspect* **109 Suppl 4**, 547-551 (2001).
86. Pham, H., Bonham, A.C., Pinkerton, K.E. & Chen, C.Y. Central neuroplasticity and decreased heart rate variability after particulate matter exposure in mice. *Environ Health Perspect* **117**, 1448-1453 (2009).
87. Morishita, M.*, et al.* The characteristics of coarse particulate matter air pollution associated with alterations in blood pressure and heart rate during controlled exposures. *J Expo Sci Environ Epidemiol* **25**, 153-159 (2015).
88. Brook, R.D.*, et al.* Hemodynamic, autonomic, and vascular effects of exposure to coarse particulate matter air pollution from a rural location. *Environ Health Perspect* **122**, 624-630 (2014).
89. Ying, Z.*, et al.* Long-term exposure to concentrated ambient PM2.5 increases mouse blood pressure through abnormal activation of the sympathetic nervous system: a role for hypothalamic inflammation. *Environ Health Perspect* **122**, 79-86 (2014).
90. Chuang, H.C.*, et al.* Nickel-regulated heart rate variability: the roles of oxidative stress and inflammation. *Toxicol Appl Pharmacol* **266**, 298-306 (2013).
91. Rowan, W.H., 3rd, Campen, M.J., Wichers, L.B. & Watkinson, W.P. Heart rate variability in rodents: uses and caveats in toxicological studies. *Cardiovasc Toxicol* **7**, 28-51 (2007).
92. Corey, L.M., Baker, C. & Luchtel, D.L. Heart-rate variability in the apolipoprotein E knockout transgenic mouse following exposure to Seattle particulate matter. *J Toxicol Environ Health A* **69**, 953-965 (2006).
93. Bigger, J.T., Fleiss, J.L., Rolnitzky, L.M. & Steinman, R.C. The ability of several short-term measures of RR variability to predict mortality after myocardial infarction. *Circulation* **88**, 927-934 (1993).
94. Fauchier, L.*, et al.* Heart rate variability in severe right or left heart failure: the role of pulmonary hypertension and resistances. *Eur J Heart Fail* **6**, 181-185 (2004).
95. Anselme, F.*, et al.* Inhalation of diluted diesel engine emission impacts heart rate variability and arrhythmia occurrence in a rat model of chronic ischemic heart failure. *Arch Toxicol* **81**, 299-307 (2007).

96. Elder, A.*, et al.* Effects of on-road highway aerosol exposures on autonomic responses in aged, spontaneously hypertensive rats. *Inhal Toxicol* **19**, 1-12 (2007).
97. Chuang, K.J., Chan, C.C., Chen, N.T., Su, T.C. & Lin, L.Y. Effects of particle size fractions on reducing heart rate variability in cardiac and hypertensive patients. *Environ Health Perspect* **113**, 1693-1697 (2005).
98. Schwartz, J.*, et al.* Traffic related pollution and heart rate variability in a panel of elderly subjects. *Thorax* **60**, 455-461 (2005).
99. Ren, C.*, et al.* Ambient temperature, air pollution, and heart rate variability in an aging population. *Am J Epidemiol* **173**, 1013-1021 (2011).
100. Godleski, J.J.*, et al.* Mechanisms of morbidity and mortality from exposure to ambient air particles. *Res Rep Health Eff Inst*, 5-88; discussion 89-103 (2000).
101. Tankersley, C.G.*, et al.* Particle effects on heart-rate regulation in senescent mice. *Inhal Toxicol* **16**, 381-390 (2004).
102. Langrish, J.P.*, et al.* Cardiovascular effects of particulate air pollution exposure: time course and underlying mechanisms. *J Intern Med* **272**, 224-239 (2012).
103. Krishna, M.T., Chauhan, A.J., Frew, A.J. & Holgate, S.T. Toxicological mechanisms underlying oxidant pollutant-induced airway injury. *Rev Environ Health* **13**, 59-71 (1998).
104. Krishnan, R.M.*, et al.* A randomized cross-over study of inhalation of diesel exhaust, hematological indices, and endothelial markers in humans. *Part Fibre Toxicol* **10**, 7 (2013).
105. Wilson, D.W.*, et al.* Exposure of mice to concentrated ambient particulate matter results in platelet and systemic cytokine activation. *Inhal Toxicol* **22**, 267-276 (2010).
106. van Eeden, S.F.*, et al.* Cytokines involved in the systemic inflammatory response induced by exposure to particulate matter air pollutants (PM(10)). *Am J Respir Crit Care Med* **164**, 826-830 (2001).
107. Kido, T.*, et al.* Particulate matter induces translocation of IL-6 from the lung to the systemic circulation. *Am J Respir Cell Mol Biol* **44**, 197-204 (2011).
108. Tsai, D.H.*, et al.* Effects of particulate matter on inflammatory markers in the general adult population. *Part Fibre Toxicol* **9**, 24 (2012).
109. Channell, M.M., Paffett, M.L., Devlin, R.B., Madden, M.C. & Campen, M.J. Circulating factors induce coronary endothelial cell activation following exposure to inhaled diesel exhaust and nitrogen dioxide in humans: evidence from a novel translational in vitro model. *Toxicol Sci* **127**, 179-186 (2012).
110. Robertson, S.*, et al.* CD36 mediates endothelial dysfunction downstream of circulating factors induced by O3 exposure. *Toxicol Sci* **134**, 304-311 (2013).
111. Febbraio, M., Hajjar, D.P. & Silverstein, R.L. CD36: a class B scavenger receptor involved in angiogenesis, atherosclerosis, inflammation, and lipid metabolism. *J Clin Invest* **108**, 785-791 (2001).

112. Lund, A.K.*, et al.* Vehicular emissions induce vascular MMP-9 expression and activity associated with endothelin-1-mediated pathways. *Arterioscler Thromb Vasc Biol* **29**, 511-517 (2009).
113. Rao, X.*, et al.* CD36-dependent 7-ketocholesterol accumulation in macrophages mediates progression of atherosclerosis in response to chronic air pollution exposure. *Circ Res* **115**, 770-780 (2014).
114. Kampfrath, T.*, et al.* Chronic fine particulate matter exposure induces systemic vascular dysfunction via NADPH oxidase and TLR4 pathways. *Circ Res* **108**, 716-726 (2011).
115. Lund, A.K.*, et al.* The oxidized low-density lipoprotein receptor mediates vascular effects of inhaled vehicle emissions. *Am J Respir Crit Care Med* **184**, 82-91 (2011).
116. Van Lint, P. & Libert, C. Chemokine and cytokine processing by matrix metalloproteinases and its effect on leukocyte migration and inflammation. *J Leukoc Biol* **82**, 1375-1381 (2007).
117. Forsyth, P.A.*, et al.* Gelatinase-A (MMP-2), gelatinase-B (MMP-9) and membrane type matrix metalloproteinase-1 (MT1-MMP) are involved in different aspects of the pathophysiology of malignant gliomas. *Br J Cancer* **79**, 1828-1835 (1999).
118. Bekes, E.M.*, et al.* Tumor-recruited neutrophils and neutrophil TIMP-free MMP-9 regulate coordinately the levels of tumor angiogenesis and efficiency of malignant cell intravasation. *Am J Pathol* **179**, 1455-1470 (2011).
119. Fang, L., Du, X.J., Gao, X.M. & Dart, A.M. Activation of peripheral blood mononuclear cells and extracellular matrix and inflammatory gene profile in acute myocardial infarction. *Clin Sci (Lond)* **119**, 175-183 (2010).
120. Grzela, K., Litwiniuk, M., Zagorska, W. & Grzela, T. Airway Remodeling in Chronic Obstructive Pulmonary Disease and Asthma: the Role of Matrix Metalloproteinase-9. *Arch Immunol Ther Exp (Warsz)* (2015).
121. Shaul, P.W. Endothelial nitric oxide synthase, caveolae and the development of atherosclerosis. *J Physiol* **547**, 21-33 (2003).
122. Silverstein, R.L. & Febbraio, M. CD36, a scavenger receptor involved in immunity, metabolism, angiogenesis, and behavior. *Sci Signal* **2**, re3 (2009).
123. Pope, C.A., 3rd*, et al.* Cardiovascular mortality and long-term exposure to particulate air pollution: epidemiological evidence of general pathophysiological pathways of disease. *Circulation* **109**, 71-77 (2004).
124. Brook, R.D.*, et al.* Long-term fine particulate matter exposure and mortality from diabetes in Canada. *Diabetes Care* **36**, 3313-3320 (2013).
125. Mercer, R.R.*, et al.* Extrapulmonary transport of MWCNT following inhalation exposure. *Part Fibre Toxicol* **10**, 38 (2013).
126. Postlethwait, E.M., Langford, S.D. & Bidani, A. Determinants of inhaled ozone absorption in isolated rat lungs. *Toxicol Appl Pharmacol* **125**, 77-89 (1994).

127. Liberda, E.N., Cuevas, A.K., Qu, Q. & Chen, L.C. The acute exposure effects of inhaled nickel nanoparticles on murine endothelial progenitor cells. *Inhal Toxicol* **26**, 588-597 (2014).
128. Vedal, S.*, et al.* National Particle Component Toxicity (NPACT) Initiative Report on Cardiovascular Effects. *Res Rep Health Eff Inst* **178**, 238 (2013).
129. Sarnat, J.A.*, et al.* Fine particle sources and cardiorespiratory morbidity: an application of chemical mass balance and factor analytical source-apportionment methods. *Environ Health Perspect* **116**, 459-466 (2008).
130. Hoffmann, B.*, et al.* Residential traffic exposure and coronary heart disease: results from the Heinz Nixdorf Recall Study. *Biomarkers* **14 Suppl 1**, 74-78 (2009).
131. Mills, N.L.*, et al.* Diesel exhaust inhalation causes vascular dysfunction and impaired endogenous fibrinolysis. *Circulation* **112**, 3930-3936 (2005).
132. Bell, M.L.*, et al.* Associations of PM(2).(5) constituents and sources with hospital admissions: analysis of four counties in Connecticut and Massachusetts (USA) for persons >/= 65 years of age. *Environ Health Perspect* **122**, 138-144 (2014).
133. McDonald, J.D., Barr, E.B. & White, R.K. Design, characterization, and evaluation of a small-scale diesel exhaust exposure system. *Aerosol Science and Technology* **38**, 62-78 (2004).
134. McDonald, J.D.*, et al.* Generation and Characterization of Gasoline Engine Exhaust Inhalation Exposure Atmospheres. *Inhalation Toxicology* **20**, 1157-1168 (2008).
135. Livak, K.J. & Schmittgen, T.D. Analysis of relative gene expression data using real-time quantitative PCR and the 2(-Delta Delta C(T)) Method. *Methods* **25**, 402-408 (2001).
136. Otterbein, L.E.*, et al.* Carbon monoxide suppresses arteriosclerotic lesions associated with chronic graft rejection and with balloon injury. *Nat Med* **9**, 183-190 (2003).
137. Campen, M., Robertson, S., Lund, A., Lucero, J. & McDonald, J. Engine exhaust particulate and gas phase contributions to vascular toxicity. *Inhal Toxicol* **26**, 353-360 (2014).
138. Forchhammer, L.*, et al.* Controlled human wood smoke exposure: oxidative stress, inflammation and microvascular function. *Part Fibre Toxicol* **9**, 7 (2012).
139. Unosson, J.*, et al.* Exposure to wood smoke increases arterial stiffness and decreases heart rate variability in humans. *Part Fibre Toxicol* **10**, 20 (2013).
140. Hunter, A.L.*, et al.* Effect of wood smoke exposure on vascular function and thrombus formation in healthy fire fighters. *Part Fibre Toxicol* **11**, 62 (2014).
141. Allen, R.W.*, et al.* An air filter intervention study of endothelial function among healthy adults in a woodsmoke-impacted community. *Am J Respir Crit Care Med* **183**, 1222-1230 (2011).

142. Mauderly, J.L. & Seilkop, S.K. The National Environmental Respiratory Center (NERC) experiment in multi-pollutant air quality health research: III. Components of diesel and gasoline engine exhausts, hardwood smoke and simulated downwind coal emissions driving non-cancer biological responses in rodents. *Inhal Toxicol* **26**, 668-690 (2014).
143. Seilkop, S.K., Campen, M.J., Lund, A.K., McDonald, J.D. & Mauderly, J.L. Identification of chemical components of combustion emissions that affect pro-atherosclerotic vascular responses in mice. *Inhal Toxicol* **24**, 270-287 (2012).
144. Ross, R. Atherosclerosis--an inflammatory disease. *N Engl J Med* **340**, 115-126 (1999).
145. Nurkiewicz, T.R.*, et al.* Nanoparticle inhalation augments particle-dependent systemic microvascular dysfunction. *Particle and fibre toxicology* **5**, 1 (2008).
146. Nurkiewicz, T.R.*, et al.* Pulmonary nanoparticle exposure disrupts systemic microvascular nitric oxide signaling. *Toxicol Sci* **110**, 191-203 (2009).
147. Sun, Q.*, et al.* Long-term air pollution exposure and acceleration of atherosclerosis and vascular inflammation in an animal model. *Jama* **294**, 3003-3010 (2005).
148. Folkmann, J.K., Vesterdal, L.K., Sheykhzade, M., Loft, S. & Moller, P. Endothelial dysfunction in normal and prediabetic rats with metabolic syndrome exposed by oral gavage to carbon black nanoparticles. *Toxicol Sci* **129**, 98-107 (2012).
149. Bai, N., Khazaei, M., van Eeden, S.F. & Laher, I. The pharmacology of particulate matter air pollution-induced cardiovascular dysfunction. *Pharmacol Ther* **113**, 16-29 (2007).
150. Aird, W.C. Endothelium in health and disease. *Pharmacological reports : PR* **60**, 139-143 (2008).
151. Nunokawa, Y. & Tanaka, S. Interferon-gamma inhibits proliferation of rat vascular smooth muscle cells by nitric oxide generation. *Biochem Biophys Res Commun* **188**, 409-415 (1992).
152. Wang, W.*, et al.* TLR4 activation induces nontolerant inflammatory response in endothelial cells. *Inflammation* **34**, 509-518 (2011).
153. Febbraio, M.*, et al.* A null mutation in murine CD36 reveals an important role in fatty acid and lipoprotein metabolism. *J Biol Chem* **274**, 19055-19062 (1999).
154. Sawada, H., Saito, Y. & Noguchi, N. Enhanced CD36 expression changes the role of Nrf2 activation from anti-atherogenic to pro-atherogenic in apoE-deficient mice. *Atherosclerosis* **225**, 83-90 (2012).
155. Su, W.Y., Jaskot, R.H. & Dreher, K.L. Particulate Matter Induction of Pulmonary Gelatinase A, Gelatinase B, and Tissue Inhibitor of Metalloproteinase Expression. *Inhal Toxicol* **12 Suppl 2**, 105-119 (2000).
156. Dagouassat, M., Lanone, S. & Boczkowski, J. Interaction of matrix metalloproteinases with pulmonary pollutants. *Eur Respir J* **39**, 1021-1032 (2012).

157. Fuller, B.F.*, et al.* Exposure of rats to environmental tobacco smoke during cerebellar development alters behavior and perturbs mitochondrial energetics. *Environ Health Perspect* **120**, 1684-1691 (2012).
158. Ottens, A.K.*, et al.* Post-acute brain injury urinary signature: a new resource for molecular diagnostics. *J Neurotrauma* **31**, 782-788 (2014).
159. Distler, U.*, et al.* Drift time-specific collision energies enable deep-coverage data-independent acquisition proteomics. *Nat Methods* **11**, 167-170 (2014).
160. Kuharev, J., Navarro, P., Distler, U., Jahn, O. & Tenzer, S. In-depth evaluation of software tools for data-independent acquisition based label-free quantification. *Proteomics* (2014).
161. Paffett, M.L.*, et al.* Ozone Inhalation Impairs Coronary Artery Dilation via Intracellular Oxidative Stress: Evidence for Serum-Borne Factors as Drivers of Systemic Toxicity. *Toxicological sciences : an official journal of the Society of Toxicology* (2015).
162. Van Eeden, S., Leipsic, J., Paul Man, S.F. & Sin, D.D. The relationship between lung inflammation and cardiovascular disease. *Am J Respir Crit Care Med* **186**, 11-16 (2012).
163. Knuckles, T.L., Lund, A.K., Lucas, S.N. & Campen, M.J. Diesel exhaust exposure enhances venoconstriction via uncoupling of eNOS. *Toxicology and applied pharmacology* **230**, 346-351 (2008).
164. Cherng, T.W.*, et al.* Mechanisms of diesel-induced endothelial nitric oxide synthase dysfunction in coronary arterioles. *Environ Health Perspect* **119**, 98-103 (2011).
165. Uittenbogaard, A., Shaul, P.W., Yuhanna, I.S., Blair, A. & Smart, E.J. High density lipoprotein prevents oxidized low density lipoprotein-induced inhibition of endothelial nitric-oxide synthase localization and activation in caveolae. *J Biol Chem* **275**, 11278-11283 (2000).
166. Fleming, I.*, et al.* Oxidized low-density lipoprotein increases superoxide production by endothelial nitric oxide synthase by inhibiting PKCalpha. *Cardiovasc Res* **65**, 897-906 (2005).
167. Wong, W.T., Ng, C.H., Tsang, S.Y., Huang, Y. & Chen, Z.Y. Relative contribution of individual oxidized components in ox-LDL to inhibition on endothelium-dependent relaxation in rat aorta. *Nutrition, metabolism, and cardiovascular diseases : NMCD* **21**, 157-164 (2011).
168. Colin-Barenque, L.*, et al.* Matrix metalloproteinases 2 and 9 in central nervous system and their modification after vanadium inhalation. *J Appl Toxicol* **28**, 718-723 (2008).
169. Palmer, K.T.*, et al.* Inflammatory responses to the occupational inhalation of metal fume. *Eur Respir J* **27**, 366-373 (2006).
170. Cornelius, L.A.*, et al.* Matrix metalloproteinases generate angiostatin: effects on neovascularization. *J Immunol* **161**, 6845-6852 (1998).
171. Pozzi, A.*, et al.* Elevated matrix metalloprotease and angiostatin levels in integrin alpha 1 knockout mice cause reduced tumor vascularization. *Proc Natl Acad Sci U S A* **97**, 2202-2207 (2000).

172. Hamano, Y.*, et al.* Physiological levels of tumstatin, a fragment of collagen IV alpha3 chain, are generated by MMP-9 proteolysis and suppress angiogenesis via alphaV beta3 integrin. *Cancer Cell* **3**, 589-601 (2003).
173. Agrawal, S.*, et al.* Dystroglycan is selectively cleaved at the parenchymal basement membrane at sites of leukocyte extravasation in experimental autoimmune encephalomyelitis. *J Exp Med* **203**, 1007-1019 (2006).
174. Bai, N. & van Eeden, S.F. Systemic and vascular effects of circulating diesel exhaust particulate matter. *Inhal Toxicol* **25**, 725-734 (2013).
175. Ormsby, R.W., Modreanu, M., Mitchell, C.A. & Dunne, N.J. Carboxyl functionalised MWCNT/polymethyl methacrylate bone cement for orthopaedic applications. *J Biomater Appl* **29**, 209-221 (2014).
176. Hamilton, R.F., Jr., Wu, Z., Mitra, S., Shaw, P.K. & Holian, A. Effect of MWCNT size, carboxylation, and purification on in vitro and in vivo toxicity, inflammation and lung pathology. *Part Fibre Toxicol* **10**, 57 (2013).
177. Lam, C.W., James, J.T., McCluskey, R., Arepalli, S. & Hunter, R.L. A review of carbon nanotube toxicity and assessment of potential occupational and environmental health risks. *Crit Rev Toxicol* **36**, 189-217 (2006).
178. Donaldson, K. & Tran, C.L. An introduction to the short-term toxicology of respirable industrial fibres. *Mutat Res* **553**, 5-9 (2004).
179. Erdely, A.*, et al.* Carbon nanotube dosimetry: from workplace exposure assessment to inhalation toxicology. *Part Fibre Toxicol* **10**, 53 (2013).
180. Mercer, R.R.*, et al.* Pulmonary fibrotic response to aspiration of multi-walled carbon nanotubes. *Part Fibre Toxicol* **8**, 21 (2011).
181. Erdely, A.*, et al.* Identification of systemic markers from a pulmonary carbon nanotube exposure. *J Occup Environ Med* **53**, S80-86 (2011).
182. Mercer, R.R.*, et al.* Extrapulmonary transport of MWCNT following inhalation exposure. *Part Fibre Toxicol* **10**, 38 (2013).
183. Takeda, S., Sato, N. & Morishita, R. Systemic inflammation, blood-brain barrier vulnerability and cognitive/non-cognitive symptoms in Alzheimer disease: relevance to pathogenesis and therapy. *Front Aging Neurosci* **6**, 171 (2014).
184. Calderon-Garciduenas, L.*, et al.* Brain inflammation and Alzheimer's-like pathology in individuals exposed to severe air pollution. *Toxicol Pathol* **32**, 650-658 (2004).
185. Bussy, C.*, et al.* Microglia Determine Brain Region-Specific Neurotoxic Responses to Chemically Functionalized Carbon Nanotubes. *ACS Nano* (2015).
186. Rivas-Arancibia, S.*, et al.* Oxidative stress caused by ozone exposure induces loss of brain repair in the hippocampus of adult rats. *Toxicol Sci* **113**, 187-197 (2010).
187. Porter, D.W.*, et al.* Acute pulmonary dose-responses to inhaled multi-walled carbon nanotubes. *Nanotoxicology* (2012).
188. Satoh, S.*, et al.* Neuroprotective properties of a protein kinase inhibitor against ischaemia-induced neuronal damage in rats and gerbils. *Br J Pharmacol* **118**, 1592-1596 (1996).

189. Gibson, C.L., Srivastava, K., Sprigg, N., Bath, P.M. & Bayraktutan, U. Inhibition of Rho-kinase protects cerebral barrier from ischaemia-evoked injury through modulations of endothelial cell oxidative stress and tight junctions. *J Neurochem* **129**, 816-826 (2014).
190. Hajri, T., Han, X.X., Bonen, A. & Abumrad, N.A. Defective fatty acid uptake modulates insulin responsiveness and metabolic responses to diet in CD36-null mice. *J Clin Invest* **109**, 1381-1389 (2002).
191. Febbraio, M.*, et al.* Targeted disruption of the class B scavenger receptor CD36 protects against atherosclerotic lesion development in mice. *J Clin Invest* **105**, 1049-1056 (2000).
192. Aoki, T., Sumii, T., Mori, T., Wang, X. & Lo, E.H. Blood-brain barrier disruption and matrix metalloproteinase-9 expression during reperfusion injury: mechanical versus embolic focal ischemia in spontaneously hypertensive rats. *Stroke* **33**, 2711-2717 (2002).
193. Cramer, S.P., Simonsen, H., Frederiksen, J.L., Rostrup, E. & Larsson, H.B. Abnormal blood-brain barrier permeability in normal appearing white matter in multiple sclerosis investigated by MRI. *Neuroimage Clin* **4**, 182-189 (2014).
194. Ujiie, M., Dickstein, D.L., Carlow, D.A. & Jefferies, W.A. Blood-brain barrier permeability precedes senile plaque formation in an Alzheimer disease model. *Microcirculation* **10**, 463-470 (2003).
195. Dergham, P.*, et al.* Rho signaling pathway targeted to promote spinal cord repair. *J Neurosci* **22**, 6570-6577 (2002).
196. Hara, M.*, et al.* Protein kinase inhibition by fasudil hydrochloride promotes neurological recovery after spinal cord injury in rats. *J Neurosurg* **93**, 94-101 (2000).
197. Fournier, A.E., Takizawa, B.T. & Strittmatter, S.M. Rho kinase inhibition enhances axonal regeneration in the injured CNS. *J Neurosci* **23**, 1416-1423 (2003).
198. Walters, C.E.*, et al.* Inhibition of Rho GTPases with protein prenyltransferase inhibitors prevents leukocyte recruitment to the central nervous system and attenuates clinical signs of disease in an animal model of multiple sclerosis. *J Immunol* **168**, 4087-4094 (2002).
199. Ueno, M.*, et al.* The expression of CD36 in vessels with blood-brain barrier impairment in a stroke-prone hypertensive model. *Neuropathol Appl Neurobiol* **37**, 727-737 (2011).
200. Wraith, K.S.*, et al.* Oxidized low-density lipoproteins induce rapid platelet activation and shape change through tyrosine kinase and Rho kinase-signaling pathways. *Blood* **122**, 580-589 (2013).
201. Gerlofs-Nijland, M.E.*, et al.* Effect of prolonged exposure to diesel engine exhaust on proinflammatory markers in different regions of the rat brain. *Particle and fibre toxicology* **7**, 12 (2010).
202. Campbell, A., Araujo, J.A., Li, H., Sioutas, C. & Kleinman, M. Particulate matter induced enhancement of inflammatory markers in the brains of apolipoprotein E knockout mice. *J Nanosci Nanotechnol* **9**, 5099-5104 (2009).

203. Oppenheim, H.A.*, et al.* Exposure to vehicle emissions results in altered blood brain barrier permeability and expression of matrix metalloproteinases and tight junction proteins in mice. *Particle and fibre toxicology* **10**, 62 (2013).
204. Levesque, S., Surace, M.J., McDonald, J. & Block, M.L. Air pollution & the brain: Subchronic diesel exhaust exposure causes neuroinflammation and elevates early markers of neurodegenerative disease. *J Neuroinflammation* **8**, 105 (2011).
205. Ren, J.*, et al.* The targeted delivery of anticancer drugs to brain glioma by PEGylated oxidized multi-walled carbon nanotubes modified with angiopep-2. *Biomaterials* **33**, 3324-3333 (2012).
206. Kateb, B.*, et al.* Internalization of MWCNTs by microglia: possible application in immunotherapy of brain tumors. *Neuroimage* **37 Suppl 1**, S9-17 (2007).
207. Tsai, H.C., Lin, J.Y., Maryani, F., Huang, C.C. & Imae, T. Drug-loading capacity and nuclear targeting of multiwalled carbon nanotubes grafted with anionic amphiphilic copolymers. *Int J Nanomedicine* **8**, 4427-4440 (2013).
208. Vittorio, O., Raffa, V. & Cuschieri, A. Influence of purity and surface oxidation on cytotoxicity of multiwalled carbon nanotubes with human neuroblastoma cells. *Nanomedicine* **5**, 424-431 (2009).
209. Forati, T.*, et al.* Effect of functionalized carbon nanotubes on the synthesis of hydroxyapatite nanoparticles. *J Nanosci Nanotechnol* **11**, 5423-5428 (2011).
210. Bussy, C.*, et al.* Microglia Determine Brain Region-Specific Neurotoxic Responses to Chemically Functionalized Carbon Nanotubes. *ACS Nano* **9**, 7815-7830 (2015).
211. Peer, D.*, et al.* Nanocarriers as an emerging platform for cancer therapy. *Nat Nanotechnol* **2**, 751-760 (2007).
212. Mehra, N.K. & Jain, N.K. Development, characterization and cancer targeting potential of surface engineered carbon nanotubes. *J Drug Target* **21**, 745-758 (2013).
213. Kafa, H.*, et al.* The interaction of carbon nanotubes with an in vitro blood-brain barrier model and mouse brain in vivo. *Biomaterials* **53**, 437-452 (2015).
214. Singh, R., Mehra, N.K., Jain, V. & Jain, N.K. Gemcitabine-loaded smart carbon nanotubes for effective targeting to cancer cells. *J Drug Target* **21**, 581-592 (2013).
215. Wu, C.H.*, et al.* Trojan-horse nanotube on-command intracellular drug delivery. *Nano Lett* **12**, 5475-5480 (2012).
216. Dockery, D.W.*, et al.* An association between air pollution and mortality in six U.S. cities. *N Engl J Med* **329**, 1753-1759 (1993).
217. Simkhovich, B.Z., Kleinman, M.T. & Kloner, R.A. Air pollution and cardiovascular injury epidemiology, toxicology, and mechanisms. *J Am Coll Cardiol* **52**, 719-726 (2008).

218. Yusuf, S.*, et al.* Effect of potentially modifiable risk factors associated with myocardial infarction in 52 countries (the INTERHEART study): case-control study. *Lancet* **364**, 937-952 (2004).
219. Wang, T.J.*, et al.* Multiple biomarkers for the prediction of first major cardiovascular events and death. *N Engl J Med* **355**, 2631-2639 (2006).
220. Bastian, N.R. & Hibbs, J.B., Jr. Assembly and regulation of NADPH oxidase and nitric oxide synthase. *Curr Opin Immunol* **6**, 131-139 (1994).
221. Hunt, B.J. & Jurd, K.M. Endothelial cell activation. A central pathophysiological process. *BMJ* **316**, 1328-1329 (1998).
222. Desmedt, M., Rottiers, P., Dooms, H., Fiers, W. & Grooten, J. Macrophages induce cellular immunity by activating Th1 cell responses and suppressing Th2 cell responses. *J Immunol* **160**, 5300-5308 (1998).
223. Day, A.J. Lipid metabolism by macrophages and its relationship to atherosclerosis. *Adv Lipid Res* **5**, 185-207 (1967).
224. Dumitrescu, C.*, et al.* Myocardial ischemia results in tetrahydrobiopterin (BH4) oxidation with impaired endothelial function ameliorated by BH4. *Proceedings of the National Academy of Sciences of the United States of America* **104**, 15081-15086 (2007).
225. Vasquez-Vivar, J.*, et al.* Superoxide generation by endothelial nitric oxide synthase: the influence of cofactors. *Proc Natl Acad Sci U S A* **95**, 9220-9225 (1998).
226. Gerrity, R.G. The role of the monocyte in atherogenesis: I. Transition of blood-borne monocytes into foam cells in fatty lesions. *Am J Pathol* **103**, 181-190 (1981).
227. Yla-Herttuala, S.*, et al.* Expression of monocyte chemoattractant protein 1 in macrophage-rich areas of human and rabbit atherosclerotic lesions. *Proc Natl Acad Sci U S A* **88**, 5252-5256 (1991).
228. Cassar, A., Holmes, D.R., Jr., Rihal, C.S. & Gersh, B.J. Chronic coronary artery disease: diagnosis and management. *Mayo Clin Proc* **84**, 1130-1146 (2009).
229. Fuster, V.*, et al.* Atherosclerotic plaque rupture and thrombosis. Evolving concepts. *Circulation* **82**, II47-59 (1990).
230. Hennerici, M.G. The unstable plaque. *Cerebrovasc Dis* **17 Suppl 3**, 17-22 (2004).
231. van der Wal, A.C. & Becker, A.E. Atherosclerotic plaque rupture--pathologic basis of plaque stability and instability. *Cardiovasc Res* **41**, 334-344 (1999).
232. Shoenfelt, J.*, et al.* Involvement of TLR2 and TLR4 in inflammatory immune responses induced by fine and coarse ambient air particulate matter. *J Leukoc Biol* **86**, 303-312 (2009).
233. Dreier, R., Wallace, S., Fuchs, S., Bruckner, P. & Grassel, S. Paracrine interactions of chondrocytes and macrophages in cartilage degradation: articular chondrocytes provide factors that activate macrophage-derived pro-gelatinase B (pro-MMP-9). *J Cell Sci* **114**, 3813-3822 (2001).
234. Rajagopalan, S., Meng, X.P., Ramasamy, S., Harrison, D.G. & Galis, Z.S. Reactive oxygen species produced by macrophage-derived foam cells

regulate the activity of vascular matrix metalloproteinases in vitro. Implications for atherosclerotic plaque stability. *J Clin Invest* **98**, 2572-2579 (1996).
235. Stawowy, P.*, et al.* Furin-like proprotein convertases are central regulators of the membrane type matrix metalloproteinase-pro-matrix metalloproteinase-2 proteolytic cascade in atherosclerosis. *Circulation* **111**, 2820-2827 (2005).
236. Gu, Z.*, et al.* S-nitrosylation of matrix metalloproteinases: signaling pathway to neuronal cell death. *Science* **297**, 1186-1190 (2002).
237. Janeway, C. Immunogenicity signals 1,2,3 ... and 0. *Immunol Today* **10**, 283-286 (1989).
238. Panayi, G.S., Corrigall, V.M. & Henderson, B. Stress cytokines: pivotal proteins in immune regulatory networks; Opinion. *Curr Opin Immunol* **16**, 531-534 (2004).
239. Scaffidi, P., Misteli, T. & Bianchi, M.E. Release of chromatin protein HMGB1 by necrotic cells triggers inflammation. *Nature* **418**, 191-195 (2002).
240. Scheibner, K.A.*, et al.* Hyaluronan fragments act as an endogenous danger signal by engaging TLR2. *J Immunol* **177**, 1272-1281 (2006).
241. Verkhratsky, A., Olabarria, M., Noristani, H.N., Yeh, C.Y. & Rodriguez, J.J. Astrocytes in Alzheimer's disease. *Neurotherapeutics* **7**, 399-412 (2010).
242. Nair, A., Frederick, T.J. & Miller, S.D. Astrocytes in multiple sclerosis: a product of their environment. *Cell Mol Life Sci* **65**, 2702-2720 (2008).
243. Silverstein, R.L., Baird, M., Lo, S.K. & Yesner, L.M. Sense and antisense cDNA transfection of CD36 (glycoprotein IV) in melanoma cells. Role of CD36 as a thrombospondin receptor. *J Biol Chem* **267**, 16607-16612 (1992).
244. Boullier, A.*, et al.* The binding of oxidized low density lipoprotein to mouse CD36 is mediated in part by oxidized phospholipids that are associated with both the lipid and protein moieties of the lipoprotein. *J Biol Chem* **275**, 9163-9169 (2000).
245. Cope, A.P., Schulze-Koops, H. & Aringer, M. The central role of T cells in rheumatoid arthritis. *Clin Exp Rheumatol* **25**, S4-11 (2007).
246. Tsai, S., Shameli, A. & Santamaria, P. CD8+ T cells in type 1 diabetes. *Adv Immunol* **100**, 79-124 (2008).
247. Mallat, Z., Taleb, S., Ait-Oufella, H. & Tedgui, A. The role of adaptive T cell immunity in atherosclerosis. *J Lipid Res* **50 Suppl**, S364-369 (2009).
248. Hoffman, R.W. T cells in the pathogenesis of systemic lupus erythematosus. *Clin Immunol* **113**, 4-13 (2004).
249. Lim, H.*, et al.* Proatherogenic conditions promote autoimmune T helper 17 cell responses in vivo. *Immunity* **40**, 153-165 (2014).
250. Engelhardt, B. Molecular mechanisms involved in T cell migration across the blood-brain barrier. *J Neural Transm* **113**, 477-485 (2006).
251. Dando, S.J.*, et al.* Pathogens penetrating the central nervous system: infection pathways and the cellular and molecular mechanisms of invasion. *Clin Microbiol Rev* **27**, 691-726 (2014).

252. Engelhardt, B. & Ransohoff, R.M. Capture, crawl, cross: the T cell code to breach the blood-brain barriers. *Trends Immunol* **33**, 579-589 (2012).
253. Yang, Y. & Rosenberg, G.A. MMP-mediated disruption of claudin-5 in the blood-brain barrier of rat brain after cerebral ischemia. *Methods Mol Biol* **762**, 333-345 (2011).
254. Shigemori, Y., Katayama, Y., Mori, T., Maeda, T. & Kawamata, T. Matrix metalloproteinase-9 is associated with blood-brain barrier opening and brain edema formation after cortical contusion in rats. *Acta Neurochir Suppl* **96**, 130-133 (2006).
255. Aiso, S*., et al.* Pulmonary toxicity of intratracheally instilled multiwall carbon nanotubes in male Fischer 344 rats. *Ind Health* **48**, 783-795 (2010).